

MATERIALS SCIENCE AND TECHNOLOGIES

**A NEW FRACTURE
MECHANICS THEORY
OF WOOD.**

EXTENDED SECOND EDITION

No part of this digital document may be reproduced, stored in a retrieval system or transmitted commercially in any form or by any means. The publisher has taken reasonable care in the preparation of this digital document, but makes no expressed or implied warranty of any kind and assumes no responsibility for any errors or omissions. No liability is assumed for incidental or consequential damages in connection with or arising out of information contained herein. This digital document is sold with the clear understanding that the publisher is not engaged in rendering legal, medical or any other professional services.

MATERIALS SCIENCE AND TECHNOLOGIES

Additional books in this series can be found on Nova's website
under the Series tab.

Additional e-books in this series can be found on Nova's website
under the eBooks tab.

MATERIALS SCIENCE AND TECHNOLOGIES

**A NEW FRACTURE
MECHANICS THEORY
OF WOOD.**

EXTENDED SECOND EDITION

T.A.C.M. VAN DER PUT



Copyright © 2017 by Nova Science Publishers, Inc.

All rights reserved. No part of this book may be reproduced, stored in a retrieval system or transmitted in any form or by any means: electronic, electrostatic, magnetic, tape, mechanical photocopying, recording or otherwise without the written permission of the Publisher.

We have partnered with Copyright Clearance Center to make it easy for you to obtain permissions to reuse content from this publication. Simply navigate to this publication's page on Nova's website and locate the "Get Permission" button below the title description. This button is linked directly to the title's permission page on copyright.com. Alternatively, you can visit copyright.com and search by title, ISBN, or ISSN.

For further questions about using the service on copyright.com, please contact:

Copyright Clearance Center

Phone: +1-(978) 750-8400

Fax: +1-(978) 750-4470

E-mail: info@copyright.com.

NOTICE TO THE READER

The Publisher has taken reasonable care in the preparation of this book, but makes no expressed or implied warranty of any kind and assumes no responsibility for any errors or omissions. No liability is assumed for incidental or consequential damages in connection with or arising out of information contained in this book. The Publisher shall not be liable for any special, consequential, or exemplary damages resulting, in whole or in part, from the readers' use of, or reliance upon, this material. Any parts of this book based on government reports are so indicated and copyright is claimed for those parts to the extent applicable to compilations of such works.

Independent verification should be sought for any data, advice or recommendations contained in this book. In addition, no responsibility is assumed by the publisher for any injury and/or damage to persons or property arising from any methods, products, instructions, ideas or otherwise contained in this publication.

This publication is designed to provide accurate and authoritative information with regard to the subject matter covered herein. It is sold with the clear understanding that the Publisher is not engaged in rendering legal or any other professional services. If legal or any other expert assistance is required, the services of a competent person should be sought. FROM A DECLARATION OF PARTICIPANTS JOINTLY ADOPTED BY A COMMITTEE OF THE AMERICAN BAR ASSOCIATION AND A COMMITTEE OF PUBLISHERS.

Additional color graphics may be available in the e-book version of this book.

Library of Congress Cataloging-in-Publication Data

ISBN: 978-1-53612-245-9

Published by Nova Science Publishers, Inc. † New York

CONTENTS

Preface		xi
Chapter 1	Introduction	1
	<i>1.1 References</i>	<i>6</i>
Chapter 2	The Boundary Value Problem of Fracture Mechanics	7
	<i>2.1. Basic Airy Stress Function</i>	<i>7</i>
	<i>2.2. The Elliptical Flat Crack Solution</i>	<i>13</i>
	<i>2.2.1. The Elliptic Hole in an Infinite Region</i>	<i>14</i>
	<i>2.2.2. The Flat Crack Solution, Explaining the Singularity Approach</i>	<i>16</i>
	<i>2.3. Derivation of the Mixed I- II- Mode Equation</i>	<i>19</i>
	<i>2.4. Remarks Regarding Crack Propagation</i>	<i>29</i>
	<i>2.5. Remarks Regarding the Empirical Confirmation</i>	<i>32</i>
	<i>2.6. References</i>	<i>33</i>

Chapter 3	Softening - Called Yield Drop and Hardening	35
	3.1. <i>Introduction</i>	35
	3.2. <i>Mode I “Softening” Called Yield Drop Explained by Hardening</i>	36
	3.3. <i>Mode I “Softening” - Called Yield Drop Curve</i>	44
	3.4. <i>Fracture Energy as Area under the Yield Drop Curve</i>	49
	3.5. <i>Explanation of Mode I Data and the Empirical Yield Drop Curve</i>	53
	3.6. <i>Crack Merging Mechanism</i>	59
	3.7. <i>Mode II Yield Drop Behavior</i>	63
	3.7.1. <i>Derivation of the Mode II Critical Crack Length for Yield Drop</i>	63
	3.7.2. <i>Mode II Fracture Strength Criterion</i>	65
	3.8. <i>References</i>	71
Chapter 4	Corrections of the Singularity Approach	73
	4.1. <i>Introduction</i>	73
	4.2. <i>The Fictitious Crack Models</i>	75
	4.3. <i>Applied Crack Growth Models</i>	78
	4.4. <i>Continuum Damage Mechanics</i>	80
	4.5. <i>Deformation Kinetics of Fracture Processes</i>	83
	4.6. <i>Derivation of the Power Law</i>	86
	4.7. <i>J-Integral Application</i>	88
	4.8. <i>References</i>	90
Chapter 5	Energy Theory of Fracture	91
	5.1. <i>Introduction</i>	91
	5.2. <i>Critical Distortional Energy as Fracture Criterion</i>	91

	<i>5.3. Revision of the Critical Energy</i>	
	<i> Release Rate Equation</i>	95
	<i>5.4. References</i>	98
Chapter 6	Energy Approach for Fracture of Notched Beams	99
	<i>6.1. Introduction</i>	99
	<i>6.2. Energy Balance</i>	100
	<i>6.3. Experimental Verification</i>	103
	<i>6.4. References</i>	106
Chapter 7	Energy Approach for Fracture of Joints Loaded Perpendicular to the Grain	109
	<i>7.1. Introduction</i>	109
	<i>7.2. Energy Balance</i>	110
	<i>7.3. Experimental Verification</i>	117
	<i>7.4. Design Equation of Eurocode 5</i>	120
	<i>7.4. References</i>	121
Chapter 8	Conclusions Regarding Fracture Mechanics	123
	<i>8.1. Conclusions Overview</i>	123
	<i>8.2. Conclusions Chapter 1 to 7</i>	123
Chapter 9	Weibull Size Effect in Fracture Mechanics of Wide Angle Notched Timber Beams	135
	<i>9.1. Overview</i>	135
	<i>9.2. Introduction</i>	136
	<i>9.3. Size Effect</i>	138
	<i>9.4. Size Effect of Wide Notched Beams</i>	142
	<i>9.5. Conclusions Regarding Size Effect</i>	146
	<i>9.6. References</i>	147

Chapter 10	Small Crack Fracture Mechanics	149
	<i>10.1. Introduction</i>	<i>149</i>
	<i>10.2. Derivation of the Geometric Correction Factor of the Center Notched Specimen</i>	<i>151</i>
	<i>10.3. Small Crack Limit Strength Behavior</i>	<i>155</i>
	<i>10.3.1. Small Crack Limit Dimensions</i>	<i>155</i>
	<i>10.3.2. Small Crack Failure Criterion</i>	<i>157</i>
	<i>10.4. Conclusions Regarding Small Crack Fracture Mechanics</i>	<i>159</i>
	<i>10.5. References</i>	<i>161</i>
Chapter 11	Strength Theory: Exact Failure Criterion for Clear Wood and Timber	163
	<i>11.1. Introduction</i>	<i>163</i>
	<i>11.2. The General Failure Criterion for Wood Polymers</i>	<i>168</i>
	<i>11.2.1. General Properties</i>	<i>168</i>
	<i>11.2.2. Initial Yield Criterion and Derivation of the Hankinson and Extended Hankinson Equations</i>	<i>174</i>
	<i>11.2.3. Transverse Strengths</i>	<i>180</i>
	<i>11.2.4. Longitudinal Strengths</i>	<i>182</i>
	<i>11.2.5. Estimation of the Polynomial Constants by Uniaxial Tests</i>	<i>191</i>
	<i>11.3. Discussion of Applied Failure Criteria</i>	<i>200</i>
	<i>11.3.1. Yield Criterion</i>	<i>200</i>
	<i>11.3.2. Critical Distortional Energy of the Isotropic Matrix</i>	<i>201</i>
	<i>11.3.3. Hankinson Equations</i>	<i>205</i>
	<i>11.3.4. Rankine Criterion</i>	<i>206</i>
	<i>11.3.5. Norris Equations</i>	<i>208</i>
	<i>11.4. Conclusions Regarding the Failure Criterion</i>	<i>212</i>
	<i>11.5. References</i>	<i>219</i>

Chapter 12	Conclusion	223
	<i>Appendix I: Dynamics of Crack Propagation</i>	223
	<i>Appendix II: Derivation of the Orthotropic Critical Distortional Energy Principle</i>	225
	<i>Appendix III: Transformation of Strength Tensors: F_{ij}</i>	231
	Author's Contact Information	235
	Index	237

PREFACE

This second edition provides extensions of derivations and new theory, based on micro crack processes leading to unification with strength theory. Therefore, the derivation of the complete strength theory of wood, also applicable to similar polymers, is added as the last Chapter 11.

The now solely applied singularity approach of fracture mechanics prevents the possibility of exact solutions and thus prevents real and reliable strength predictions. The singularity Airy stress function of the mixed mode I-II boundary value solution predicts uncoupled strength criteria and the existence of infinite strengths. It therefore is necessary to leave the singularity approach and to apply the general applicable limit analysis theory for the special boundary value problem of notches in wood. It then is possible to derive the mixed “mode I – II” - interaction equation, with the relations between the mode I and mode II stress intensities and energy release rates. Because initial fracture starts in the isotropic matrix, it is necessary to solve the isotropic boundary value problem as basis for the total stresses. Therefore, for

combined mode I - II loading, there is always virtual oblique crack extension, in the opening mode, by the same uniaxial ultimate tensile stress (cohesive strength) at the crack boundary. The total stresses then have to satisfy the failure criterion, which is shown to follow the orthotropic critical distortional energy criterion, determining also the critical energy release rate equation.

It is shown that fracture strain softening does not exist and is not a material property as assumed. The derivation of the softening, called yield drop curve is given with the explanation of the measurements. It is also shown that the area under the yield drop curve method, does not always give the right fracture energy.

Further is discussed: the derivation of the power law; the energy method of notched beams and of joints loaded perpendicular to the grain; the Weibull size effect in fracture mechanics, and the necessary rejection of the applied crack growth models and fictitious crack models.

Ultimate strength theory is discussed separately in Chapter 11, as a separate subject, although it is shown in the previous chapters to be necessary to explain and derive all laws of fracture mechanics.

Discussed are the extension of the derivation and explanation of:

- the failure criterion of wood (with hardening) and the meaning of the constants;
- the necessary data fitting conditions by the derived relations between the constants;
- the orthotropic extension of the critical distortional energy principle of yield;
- the generalized and extended Hankinson equations; the Norris- Tsai Wu- Hoffmann- Coulomb- and Wu fracture criteria.

- the extended Tresca criterion for wood-matrix failure at final yield;
- the determination of all constants of the failure criterion from simple uniaxial, oblique-grain compression and tension tests.
- the hypothesis of the replacement of the normality rule by the intrinsic minimum work for dissipation, with hardening state constants, for quasi orthotropic materials like wood.

Chapter 1

INTRODUCTION

Limit analysis is a technically exact approach for reliable upper- and lower bound estimations of the ultimate load. Structural design and strength calculations therefore have to be based on limit analysis, at least on the lower bound equilibrium method by choosing an equilibrium stress system, covering the whole body, which suffices boundary conditions and nowhere surmounts the failure or yield criterion. The high value of G_c , the critical energy release rate, with respect to the surface energy, shows, that there is sufficient plasticity for the linear elastic- full-plastic approach of limit analysis. Because the isotropic wood-matrix is determining the initial fracture, linear elastic fracture mechanics (LEFM) applies perfectly for the initial fracture of wood. Plastic deformation of the polymeric reinforcement occurs at the creases at the crack tip, called the fracture process zone. This zone is also the location of micro crack and small crack multiplication and propagation. Thus, wood shows local small scale yielding at the crack tip. The first yield occurs at the highest elastic stress at the crack boundary, which is also the location of the highest ultimate

strain after yield and thus is the location of the crack extension. This zone of confined plasticity can also be replaced by the equivalent linear elastic ultimate stress value (similar to the applied linear elastic bending strength diagram to represent full plastic bending compression flow). The difference is an internal equilibrium system, which, as with all initial stresses and deformations, does not affect the collapse load, according to limit analysis theorems, based on virtual displacements behavior. This explains why, outer regarding the yield stress at the elastic plastic crack boundary, also LEFM may apply up to failure by the empirical ultimate tensile stress at the crack boundary (as replacement of the confined plasticity solution).

The so called non-linear fracture mechanics approach, which only applies for singularity solutions, e.g., as correction of infinite stresses, is superfluous, because it is covered by limit analysis (see Chapter 4). The always applied singularity approach is not exact, because e.g., the Airy stress function solution wrongly predicts failure when whether mode I and/or mode II (without interaction) becomes ultimate at mixed mode fracture. It is therefore necessary to reject the singularity solution.

In Chapter 2, the derivation of the exact, non-singular, mixed mode failure criterion is given. Transformation to polar coordinates, shows that the singularity equations follow directly from the exact non-singular solution and should be corrected accordingly. In [1, 2], the given equation: $\sigma_{ij} = F_{ij}(\theta) \cdot K_I / \sqrt{2\pi r}$ applies for a stress σ perpendicular to crack with a length of $2c$. For a collinear crack extension: $\theta=0$ and $F_{ij}(0)=1$ and $\sigma_{22} = K_I / \sqrt{2\pi r}$, where K_I is an arbitrary shortcut for “ $\sigma\sqrt{\pi c}$,” which follows from the exact solution, given in § 2.2.2, (see also: [3, 4]). This is not a parameter following from the dimensional analysis as stated in [2], page 78, and K_I is not the limit of

$\sigma_y \sqrt{2\pi r}$, for crack boundary $r \rightarrow 0$ and strength $\sigma_y \rightarrow \infty$. Both r and σ_y are constant. For micro crack extension, (see paragraph 10.2) it is possible for a freely chosen singularity solution of the Airy stress function, containing points where $\sigma \rightarrow \infty$, when $c \rightarrow 0$, with K_I as limit of $\sigma \sqrt{\pi c}$. This is the only possible singularity, which is not a necessary one, but freely chosen as a possible approximate solution.

It is shown that the area under the load-displacement yield drop curve gives the total external work on the test specimen and not the fracture energy as is wrongly assumed. The fracture energy follows from half this area which is equal to the critical strain energy release rate at initial crack extension. For wood this is correctly applied for mode II (see Figure 3.4.3). For mode I however, as for other materials, the total area is incorrectly regarded as fracture energy, which is a factor 2 too high. The finite element method regards the area of the loading-unloading hysteresis loop, Area(OABO) in Figure 3.4.3, as fracture energy, which indeed, correctly is equal to half the area under the load displacement curve ($0.5 \cdot \text{Area}(ABCD)$).

The derivations of Chapter 6 and 7 lead to an adaption of the energy approach for the fracture of beams with square end notches and of joints loaded perpendicular to the grain, providing a simple design method. It is further shown that all corrective, so called, non-linear fracture mechanics models, such as the Dugdale model, the fictitious crack model and the crack growth models, are not exact and thus not reliable.

It is shown that failure according to the modes I and II is not simply related to the dissipated stress type. The so called mode I may occur by dissipation of elastic shear stress energy only and the so called mode II, by dissipation of bending stress energy only. Determining for the strength is the stress combination at the

fracture site (as follows also from the crack closure technique). Therefore, these local stresses should satisfy the derived mixed mode failure criterion, which is shown to follow the critical distortional energy criterion for initial crack extension and follows the Coulomb criterion after “hardening.” It is shown that strain softening does not exist (as assumed by cohesive zone models) and thus is not a material property. This “softening”- called yield drop, is an elastic unloading process. At loading, in a constant strain rate test, the unloading rate due to the kinetic damage process [5], is much higher than the loading rate, causing unloading of the specimen. Increasing the loading rate may change this apparent softening behavior into apparent “hardening.” “Softening”-called yield drop behavior therefore is not possible in a constant loading rate test and not in a dead load to failure test, which ends in sudden failure (at the speed of sound). This yield drop stress, due to crack extension, is a nominal stress based on unnotched specimen dimensions, thus is the mean actual stress outside the fractured area, while the actual fracture stress, in the fracture plane (at the ligament), increases and remains ultimate. Apparent and real softening, (e.g., thermal softening), are fully explained by molecular deformation kinetics processes [5], and here, by limit analysis without assuming the impossible negative dissipation, decreasing flow stress, and negative modulus of elasticity of the fictitious crack models. The derivation of the yield drop curve of the “Griffith strength” (which is based on the ultimate actual stress in the fracture plane) is given in § 3.3. It appears that small crack extension and crack merging in the high loaded intact clear wood part of the fracture plane explains yield drop and fracture in general, which should replace the Griffith law for overcritical long initial crack lengths. In that case the Griffith law only gives the crack closure energy which is then lower than the crack formation energy. The Griffith law, as extremum principle, applies for the

critical crack length at the top of the initial loading curve. But also for the main part of unloading at yield drop, this principle applies for the then current crack lengths. The Griffith stress is a nominal stress, based on the intact, uncracked, not ultimate, but elastic loaded section, and thus is the actual stress outside the fracture plane, and not the actual ultimate fracture stress on the intact material in the fracture plane.

It is shown in § 2.3, that the oblique virtual crack extension in the isotropic matrix, by any stress combination, follows the Coulomb- equation (also called Wu-equation for wood), which implies that failure always occurs by the same actual ultimate uniaxial tensile stress in the matrix, at the crack boundary near the crack tip. This uniaxial tensile failure, as a measure of the cohesion strength, leads to the mixed mode Coulomb-equation, eq.(2.3.10), as exact failure criterion. This applies as initial crack extension, for the isotropic Airy stress function of the isotropic matrix stresses, and for the orthotropic total stresses after multiplication with the derived stiffness factors. Only for mode I loading is crack extension collinear. For shear, mode II loading, and for combined mode I and II loading, initial, virtual, oblique crack extension is determining providing the lower bound solution, as well for the isotropic matrix, as for the total orthotropic case.

Following, it is further discussed: the derivation of the power law; the energy method of notched beams and of joints loaded perpendicular to the grain; the explanation of the Weibull size effect in fracture mechanics, and the necessary rejection of the applied crack growth models and fictitious crack models.

1.1 REFERENCES

- [1] RILEM state of the art report on fracture mechanics, *Espoo*, 1991.
- [2] I. Smith, E. Landis, M. Gong, Fracture and Fatigue in Wood, *J. Wiley & Sons*, 2003.
- [3] van der Put, T.A.C.M., *A New Fracture Mechanics Theory of Wood*, Nova Science Publishers, New York, 2011.
- [4] van der Put, T.A.C.M. *Adv Mech Eng Res*, Vol. 2. Chap. 1: Fracture Mechanics of Wood and Wood like Reinforced Polymers, Nova Science Publishers, Inc. New York, 2011.
- [5] van der Put, T.A.C.M., Deformation and damage processes in wood, Delft Univ. press, 1989.

(See files, regarding [3 to 5] on: dwsf.nl, or: iew.s.nl or: Researchgate.net).

Chapter 2

THE BOUNDARY VALUE PROBLEM OF FRACTURE MECHANICS

2.1. BASIC AIRY STRESS FUNCTION

For the solution of the crack-boundary value problem of notches in wood, the orthotropic Airy stress function is normally based on evenly distributed reinforcement which acts as a continuum, satisfying the equilibrium, compatibility and strength conditions. This behaviour is only possible by the interaction of reinforcements through the matrix. Thus, the equilibrium conditions and strength criterion of the matrix, as determining element, have to be satisfied. This is also necessary because the isotropic matrix fails earlier than the reinforcement, and determines initial “yield” behavior. It is therefore necessary to solve the Airy stress function for the stresses in the isotropic matrix and then to derive the total (orthotropic) stresses from this solution. This is not applied in other approaches mentioned e.g., in Chapter 2, of [1]. In fact none of the usually applied singularity

solutions is exact, leading not to the exact mixed mode failure criterion (i.e. the Coulomb- or Wu- equation, eq. (2.5.10)) and thus, should in fact be rejected as a possible solution.

In total stresses, the stress-strain relations for the two-dimensional flat crack problem are:

$$\begin{aligned}\varepsilon_x &= c_{11}\sigma_x + c_{12}\sigma_y; \quad \varepsilon_y = c_{12}\sigma_x + c_{22}\sigma_y; \\ \gamma_{xy} &= c_{66}\tau_{xy}.\end{aligned}\tag{2.1.1}$$

This can be written:

$$\begin{aligned}\varepsilon_x &= \sigma_x / E_x - \nu_{21}\sigma_y / E_y; \\ \varepsilon_y &= -\nu_{21}\sigma_x / E_y + \sigma_y / E_y; \\ \gamma_{xy} &= \tau_{xy} / G_{xy}\end{aligned}\tag{2.1.2}$$

The Airy function follows from:

$$\sigma_x = \frac{\partial^2 U}{\partial y^2}; \quad \sigma_y = \frac{\partial^2 U}{\partial x^2}; \quad \tau_{xy} = -\frac{\partial^2 U}{\partial x \partial y},\tag{2.1.3}$$

satisfying the equilibrium equations:

$$\frac{\partial \sigma_x}{\partial x} + \frac{\partial \tau}{\partial y} = 0 \quad \text{and} \quad \frac{\partial \tau}{\partial x} + \frac{\partial \sigma_y}{\partial y} = 0\tag{2.1.4}$$

Substitutions of eq. (2.1.1), using eq. (2.1.3):

$$\varepsilon_x = c_{11} \frac{\partial^2 U}{\partial y^2} + c_{12} \frac{\partial^2 U}{\partial x^2}, \text{ etc., in the compatibility condition:}$$

$$\frac{\partial^2 \varepsilon_x}{\partial y^2} + \frac{\partial^2 \varepsilon_y}{\partial x^2} = \frac{\partial^2 \gamma_{xy}}{\partial x \partial y}, \quad (2.1.5)$$

gives:

$$c_{22} \frac{\partial^4 U}{\partial x^4} + (c_{66} + 2c_{12}) \frac{\partial^4 U}{\partial x^2 \partial y^2} + c_{11} \frac{\partial^4 U}{\partial y^4} = 0 \quad (2.1.6)$$

The general solution of eq. (2.1.6) is: $U = \sum_i^4 F_i(x + \mu y)$,

where μ is a root of the characteristic equation: $c_{11}\mu^4 + (c_{66} + 2c_{12})\mu^2 + c_{22} = 0$, giving:

$$\mu^2 = \frac{c_{66} + 2c_{12}}{2c_{11}} \cdot \left(-1 \pm \sqrt{1 - \frac{4c_{22}c_{11}}{(c_{66} + 2c_{12})^2}} \right), \quad (2.1.7)$$

thus giving 4 imaginary roots. Introducing the complex variables z_1 and z_2 , defined by: $z_1 = x + \mu_1 y \equiv x' + iy'$ and $z_2 = x + \mu_2 y \equiv x'' + iy''$, the solution of eq.2.1.6 assumes the form:

$$U = F_1(z_1) + F_2(z_2) + \bar{F}_1(z_1) + \bar{F}_2(z_2), \quad (2.1.8)$$

where the bars denote complex conjugate values. The stresses, displacements and boundary conditions now can be written in the general form of the derivatives of these functions. There are standard methods to solve some boundary value problems (e.g., by Fourier transforms of equations of the boundary conditions) but in

principle, functions have to be guessed or chosen, or expanded as polynomials, or Fourier series or power series in: z or z^{-1} , etc. The exact non-singular solution is given in § 2.2.1.

As alternative, eq. (2.1.6) also can be given as:

$$\left(\frac{\partial^2}{\partial x^2} + \alpha_1 \frac{\partial^2}{\partial y^2} \right) \left(\frac{\partial^2}{\partial x^2} + \alpha_2 \frac{\partial^2}{\partial y^2} \right) U = 0 \quad (2.1.9)$$

where $\alpha_1 \alpha_2 = c_{11} / c_{22}$ and $\alpha_1 + \alpha_2 = (c_{66} + 2c_{12}) / c_{22}$.

Introducing 3 sets of polar coordinates for this case, $x + iy = re^{i\theta}$, $x + iy / \sqrt{\alpha_1} = re^{i\theta_1}$, $x + iy / \sqrt{\alpha_2} = re^{i\theta_2}$, eq.(2.1.9) has e.g., elementary solutions as: $r_1^{\pm m} \cos(m\theta_1)$, $r_1^{\pm m} \sin(m\theta_1)$, $r_2^{\pm m} \cos(m\theta_2)$, $r_2^{\pm m} \sin(m\theta_2)$, and solutions may be chosen in the form of series of these types. For wood material, the elementary solution in $r^{\pm m}$ are e.g., chosen in [2], which in principle leads to:

$$\{\sigma_r, \sigma_\theta, \sigma_{r\theta}\} = \frac{K_A}{(2\pi r)^s} \{f_1(\theta), f_2(\theta), f_3(\theta)\} \quad (2.1.10)$$

and

$$\{\sigma_r, \sigma_\theta, \sigma_{r\theta}\} = \frac{K_B}{(2\pi r)^q} \{f_1(\theta), f_2(\theta), f_3(\theta)\} \quad (2.1.11)$$

with $q \leq s$. The chosen solution is such that it applies in the vicinity of the notch root as stress singularity at $r = 0$. Because for $q < s$, and r small, the stresses of eq. (2.1.10) are always higher than those of eq. (2.1.11), the solution, eq. (2.1.11), should be rejected based on the boundary conditions at failure (the highest

lower bound solution is also most probable). It therefore is not right to regard 2 singular stress fields, only eq. (2.1.10) applies, as an approximate solution, only applicable for the strength of the uniaxial stress in the main material direction.

Because wood is a reinforced material where the reinforcement interacts through the matrix and also the primary crack formation is in the matrix, the failure condition should be based on the strength of the matrix and first the Airy stress function of the matrix-stresses should be solved.

As orthotropic solution, eq. (2.1.10), of U of eq. (2.1.9), always show only powers smaller than $s = 0.5$ (the value of the common isotropic singularity approach). For instance, one finite element solution did show $s = 0.45$ near a rectangular notch, while another investigation of the same notch type did show values of;

$s = 0.45$ for σ and $s = 0.10$ for τ , while by the finite difference method, powers were found of $s = 0.437$ for the same rectangular notch of 90° and $s \approx 0.34$ for much wider notch angles. This shows that no compatibility, at initial failure of the (linearly lower) stresses and strains in the isotropic wood matrix are possible. For wood, the nearly always applied solution, with (isotropic) $s = 0.5$, represents flow of the matrix while there is still an elastic contribution of reinforcement, thus following in principle, the same starting point as the in § 2.3 given derivation of the non-singularity approach.

Wood acts as a reinforced material because lignin is isotropic and hemicellulose and cellulose are transversely isotropic, which means that only one stiffness factor in the main direction has a n -fold higher stiffness in proportion to the higher stiffness of the reinforcement with respect to the matrix. Thus, wood material can be treated to contain a shear-reinforcement and a tensile reinforcement in the main direction, and for equilibrium of the matrix stresses then applies:

$$\frac{\sigma_x}{n_1} = \frac{\partial^2 U}{\partial y^2}; \quad \sigma_y = \frac{\partial^2 U}{\partial x^2}; \quad \tau_{xy} = -\frac{\partial^2 U}{\partial x \partial y}, \quad (2.1.12)$$

Instead of using the matrix stresses and the matrix stiffness, also the orthotropic n-fold higher total stresses and n-fold higher stiffness can be used to give the same compatibility condition (thus the same condition for matrix and reinforcement). Inserting eq. (2.1.5) in the compatibility equation, the total stresses, expressed in the isotropic Airy stress function U of the matrix stresses, gives:

$$c_{22} \frac{\partial^4 U}{\partial x^4} + (n_6 c_{66} + (1+n_1)c_{12}) \frac{\partial^4 U}{\partial x^2 \partial y^2} + n_1 c_{11} \frac{\partial^4 U}{\partial y^4} = 0 \quad (2.1.13)$$

For the isotropic matrix: $n_1 c_{11} / c_{22} = 1$ and $(n_6 c_{66} + (1+n_1)c_{12}) / c_{22} = 2$ giving:

$$\frac{\partial^4 U}{\partial x^4} + 2 \frac{\partial^4 U}{\partial x^2 \partial y^2} + \frac{\partial^4 U}{\partial y^4} = \nabla^2 (\nabla^2 U) = 0 \quad (2.1.14)$$

Thus:

$$n_1 = \frac{c_{22}}{c_{11}} = \frac{E_x}{E_y}; \quad n_6 = \left(2 - \frac{c_{12}}{c_{22}} - \frac{c_{12}}{c_{11}} \right) \cdot \frac{c_{22}}{c_{66}} = (2 + \nu_{21} + \nu_{12}) \cdot \frac{G_{xy}}{E_y} \quad (2.1.15)$$

This new orthotropic-isotropic transformation of the Airy stress function and the calculation method based on the stresses of the matrix, are now being used. It now is possible to use the isotropic solutions of U to find the matrix stresses (which should

not surmount the matrix strength) and to multiply these matrix stresses with the n -factors of eq. (2.1.15) for the applied orthotropic stresses of initial flow of the regarded loading case. This is applied in § 2.2 by solving first the matrix stresses. This therefore is equivalent to the orthotropic solution of the singularity approach, based on a modified isotropic Airy stress function and an isotropic singularity $r^{-0.5}$, which now is always applied.

2.2. THE ELLIPTICAL FLAT CRACK SOLUTION

As shown above, the applied singularity approach with $s = 0.5$, only applies for uniaxial loading and thus prevents the solution of mixed mode loading cases and prevents the derivation of a right failure criterion. Instead of such a criterion, critical values are assumed of the strain energy density, the J-integral, or the maximal principal stress, or a non local stress function, all at a distance away from the crack tip, thus away from the fracture site. A real failure criterion can only be based on the actual ultimate stress in the material which occurs at the crack-boundary. A real physical crack form is the flat elliptical crack, which is the first expanded of any form of the crack boundary, and because the crack is flat, the higher expanded terms have a negligible, in the limit a zero, contribution. When “flow” occurs around the crack tip, the ultimate strain condition (or ultimate equivalent stress, see Chapter 1), at the crack-boundary determines failure and the direction of the crack extension. The elastic-plastic boundary (of limit analysis) then acts as an enlarged crack tip boundary. Thus the limit analysis approach incorporates linear elastic -, as well as non-linear fracture mechanics. There is no distinction between the two.

2.2.1. The Elliptic Hole in an Infinite Region

The classical way of analyzing the elliptic crack problem is to use complex variables and elliptic coordinates. The Airy stress function can be expressed in terms of two analytic functions [3], of the complex variable $z (= x + iy)$ and the transformation to elliptic coordinates in Figure 2.1, gives:

$$\begin{aligned} z = x + iy &= c \cdot \cosh(\zeta + i\eta) \text{ or: } x = c \cdot \cosh(\zeta) \cdot \cos(\eta); \\ y &= c \cdot \sinh(\zeta) \cdot \sin(\eta). \end{aligned} \quad (2.2.1)$$

For an elliptic hole, $\zeta = \xi_0$, in an infinite region with uniaxial stress p at infinity in a direction inclined at β to the major axis Ox of the ellipse, the Airy stress function U , satisfying:

$$\nabla^2 (\nabla^2 U) = 0, \quad (2.2.2)$$

and satisfying the conditions at infinity and at the surface $\zeta = \xi_0$, showing no discontinuity of displacement, thus is the solution giving:

$$U = R\{z\phi(z) + \chi(z)\}, \text{ with [3]:} \quad (2.2.3)$$

$$4\phi(z) = p \cdot c \cdot \exp(2\xi_0) \cdot \cos(2\beta) \cdot \cosh(\zeta) + p \cdot c \cdot (1 - \exp(2\xi_0 + 2i\beta)) \cdot \sinh(\zeta) \quad (2.2.4)$$

$$4\chi'(z) = -p \cdot c \cdot [\cosh(2\xi_0) - \cos(2\beta) + \exp(2\xi_0) \cdot \sinh(2\{\zeta - \xi_0 - i\beta\})] \cdot \operatorname{cosech}(\zeta) \quad (2.2.5)$$

where $\zeta = \xi + i\eta$. For the stresses at the boundary, due to a stress p at an angle β to the crack, is:

$$\begin{aligned} \sigma_\eta - \sigma_\xi + 2i\tau_{\xi\eta} &= 2[\bar{z}\varphi''(z) + \chi''(z)]e^{i\delta} \text{ and:} \\ \sigma_\xi + \sigma_\eta &= 2[\varphi'(z) + \overline{\varphi'(z)}] = 4R\{\varphi'(z)\} \end{aligned} \quad (2.2.6)$$

and the tangential stress σ_t at the surface $\xi = \xi_0$ is simply known from the last equation because here $\sigma_\xi = 0$. Thus: determining for the strength, according to strength theory, is the ultimate tangential uniaxial ultimate stress σ_t at the crack surface $\xi = \xi_0$ due to a stress p at an angle β (of Figure 2.3.1) to the crack. Thus:

$$\sigma_t = 2[\varphi'(\xi_0 + i\eta) + \varphi'(\xi_0 - i\eta)] = \frac{p(\sinh(2\xi_0) + \cos(2\beta) - \exp(2\xi_0) \cdot \cos(2(\beta - \eta)))}{\cosh(2\xi_0) - \cos(2\eta)} \quad (2.2.7)$$

while $\chi'(z)$ has to vanish at: $\xi = \xi_0$.

Eq. (2.2.7) can be extended for two mutual perpendicular principal stresses p_1 and p_2 (see Figure 2.3.1) by a simple addition leading to eq. (2.3.1) below.

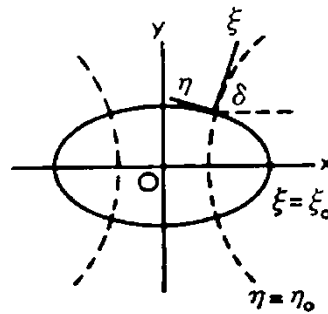


Figure 2.1. Elliptic hole and coordinates.

2.2.2. The Flat Crack Solution, Explaining the Singularity Approach

The stresses in the wood-matrix of the limit case of the elliptical notch with ξ_0 approaching zero appear to be comparable with the results of the mathematical flat crack solution of the singularity approach. To derive these singularity equations (as special case of the general exact solution), new coordinates X, Y with the origin in the focus of the ellipse are necessary (see Figure 2.2).

Thus:

$$X = x - c = c(\xi^2 - \eta^2)/2, Y = y = c\xi\eta \quad (2.2.8)$$

or in polar coordinates:

$$r = (X^2 + Y^2)^{0.5}, X = r\cos(\theta), Y = r\sin(\theta) \quad (2.2.9)$$

and from eq.(2.2.8):

$$\xi^2 + \eta^2 = 2(X^2 + Y^2)^{0.5} / c = 2r / c \quad (2.2.10)$$

$$\begin{aligned} \xi &= \sqrt{2r/c} \cdot \cos(\theta/2), \eta = \sqrt{2r/c} \cdot \sin(\theta/2), \\ \eta / \xi &= \tan(\theta/2) = \tan(\delta) \end{aligned} \quad (2.2.11)$$

Using these relations in the stresses $\sigma_\eta, \sigma_\xi, \tau_{\xi\eta}$ of § 2.2.1 and applying the singularity, $\xi_0 = 0$ in the general solution of the elliptic Airy stress function, then the tangential stress σ_θ along a

crack boundary r_0 , due to a stress p at infinity at an angle β with the notch is:

$$\left(8r/cp^2\right)^{0.5} \sigma_{\theta} = -3\sin(\theta/2)\cos^2(\theta/2)\sin(2\beta) + 2\cos^3(\theta/2)\sin^2(\beta) \quad (2.2.12)$$

For a small value of r , as applies for any flat crack with $\sqrt{r} \ll \sqrt{2c}$, so that all terms containing not the factor $r^{-0.5}$ are negligible and omitted. The other stresses then are:

$$\left(8r/cp^2\right)^{0.5} \sigma_r = \sin(\theta/2)(1-3\sin^2(\theta/2))\sin(2\beta) + 2\cos(\theta/2)(1+\sin^2(\theta/2))\sin^2(\beta) \quad (2.2.13)$$

$$\left(8r/cp^2\right)^{0.5} \tau_{r\theta} = \cos(\theta/2)(3\cos^2(\theta/2)-2)\sin(2\beta) + 2\cos^2(\theta/2)\sin(\theta/2)\sin^2(\beta) \quad (2.2.14)$$

For wood, using the always applied singularity method, the flat crack in the grain direction is supposed to propagate in that direction (collinear). Thus $\theta = 0$, and eq. (2.2.12) becomes [4]:

$$\left(8r/cp^2\right)^{0.5} \sigma_{\theta} = 2\sin^2(\beta) \text{ and is: } \sigma_r = \sigma_{\theta} \text{ and:}$$

$$\tau_{r\theta} = \sigma_{\theta} \cotg(\beta). \quad (2.2.15)$$

Mode I failure $\sigma_{\theta} = \sigma_r$ occurs when $\beta = \pi/2$. Thus when:
 $\tau_{r\theta} = 0$ and:

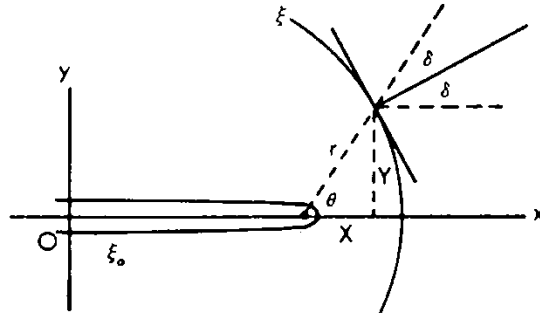


Figure 2.2. Confocal coordinates.

$$p = \sigma_t \sqrt{(2r/c)} \quad (2.2.16)$$

For pure shear loading, and thus for superposition of $p_1 = S$ at $\beta = \pi/4$ and $p_2 = -S$ at $\beta = 3\pi/4$ in eq. (2.2.12) and in the other equations of the solution, crack extension $\theta = 0$:

$$(2r/cS^2)^{0.5} \tau_{r\theta} = (\cos(\theta/2) \cdot (3\cos^2(\theta/2) - 2)) \Big|_{\theta=0} = 1 \quad (2.2.17)$$

or:

$$S = \tau_{r\theta} \sqrt{(2r/c)} \quad (2.2.18)$$

Now with $\sigma_r = \sigma_\theta = 0$, leading to an ultimate shear failure criterion (without interaction with normal stresses) although real shear failure is plastic and a real collinear pure mode II fracture does not exist. Eqs. (2.2.16) and (2.2.18) thus are in fact maximum stress conditions for the strengths in the main planes. Fracture is predicted to occur when the tensile strength is reached perpendicular to the grain and / or when the "shear strength" in this

plane is reached. Thus: $K_I \leq K_{Ic}$ and/or $K_{II} \leq K_{IIc}$ for all stress states. This also is predicted for the n-fold higher quasi orthotropic stresses and is empirically shown to be incorrect (see eq. (2.2.16) and eq. (2.2.18) in Figure 2.3.4). This also is shown by the theory equation, eq. (2.3.10) to be incorrect because according to eq. (2.3.10), failure is always by the actual uniaxial maximal tangential tensile stress along the crack tip boundary, causing oblique crack extension (see Figure 2.3.1, 2.3.2, 2.4.1, 2.4.2). Thus the always applied singularity approach gives no correct results for mixed mode failure. The right failure condition for combined stresses, eq. (2.3.10), is derived below in § 2.3.

The singularity approach regards $r \rightarrow 0$, which implies that the strength $\sigma_t \rightarrow \infty$, which is not possible. The strength is finite and also the radius $r = r_0$ of the equivalent crack boundary (thus of the fracture process zone) is shown in § 2.3 to be constant for a constant stress intensity factor. Thus for a real singularity solution, the applied stress becomes high when the crack becomes small. This is derived in § 10.2.

2.3. DERIVATION OF THE MIXED I- II- MODE EQUATION

A general failure criterion [5] follows from the determining equivalent ultimate stress, mentioned in Chapter 1, which occurs at the crack boundary, near the crack tip.

By an extension of eq. (2.2.7) (by superposition) to $p_1 = \sigma_1$ inclined at an angle $\pi/2 + \beta$ to the Ox-axis and $p_2 = \sigma_2$ inclined at an angle β , (see Figure 2.3.1), eq. (2.2.7) turns to:

$$\sigma_t = \frac{2\sigma_y \sinh(2\xi_0) + 2\tau_{xy} [(1 + \sinh(2\xi_0)) \cdot \cot(2\beta) - \exp(2\xi_0) \cdot \cos(2(\beta - \eta)) \operatorname{cosec}(2\beta)]}{\cosh(2\xi_0) - \cos(2\eta)}, \quad (2.3.1)$$

where the stresses are given in notch coordinates with the x-axis along the crack. For small values of ξ_0 and η (thus for flat notches), this equation becomes:

$$\sigma_t = \frac{2(\xi_0 \sigma_y - \eta \tau_{xy})}{\xi_0^2 + \eta^2} \quad (2.3.2)$$

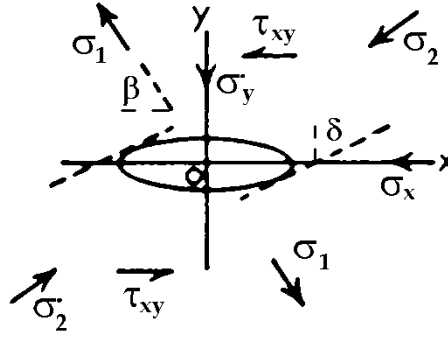


Figure 2.3.1. Stresses in the notch plane Ox.

The maximum (critical) value of the tangential tensile stress σ_t , for initial failure, depending on location η , is found by: $d\sigma_t / d\eta = 0$, giving the critical value of η :

$$-2\tau_{xy} / (\xi_0^2 + \eta^2) - (2(\xi_0 \sigma_y - \eta \tau_{xy}) \cdot 2\eta) / (\xi_0^2 + \eta^2)^2 = 0,$$

or:

$$-\tau_{xy}(\xi_0^2 + \eta^2) = 2\eta(\xi_0\sigma_y - \eta\tau_{xy}) = \eta\sigma_t(\xi_0^2 + \eta^2) \quad (2.3.3)$$

where the second equals sign is due to the substitution of eq. (2.3.2).

From the first and last term, it follows that:

$$\eta\sigma_t = -\tau_{xy} \quad (2.3.4)$$

and from the first 2 terms:

$$\eta / \xi_0 = (\sigma_y \pm \sqrt{\sigma_y^2 + \tau_{xy}^2}) / \tau_{xy} \quad (2.3.5)$$

The elimination of η , from eqs. (2.3.4) and (2.26) or from eq. (2.3.5) and eq. (2.3.2) gives:

$$\xi_0\sigma_t = \sigma_y \pm \sqrt{\sigma_y^2 + \tau_{xy}^2} \quad \text{and this can be written:}$$

$$1 = \frac{\sigma_y}{\xi_0\sigma_t/2} + \frac{\tau_{xy}^2}{\xi_0^2\sigma_t^2} = \frac{\sigma_y}{f_t} + \frac{\tau_{xy}^2}{f_v^2} \quad (2.3.6)$$

This is the ultimate stress equation of strength theory with strengths: $f_t = \xi_0\sigma_t/2$ and $f_v = \xi_0\sigma_t$, where ξ_0 depends on the structural form of the short notch. When the first expanded term of the notch form expansion, is spherical instead of elliptical as e.g., for a dislocation, then: $2r_0 \approx c$, or: $\xi_0 \approx 1$. Then, because there is a shear displacement of the dislocation, σ_t is the ultimate shear stress.

Transformation from elliptic to polar coordinates by eq. (2.2.11): $\xi_0 = \sqrt{2r_0/c} \cdot \cos(\delta)$ shows that fracture mechanics only apply when r_0 and σ_t , are constant and $c \gg 2r_0$. Thus σ_t is the equivalent cohesion strength and r_0 is the invariant radius of the fracture process zone near the crack tip of a flat crack.

The flat crack solution then leads to:

$$1 = \frac{\sigma_y \sqrt{\pi c}}{\sigma_t \sqrt{\pi r_0 / 2} \cdot \cos(\delta)} + \frac{(\tau_{xy} \sqrt{\pi c})^2}{(\sigma_t \sqrt{2\pi r_0} \cdot \cos(\delta))^2} = \frac{K_I}{K_{Ic} \cos(\delta)} + \frac{K_{II}^2}{(K_{IIc} \cos(\delta))^2} \quad (2.3.7)$$

showing that for combined (mixed mode) fracture, when $\delta \neq 0$, the apparent stress intensity factors of Irwin, $K_{Ic} \cos(\delta)$, $K_{IIc} \cos(\delta)$ are not constant. The value of δ is stress dependent and depends on the combined loading according to:

$$\operatorname{tg}(\delta) = \frac{\sigma_y}{\tau_{xy}} \pm \sqrt{\frac{\sigma_y^2}{\tau_{xy}^2} + 1} \quad (2.3.8)$$

for the stresses in the isotropic matrix. For pure mode I: $\delta = 0$, $\tau_{xy} = 0$, is K_{Ic} equal to the Irwin value. For pure shear loading of the isotropic matrix, $\sigma_y = 0$ and $\delta = 45^\circ$, and the stress intensity is lower than the Irwin value, thus:

$$K_{IIc} \cos(\pi / 4) = K_{IIc} / \sqrt{2} = 0.71 \cdot K_{IIc} . \quad (2.3.9)$$

This is measured in [6] according to Figure 2.3.2, for a relatively small initial crack length, in Agathis lumber, (density $480 \pm 10 \text{ kg/m}^3$; 12% m.c. 20°C). The lumber had no defects such as knots or grain distortions so that the specimens consisted of clear wood.

Thus, according to the exact lower bound solution of limit analysis, the combined mode I – II and pure mode II fractures, a matter of virtual oblique crack extension by reaching the maximal equivalent uniaxial tensile stress (at the maximal strain) along the crack tip boundary. The oblique angle δ of eq. (2.3.8) is indicated in Figure 2.3.3. This oblique crack extension criterion applies generally (not only for clear wood), as lower bound criterion of limit analysis.

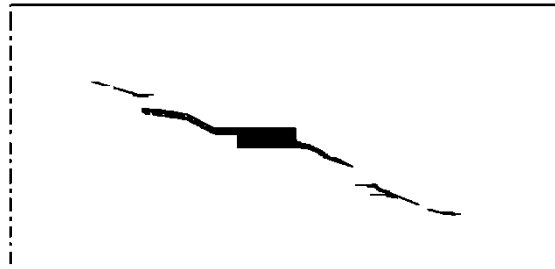


Figure 2.3.2. Fracture by pure shear loading by oblique crack extension at the uniaxial ultimate tensile stress (opening mode) near the crack tip in the asymmetric four point bending test with small center-slit. (Sketch after photo of [6]).

For timber with many defects however, an approximate collinear crack extension, with small $\delta \approx 0$ occurs, due to a small crack extension towards the macro crack tip and certainly due to previous razor blade splitting (activating directly the reinforcement), causing small crack extension according to Figure 2.4.2, so that eq. (2.3.7) becomes the Coulomb equation:.

$$\frac{K_I}{K_{Ic}} + \frac{(K_{II})^2}{(K_{IIc})^2} = 1 \quad (2.3.10)$$

The fact that $K_{Ic} = \sigma_y \sqrt{\pi c_c} = \sigma_t \sqrt{\pi r_0 / 2}$ is constant as a necessary prerequisite for the existence of fracture mechanics with constant K_{Ic} , indicates that r_0 is the radius of the fracture process zone (which represents a kind of structural crazing), which size is invariant. Thus micro crack behavior within the fracture process zone determines macro crack extension. This is discussed in § 3.6 and Chapter 10.

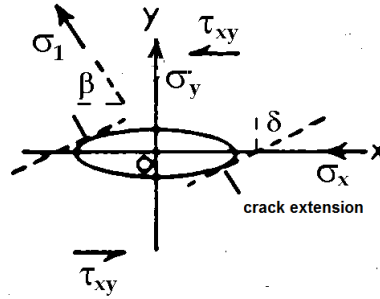


Figure 2.3.3. Uniaxial tensile failure at any mixed I-II mode fracture.

The derivation of eq. (2.3.7) also gives the relation between K_{Ic} and K_{IIc} . For the stresses in the isotropic matrix this is:

$$K_{IIc} / K_{Ic} = (\sigma_t \sqrt{2\pi r_0}) / (\sigma_t \sqrt{2\pi r_0} / 2) = 2 \quad (2.3.11)$$

The matrix stresses are also determining for Balsa wood, which is highly orthotropic, but is light, and thus has a low reinforcement content and shows total failure soon after matrix failure and thus shows at failure, the isotropic ratio of

$K_{IIc} / K_{Ic} \approx 2$ of the isotropic matrix material, as verified by the measurements of Wu on Balsa by: $K_{IIc} \approx 140 \text{ psi} \cdot \text{in}^{0.5}$ and $K_{Ic} \approx 60 \text{ psi} \cdot \text{in}^{0.5}$ (K_{IIc} is higher than 2×60 due to hardening at compression and K_{Ic} is lower than 70 due to early instability of the test rig in a tensile test, at the initial tensile strength).

Eq. (2.3.10) is generally applicable also when σ_y is a compression stress as follows from the measurements of Figure 2.3.4. When the compression is high enough to close the small notches, ($\sigma_{y,cl} \approx 2G_{xy}\xi_0$), τ_{xy} has to be replaced, in eq. (2.3.6), by the effective shear stress:

$$\tau_{xy}^* = \tau_{xy} + \mu(\sigma_y - \sigma_{y,cl}) \quad (2.3.12)$$

or:

$$1 = \frac{\sigma_{y,cl}}{\xi_0 \sigma_t / 2} + \frac{(\tau_{xy}^*)^2}{\xi_0^2 \sigma_t^2}, \quad (2.3.13)$$

which fully explains fracture by compression perpendicular to the notch plane (see Figure 2.3.4). In these equations, μ is the friction coefficient.

For species with denser layers than those of Balsa, a much higher value of K_{IIc} (than twice the value of K_{Ic}), is measured because due to the reinforcement, η becomes smaller than the initial isotropic critical value of eq. (2.3.5) at further stretching. To read the equation in applied total orthotropic stress values, the matrix stress τ_{iso} has to be replaced by τ_{ort} / n_6 and the maximum

slope of the tangent, slope δ in Figure 2.2, the location of the failure stress is:

$$|\tan \delta| = |\eta_m| / \xi_0 = K_{Ic} / K_{IIc} = 1 / 2n_6 \quad (2.3.14)$$

For small values of $\eta = -|\eta|$, eq. (2.3.2) can be written, neglecting $(\eta/\xi_0)^2$:

$$\frac{\sigma_y}{\xi_0 \sigma_t / 2} = 1 + \frac{\eta^2}{\xi^2} - \frac{\tau_{xy}}{\xi_0^2 \sigma_t / (2|\eta|)} \approx 1 - \frac{\tau_{xy}}{\xi_0^2 \sigma_t / (2|\eta|)} \quad (2.3.15)$$

where $|\eta|$ is the absolute value of negative η . Thus:

$$\frac{K_I}{K_{Ic}} + \frac{K_{II}}{K_{IIc}} \approx 1 \quad (2.3.16)$$

This is a lower bound, with:

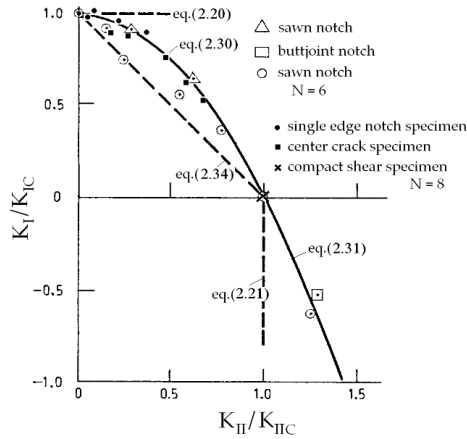


Figure 2.3.4. Combined mode I-II fracture strength [7]
 (eq.(2.20); (2.21); (2.30); (2.31); (2.34) of § 3.8 - [1] are: eq.(2.2.16); (2.2.18)
 (2.3.10); (2.3.13); (2.3.16).

$$K_{IIc} = \left(\xi_0 / |\eta_m| \right) \cdot K_{Ic} \quad (2.3.17)$$

and the maximal value of $\eta = \eta_m$ is found by measuring K_{Ic} and K_{IIc} , giving a value of about $\xi_0 / \eta_m \approx 7.7$, showing that the disregard of $(\eta / \xi_0)^2 = 0.017$ with respect to 1 is possible. Measurements between the lines eqs. (2.3.10) and (2.3.16) in Figure 2.3.4, thus indicate a strong difference between K_{IIc} and K_{Ic} of the local structure that is crossed by the propagating crack.

As mentioned, to obtain real orthotropic stresses, $\tau_{iso} = \tau_{ort} / n_6$ has to be inserted in eq. (2.3.6), giving:

$$1 = \frac{\sigma_y}{\xi_0 \sigma_t / 2} + \frac{\tau_{iso}^2}{\xi_0^2 \sigma_t^2} = \frac{\sigma_y}{\xi_0 \sigma_t / 2} + \frac{\tau_{ort}^2}{\xi_0^2 \sigma_t^2 n_6^2} = \frac{K_I}{K_{Ic}} + \frac{(K_{II})^2}{(K_{IIc})^2} \quad (2.3.18)$$

and it follows that:

$$\frac{K_{IIc}}{K_{Ic}} = \frac{\xi_0 \sigma_t n_6}{\xi_0 \sigma_t / 2} = 2n_6 \quad (2.3.19)$$

According to eq. (2.1.15), is for small clear specimens: $2n_6 = 2 \cdot (2 + \nu_{21} + \nu_{12}) \cdot (G_{xy} / E_y) = 2(2 + 0.57) / 0.67 = 7.7$ for Spruce and $2(2 + 0.48) / 0.64 = 7.7$ for Douglas Fir in TL-direction. The densities are respectively 0.37 and 0.50; moisture content of 12%). Thus, for $K_{Ic} \approx 265 \text{ kN/m}^{1.5}$ is $K_{IIc} = 7.7 \cdot 265 = 2041 \text{ kN/m}^{1.5}$ in TL – direction. This agrees with measurements [1]. In RL-direction this factor is 3.3 to 4.4. Thus,

when K_{IIc} is the same as in the TL-direction, the strength in RL-direction is predicted to be a factor 1.7 to 2.3 higher with respect to the TL-direction. This however applies at high crack velocities (“elastic” failure) and is also dependent on the site of the notch. At common loading rates a factor lower than $410/260 = 1.6$ is measured [1] and at lower cracking speeds [7, 1], this strength factor is expected to be about 1 when fracture is in the “isotropic” middle lamella. It then thus is independent of the TL and RL-direction according to the local stiffness and rigidity values. To know the mean influence, it is necessary to analyze fracture strength data dependent on the density and the elastic constants of n_6

From the rate dependency of the strength, follows an influence of viscous and viscoelastic processes. This has to be analyzed according to Deformation Kinetics theory [8]. A further problem is the possible early instability of the mode I-test equipment. In that case constants should be compared by related mode II data.

Empirical verification of the above derived theory equation, eq. (2.3.18), which is a Coulomb equation, called Wu-equation for wood, is not only obtained by [9], but also by tests of [10], done at the TL-system on eastern red spruce at normal climate conditions using different kinds of test specimens. The usual finite element simulations provided the geometric correction factors, and the stress intensity factors. The lack of fit test was performed on these data, at the usual variability for wood, assuming the five different, often suggested failure equations of Table 2.1. The statistical lack of fit values in the table show, that only the Wu-failure criterion, the third equation of Table 2.1, cannot be rejected due to lack of fit. The Wu-equation is shown to also fit clear wood and timber strength data in [11, 12], as expected from the theory.

Table 2.1. Lack of fit values for different failure criteria [10]

Failure criterion	<i>p</i> -value
$K_I / K_{Ic} = 1$	0.0001
$K_I / K_{Ic} + K_{II} / K_{IIc} = 1$	0.0001
$K_I / K_{Ic} + (K_{II} / K_{IIc})^2 = 1$	0.5629
$(K_I / K_{Ic})^2 + K_{II} / K_{IIc} = 1$	0.0784
$(K_I / K_{Ic})^2 + (K_{II} / K_{IIc})^2 = 1$	0.0001

2.4. REMARKS REGARDING CRACK PROPAGATION

Because the mixed mode failure criterion shows that cracks tend to propagate in the direction perpendicular to the greatest principal tangential tensile stress in the crack boundary as shown in Figures 2.3.2 and 2.3.3, an initial mode I fracture (opening mode) always occurs.

In Figure 2.4.1-b, the mixed mode crack propagation starts at an angle with its plane (due to initial matrix failure), but (due to the reinforcement), may bend back along the fractured zone. Stage b of this crack propagation is due to small-cracks merging in the fractured zone, which propagate to the macro-crack tip. For wood, stage b occurs in a parallel crack plane as given by Figure 2.4.2. This skipping across fibers is a form of oblique crack extension in a zigzag way, jumping when the equilibrium crack length is reached for the unloading stress level. Real collinear shear crack extension does not exist because the tensile stress there is zero and then only plastic shear sliding is possible at a much higher ultimate shear stress.

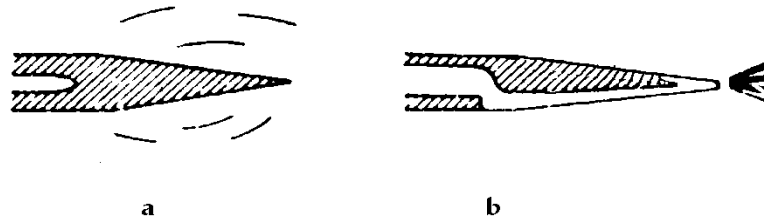


Figure 2.4.1. a) Craze at the crack tip and: b) Possible crack extension along the fractured zone in glassy polymers.

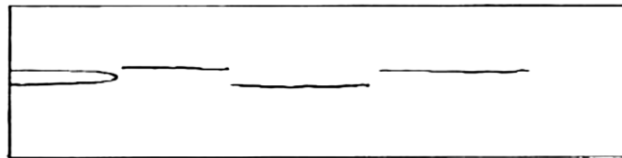


Figure 2.4.2. Scheme of Wu, of crack extension by skipping across fibers at pure shear loading, showing "mode" II failure to be a tensile failure outside the collinear plane of pure maximal shear stress. (This also can be regarded as a zig zag, small oblique angle, tensile crack propagation, in accordance with theory).

For multiple small- crack merging, collinear crack extension is possible by interference of tensile stresses, causing tensile failure in the weakest plane (along the grain) as given by Figure 2.4.3, where each small crack is propagating in the two directions towards the neighboring cracks. This is the principle of the small crack merging mechanism discussed in § 3.6.

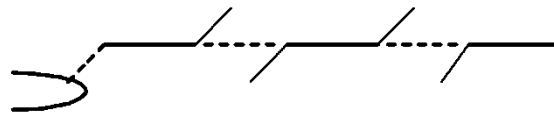


Figure 2.4.3. Collinear small crack merging.

Figure 2.4.4 explains why, in the mode II standard test, under shear loading, not a sliding mode II, but elastic, sliding unloading occurs, after an opening mode I tensile failure. This "mode II" test is represented by case $a + a''$. If the sign of the lower reaction

force V of this case is reversed and $P = 0$, the loading of the mode I, double cantilever beam (DCB) test is obtained, identical to loading case c with $N = 0$. In Figure 2.4.4, case $a + a''$ is split in case a and in case a'' , as loading of the upper and the lower cantilever. Case a is identical to case a' which is similar to end-notched beams discussed in Chapter 6. This case behaves like the mode I fracture test as can be seen by loading case c . The loading near the crack tip, given by case a , can be seen as the result of superposition of the stresses of cases b and c , where the loading of case b is such that the un-cracked state of the beam, case b' , occurs. The loading of case c is such that the sum of cases b and c gives loading case a . Case c is the real crack problem and the critical value of strain energy release rate G_c can be found by calculating the differences of elastic strain energies between case a' and b' , the cracked and un-cracked system. Case c shows the loading of the mode I – DCB-test by V and M , combined with shear loading by N and thus, the energy release rate will be somewhat smaller (by this combination with N) than the value of the pure DCB-test.

For the loading case a'' , the same stresses occur as in case a , however with opposite directions of M and V with respect to those of case c , according to case c'' , causing crack closure. To prevent that crack closure c'' , and friction, dominate above crack opening c , the crack slit has to be filled with a Teflon sheet. By superposition of cases c and c'' , case $c + c''$ of shear loading of pure mode II occurs, as crack problem due to the total loading. The normal load couple of $2N$ is just the amount to close the horizontal shift of both beam ends with respect to each other at that loading stage. This explains the applicability of the virtual crack closure (VCC-) technique. Because the upper cantilever is stronger for shear than the lower cantilever, because of higher compression

both perpendicular to and along the grain (see Figure 5.1 for the compression with parabolic increasing shear strength), mechanism c will dominate above c'' , when the lower cantilever starts to flow in shear or fails at the support. Thus mode I, case c tensile failure occurs.

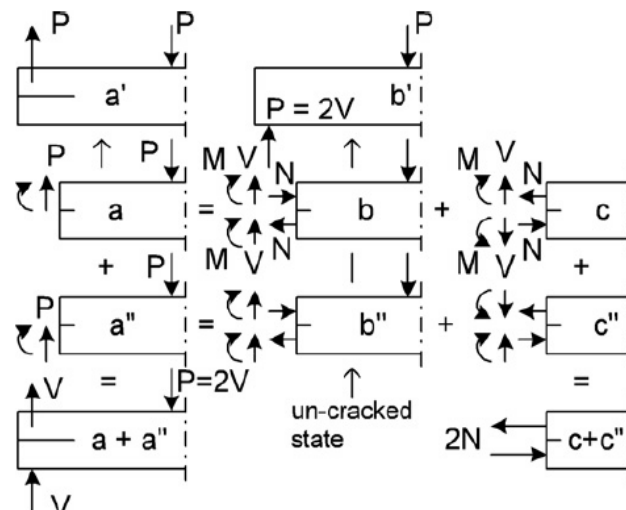


Figure 2.4.4. Mode II standard test loading of the single end notch beam.

Thus, as derived in § 2.3, there always occurs mode I failure, for any combined mode I – II stress combination, for any specimen type after stress redistribution.

2.5. REMARKS REGARDING THE EMPIRICAL CONFIRMATION

Measurements are given in Figure 2.3.4. The points are mean values of series of 6 or 8 specimens. The theoretical line eq. (2.3.10) is also the mean value of the data of Wu on extended

material properties. Only the Australian sawn notch data deviates from this parabolic line and lie between eq. (2.3.10) and the theoretical lower bound eq. (2.3.16). This is explained by the theory of a too high K_{IIc}/K_{Ic} -ratio, indicating a manufacturing mistake. Using general mean values of the constants, the prediction that $K_{IIc}/K_{Ic} = 2 \cdot (2 + \nu_{21} + \nu_{12}) \cdot (G_{xy}/E_y)$ agrees with the measurements. However, precise local values of the constants at the notches are not measurable and there is an influence of the loading rate and cracking speed. Thus safe lower bound values have to be used in practice. Figure 2.3.4 shows that all measurements, including fracture by compression, are explained by theory.

2.6. REFERENCES

- [1] RILEM state of the art report on fracture mechanics, *Espoo*, 1991.
- [2] R.H. Leicester, Design specifications for notched beams in AS 1720, CIB-W18/38-6-1, meeting 38, Karlsruhe, Germany, August 2005.
- [3] Timoshenko S. and Goodier J.N., Theory of elasticity, McGraw-Hill book comp., N.Y. 1951, 179-204.
- [4] van der Put T.A.C.M., A new fracture mechanics theory for orthotropic materials like wood, *Engin. Fract. Mech.* 74, (2007) 771-781. – or: [http://iewns.nl/C\(2007b\)](http://iewns.nl/C(2007b)).
- [5] van der Put, T.A.C.M., Explanation of the mixed mode interaction equation, COST 508 workshop 2, Bordeaux, April 1992

- [6] Susanti CME, Nakao N., Yoshihara H. Examination of the Mode II fracture behavior of wood with a short crack in an asymmetric four-point bending test. *Eng. Fract. Mech.* 78, 16 (2011) p 2775-2788.
- [7] Leicester R.H., Fracture strength of wood, First Australian Conf. on Engin. Materials, Univ. of New South Wales, 1974.
- [8] van der Put, T.A.C.M., Deformation and damage processes in wood, Delft Univers. press, 1989.
- [9] Wu E.M., Application of fracture mechanics to anisotropic plates, *ASME J. Appl. Mech.* Series E, 34 4, Dec. 1967, pp. 967-974.
- [10] Mall S., Murphy J.F., Shottafer J.E., Criterion for Mixed Mode Fracture in Wood, *J. Eng. Mech.* 109(3) 680-690, June 1983.
- [11] van der Put T.A.C.M., A continuum failure criterion applicable to wood, *J Wood Sci* (2009) 55:315–322. or: [http://iewws.nl/A\(2009\)](http://iewws.nl/A(2009)).
- [12] van der Put T.A.C.M., A general failure criterion for wood, van der Put T.A.C.M. Proceed. 15th CIB-IUFRO Timber Eng. Group Meeting, Boras, 1982, Sweden. or: [http://iewws.nl/A\(1982\)](http://iewws.nl/A(1982)).

Chapter 3

SOFTENING - CALLED YIELD DROP AND HARDENING

3.1. INTRODUCTION

A derivation is given of the yield drop curve, the occurring meta stable part of the Griffith locus. It follows from the derivation that strain softening does not exist.

For long over-critical initial crack lengths, the elastic crack closure energy, per unit area, is not equal to, but less than the critical energy release rate and the clear wood ultimate stress criterion applies for the still intact, ultimate loaded clear wood material adjacent to the macro-crack [1]. Thus clear wood micro-crack extension then is determining for failure.

The derivation of yield drop is discussed and it is shown in § 3.4 that the area under the load-displacement yield drop curve of Figures 3.4.1, 3.4.2, 3.6 or 3.7, divided by the crack area, is not the fracture energy, but the total external work on the specimen. The fracture energy follows from half this area under the loading curve,

what is equal to the critical strain energy release rate at the start of yield drop, which is the start of macro-crack extension. For wood, this correctly is applied for mode II, see Figure 3.4.3, where the elastic part of stored energy is subtracted from the total applied energy, given by the loading curve, to get the right nominal fracture energy. For mode I however, wrongly, the total area is regarded to be the fracture energy as is done by the fictitious crack models.

3.2. MODE I “SOFTENING” CALLED YIELD DROP EXPLAINED BY HARDENING

Apparent softening- like yield drop, only exists for the nominal stress thus, for the actual elastic stress far outside the fracture plane. The Griffith stress, eq. (3.2.8), is acting on the section $b \cdot t$ of Figure 3.1. This actual stress of the intact part of this specimen, outside the fracture plane, shows “softening- called” yield drop, following the Griffith locus, which is not strain softening (at failure), but is elastic unloading of intact, undamaged material, due to the reduction of intact, ultimate loaded material in the fracture plane by crack extension. The actual stress at the fractured section shows hardening and quasi hardening by the stress spreading effect, and increases, thus showing no softening as will be derived below. The same applies for the necked actual cross section area of a steel rod (and for the reduced fracture area of other materials). Clearly the term strain softening has to be replaced by “elastic unloading,” occurring when the unloading damage process is faster than the loading rate by the constant strain rate test. Because of sufficient plasticity, limit analysis applies and linear elastic fracture mechanics can be applied up to

the ultimate stress at the elastic-plastic boundary around the crack tip. The dissipation by micro crack formation, plastic deformation and friction within this boundary, called fracture process zone, then is regarded to be part of the fracture energy of macro crack extension. Thus the limit analysis equilibrium method is applicable.

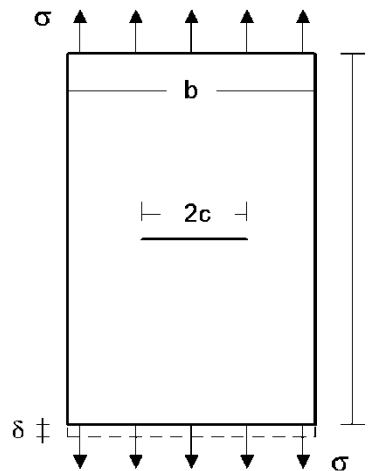


Figure 3.1. Center notched specimen $b \times l$ and thickness t , containing a flat crack of $2c$.

When a specimen is loaded until just before the start of yield drop and then unloaded and reloaded, the behavior has become elastic-full plastic, and the real stress differs in an internal equilibrium system with linear elastic loading case. Because limit analysis applies based on virtual displacements, this internal equilibrium system and other initial stresses and displacements have no influence on the value of the collapse load (when initial dimensions are regarded in the calculation). Therefore, Code calculations can be based on a reduced E -modulus, up to the ultimate state and also therefore replacement, in e.g., [2, 3, 6, 8],

and [9], etc., of the measured: compliance: $1/E_1$, by the very bad fit: $\sqrt{a_{11}a_{22}/2} \cdot \left(\sqrt{a_{22}/a_{11}} + (2a_{12} + a_{66})/(2a_{11}) \right)^{0.5}$, is not needed and therefore also the derivation below, of the yield drop curve of the fractured specimen, based on the effective E -modulus, is appropriate.

In Figure 3.1, a mode I, center notched test specimen is given with a length “ l ,” a width “ b ” and thickness “ t ,” loaded by a stress σ showing a displacement increase δ of the loaded boundary due to small crack extension. The work done by the constant external stress σ on this specimen, during this crack extension, is equal to:

$$\sigma \cdot b \cdot t \cdot \delta = 2W = 2(\sigma \cdot b \cdot t \cdot \delta / 2) \quad (3.2.1)$$

This is twice the increase of the strain energy W of the specimen. Thus, the other half of the external work, also equal to W , is the fracture energy used for crack extension. Thus the fracture energy is equal to half the applied external energy which is equal to the strain energy increase W and follows for the total crack length, from the difference of the strain energies of a body containing a crack and the same body without a crack:

$$\frac{\sigma^2}{2E_{eff}} b l t - \frac{\sigma^2}{2E} b l t = W \quad (3.2.2)$$

The fracture energy is also equal to the strain energy decrease at fixed grips conditions when $\delta = 0$:

$$W = t \sigma \int_{-c}^{+c} v da = \pi \sigma^2 c^2 t / E \quad (3.2.3)$$

where the last two terms give the strain energy to open (or to close) the flat elliptical crack of length $2c$ and where “ v ” is the displacement of the crack surface in the direction of stress σ . From eq. (3.2.2) and eq. (3.2.3), it follows that:

$$\frac{\sigma^2}{2E_{eff}}blt - \frac{\sigma^2}{2E}blt = \pi\sigma^2c^2t/E \quad (3.2.4)$$

Thus the effective Young’s modulus of the specimen of Figure 3.1, containing a crack of $2c$, is:

$$E_{eff} = \frac{E}{1 + 2\pi c^2 / bl} \quad (3.2.5)$$

The extremum principle of the normality rule, or energy equilibrium condition of the critical crack length is:

$$\frac{\partial}{\partial c}(W - G_c 2ct) = 0 \quad (3.2.6)$$

where G_c is the fracture energy for the formation of the crack surface $2ct$ per unit crack area. With W of eq. (3.2.2) or of eq. (3.2.3), eq. (3.2.6) becomes:

$$\frac{\partial}{\partial c} \left[\frac{\pi\sigma^2c^2t}{E} - G_c 2ct \right] = 0,$$

or:

$$\frac{\partial}{\partial c} \left[\frac{\sigma^2 b l t}{2E} \left(1 + \frac{2\pi c^2}{bl} \right) - \frac{\sigma^2 b l t}{2E} - G_c 2ct \right] = 0 \quad (3.2.7)$$

giving both the nominal Griffith strength:

$$\sigma_g = \sqrt{\frac{G_c E}{\pi c}} \quad (3.2.8)$$

which is the actual stress P/bt outside the fractured section on the intact area bt of the specimen of Figure 3.1. For strength problems, the necessary real, actual stress in the weakest actual cross section (ligament) with width: $b - 2c$, where fracture occurs, is:

$$\sigma_r = \sqrt{\frac{G_c E}{\pi c}} \cdot \frac{b}{b-2c} = \sqrt{\frac{G_c E}{\pi b}} \cdot \frac{1}{(\sqrt{c/b}) \cdot (1-2c/b)} \quad (3.2.9)$$

and it follows that:

$$\frac{\partial \sigma_r}{\partial (c/b)} = \sqrt{\frac{G_c E}{\pi b}} \cdot \frac{6c/b - 1}{2(c/b) \cdot (1-2c/b)} > 0, \quad (3.2.10)$$

when $c/b > 1/6 = 0.167$. This always applies for the critical crack length. Thus, $\partial \sigma_r / \partial c > 0$, and the real stress increases with the crack length and no softening behavior exists at the damage site. For larger initial cracks, the geometrical correction factor Y of § 10.2, should be accounted for. Then:

$$\begin{aligned}\sigma_r &= \frac{1}{Y} \sqrt{\frac{G_c E}{\pi c}} \cdot \frac{b}{b-2c} = \sqrt{1-(2c/b)^2} \sqrt{\frac{G_c E}{\pi b}} \cdot \frac{1}{(\sqrt{c/b}) \cdot (1-2c/b)} \\ &= \sqrt{\frac{G_c E}{\pi b}} \cdot \frac{\sqrt{(1+2c/b)}}{(\sqrt{c/b}) \cdot \sqrt{(1-2c/b)}},\end{aligned}$$

$$\text{and: } \frac{\partial \sigma_r}{\partial (c/b)} > 0 \text{ gives: } 2 \frac{c^2}{b^2} + 2 \frac{c}{b} - 0.5 > 0,$$

$$\text{or: } \frac{c}{b} > \frac{\sqrt{2}-1}{2} = 0.207 \quad (3.2.11)$$

This always happens because the critical value of eq. (3.3.3): $c_c/b = 1/\sqrt{6\pi} = 0.23$, is higher than 0.207. After initial yield, the real actual stress σ_a increases with the increase of the crack length, and “hardening” behavior characterizes the critical stress (not softening). However, a maximal ultimate value for this clear wood strength applies at the maximal possible stress spreading. Thus, the constant maximal value of the nominal energy release rate, basic for the Griffith theory, ends. The nominal stress follows the Griffith locus, eq. (3.3.2), (see Figure 3.6), as failure condition, which also is the condition of no damage acceleration. (Instable failure will not occur when the testing rig is sufficiently stiff, see Appendix I). The stress for the critical crack length of $c/b = 1/6$, of eq.(3.2.10) is: $\sigma_c = \sqrt{G_c E / \pi c} = \sqrt{G_c E / (\pi b / 6)}$ and the actual stress at the fracture plane is: $\sigma_{c,a} = \sqrt{G_c E / (\pi b / 6)} (b / (b - b/3)) = 1.5 \sqrt{G_c E / (\pi b / 6)}$, and thus is 1.5 times the nominal Griffith stress. Therefore, macro crack extension demands hardening (not softening), and demands an increase of the tensile strength. The

possible tensile strength increase follows from the exact stress spreading theory of [4]. Although derived for local compression, the sign of the shear stresses may be reversed and the same spreading rules apply for tension. For $c/b = 1/6$, according to Figure 3.1, there is a spreading of the stress on $b - 2c = 4c$ solid material to the full width: $b = 6c$. Thus the tensile strength is: $1.1\sqrt{6/4} \cdot \sigma_m \approx 1.35 \cdot \sigma_m$, or 1.35 times the uniaxial tensile strength σ_m . The nominal, fully spread, stress then is $1.1 \cdot \sqrt{4/6} \cdot \sigma_m = 0.9 \cdot \sigma_m$. Thus $1.5\sigma_g = 1.35\sigma_m$ or: $\sigma_g = 0.9\sigma_m$, thus:

$$\sqrt{(6G_c E)/(\pi b)} = 0.9\sigma_m. \quad (3.2.12)$$

In the same way, when the crack extends after twice this initial length, to: $c/b = 1/3$, then the actual stress becomes 3 times the Griffith stress, while the strength is $1.9 \sigma_m$, and the fully spread stress would be $0.64 \cdot \sigma_m$. Thus $3\sigma_{g2} = 1.9\sigma_m$, or $\sigma_{g2} = 0.63\sigma_m$, or:

$$\begin{aligned} \sqrt{(3G_c E)/(\pi b)} &= 0.63\sigma_m \rightarrow \\ \sqrt{(6G_c E)/(\pi b)} &= \sqrt{2} \cdot 0.63\sigma_m \approx 0.9\sigma_m \end{aligned} \quad (3.2.13)$$

From eq. (3.2.12) and eq. (3.2.13) it follows that the nominal stress intensity G_c (fracture energy) does not decrease at the main part of yield drop and crack extension. Mathematically, the following calculation was followed regarding the strength of the specimen of Figure 3.1. The actual stress in the fracture plane is due to the spreading effect:

$$\sigma_a = 1.1 \cdot \sigma_m \sqrt{\frac{b}{b-2c}} \quad (3.2.14)$$

where σ_m is the uniaxial tensile strength. In the intact plane, where the stress is fully spread, it is:

$$\sigma_a = 1.1 \cdot \sigma_m \sqrt{\frac{b-2c}{b}} \quad (3.2.15)$$

The actual Griffith stress in the fracture plane is:

$$\sigma_g = \sqrt{\frac{G_c E}{\pi c}} \frac{b}{b-2c} \quad (3.2.16)$$

From eq. (3.2.14) and eq. (3.2.16), it follows that:

$$\begin{aligned} \sigma_a &= 1.1 \cdot \sigma_m \sqrt{\frac{b}{b-2c}} = \sqrt{\frac{G_c E}{\pi c}} \frac{b}{b-2c}, \\ \text{or: } \sqrt{\frac{G_c E}{\pi c}} &= 1.1 \cdot \sigma_m \sqrt{\frac{b-2c}{b}} \end{aligned} \quad (3.2.17)$$

The nominal Griffith stress thus is equal and identical to the fully spread stress (the actual stress in undamaged material according to eq. (3.2.15)). This shows that the spreading effect causes a constant value of G_c during yield drop. The hardening (by the spreading effect), compensates the decreasing, still intact, material in the fracture plane during yield drop. This however ends when the maximal possible stress spreading is reached. Then the maximal “hardening” is reached and then a constant ultimate stress criterion applies (shown in § 3.7) and the Griffith law for macro crack extension does not apply anymore and thus is not able to explain fracture at low stresses. Then the ultimate stress criterion applies. This is the case below the factor 0.38 yield drop unloading level (see Figure 3.7). The total fracture cannot be due

to single macro crack extension. Necessary is clear wood fracture, (of the high loaded intact parts of the fracture plane), causing micro crack extension towards the macro crack tip, to explain macro crack extension at low nominal stresses (see § 3.3). Because unloading outside the fracture plane follows the stiffness and strength decrease of the specimen due to crack extension, the mathematical expression of this influence has to be discussed in the next § 3.3.

3.3. MODE I “SOFTENING” - CALLED YIELD DROP CURVE

Yield drop, (wrongly called softening) is only possible for nominal stresses, thus for the actual stress outside the fracture plane and should be described by the limit analysis damage theory of Deformation Kinetics [5]. But an alternative lower bound description is possible by the Griffith theory as follows: The critical strain of specimen of Figure 3.1, at which the initial crack will grow is according to eq. (3.2.5):

$$\varepsilon_g = \sigma_g / E_{eff} = \sigma_g \cdot (1 + 2\pi c^2 / bl) / E \quad (3.3.1)$$

Substitution of $c_c = G_c E / \pi \sigma_g^2$, of the ultimate state according to eq. (3.2.8), gives:

$$\varepsilon_g = \sigma_g / E + 2G_c^2 E / \pi \sigma_g^3 bl \quad (3.3.2)$$

This is the equation of critical (metastable) equilibrium states, representing the yield drop curve due to the Griffith stress eq.

(3.2.8), which is the actual stress on the intact part of the specimen, outside the fracture plane (and is the nominal stress at the fracture plane). It is shown by the dynamics of crack propagation (Appendix I), that the velocity of crack propagation is zero at the initial critical crack length and that the Griffith relation eq. (3.2.8), is the condition for zero acceleration of crack extension. Thus the crack of Griffith length is in unstable equilibrium but does not propagate. For crack propagation a slightly higher stress is necessary. The “softening” called yield drop curve, eq. (3.3.2), is called “Griffith locus” and has a vertical tangent $d\varepsilon_g/d\sigma_g = 0$, or: $\sigma_g^2 = G_c E / \sqrt{\pi b l / 6} = G_c E / \pi c_c$, thus occurring at a crack length of:

$$c_c = \sqrt{b l / 6 \pi}, \quad (3.3.3)$$

which is, with σ_c according to eq. (3.3.5), the top of the curve of Figure 3.2. The effective length l of the specimen of Figure 3.1 is the St. Venant distance, thus $l \approx b$. Therefore $c_c = \sqrt{b^2 / 6 \pi} = 0.23b$. For small initial cracks is $l \approx 2c$ and $c_c = b / 3\pi = b / 9.42 \approx 0.1b < b/6$, thus acting as clear wood fracture. Due to the steepness of the curve at the top, the first yield drop already may start earlier at: $0.57 \cdot 0.23b = 0.13b$, according to eq. (3.5.3). The locus below this top has a negative slope (following eq. (3.3.6)), as it should be at unloading, because a positive slope, represents crack recovery, which is not possible.

Eq. (3.3.2) shows a positive damage rate $d\varepsilon_g$, and negative stress rate, $d\sigma_g$, and that $\sigma_g \leq \sigma_c$. Thus σ_c is the top of the yield drop curve (see Figure 3.2).

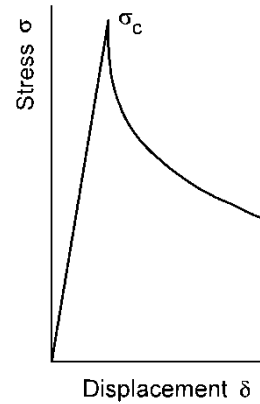


Figure 3.2. Yield drop curve according to eq.(3.3.2) for specimens of Figure 3.1 or Figure 3.5.

For a (small) cracks distribution, it applies that when their distance is higher than 2 times the St. Venant distance, the strength of the plate is about the same as when each small crack was alone in the plate. Thus for a critical distribution of small cracks in a repeating pattern, b and l in eq. (3.3.3) are the St Venant crack distances and the critical crack distance for extension therefore is about 2.2 times the crack length, because when $b \approx 2.2 \cdot (2c_c)$ and $l \approx 2.2 \cdot (2c_c)$, then $bl = b^2 \approx 19c_c^2 \approx 6\pi c_c^2$, according to eq. (3.3.3). This also applies for a single crack, or extended small cracks after merging to one crack, because the stress flow around the crack needs the St Venant's distance below and above the crack to be on full stress to be able to extend the present, small cracks further.

Thus the critical crack density for the start of yield drop, is reached, when the intermediate crack distance is about the crack length. This critical distance also is predicted by Deformation Kinetics, discussed in § 4.5, and is used in § 3.6 to explain yield drop by small-crack propagation in clear wood at the fracture plane (the ligament). Thus, when the intermediate crack distance is the St Venant distance, the stress and strength is about the same as

if the crack is alone in an infinite plate. This critical density is given by row A of Figure 3.8, which determines the critical crack density, because a lower crack distance (e.g., due to crack extension) then reduces the strength and starts yield drop. According to eq. (3.3.3), the yield drop line eq. (3.3.2), can be written:

$$\varepsilon_g = \frac{\sigma_g}{E} \left(1 + \frac{\sigma_c^4}{3\sigma_g^4} \right), \quad (3.3.4)$$

$$\text{where: } \sigma_c = \sqrt{EG_c / \pi c_c} \quad (3.3.5)$$

is the ultimate load with c_c according to eq. (3.3.3). The negative slope of the “metastable” part of the Griffith locus, being the yield drop line, then is:

$$\frac{\partial \sigma_g}{\partial \varepsilon_g} = - \frac{E}{\frac{\sigma_c^4}{\sigma_g^4} - 1} \quad (3.3.6)$$

Vertical yield drop occurs at the top at $\sigma_g = \sigma_c$, and the strain then is: $\varepsilon_{gc} = (\sigma_c / E) \cdot (1 + 1/3)$ and eq. (3.3.4) becomes:

$$\frac{\varepsilon_g}{\varepsilon_{gc}} = 0.75 \cdot \left(\frac{\sigma_g}{\sigma_c} + \frac{\sigma_c^3}{3\sigma_g^3} \right), \quad (3.3.7)$$

More in general, eq. (3.3.4) can be written, when related to a chosen stress level σ_{g1} :

$$\frac{\varepsilon_g}{\varepsilon_{g1}} = \frac{\sigma_g}{\sigma_{g1}} \cdot \frac{1 + \sigma_c^4 / 3\sigma_g^4}{1 + \sigma_c^4 / 3\sigma_{g1}^4} \quad (3.3.8)$$

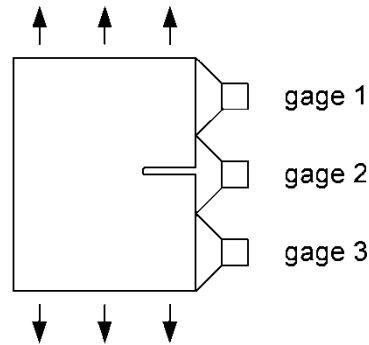


Figure 3.3. Measuring nonsense data at gage 2, (see[6]).

When the occurring yield drop curve starts to differ from the Griffith locus, σ_c decreases, causing a steeper decline of the total curve. This failure by a small-crack merging mechanism is discussed in § 3.6. To measure the fracture energy as area under the yield drop curve (discussed in §3.4), the displacement of the loading jack due to the mean deformation of the specimen has to be known. This cannot be obtained by measuring the gage displacement over a crack (see Figure 3.3), because it is not known what then is measured and this local unloading around the open crack is mainly proportional to the crack length itself, and to possible rotation and is not simply related to the constant ultimate stress state of the ligament and to the decreasing external loading.

3.4. FRACTURE ENERGY AS AREA UNDER THE YIELD DROP CURVE

As long as the fictitious crack models continue to calculate the fracture energy from the total area under the stress-displacement curve, the proof has to be repeated that only half this area has to be accounted for. This follows from the basic theory of the energy method, leading to eq. (3.2.1) and eq. (3.2.2), which of course is confirmed by the loading curve (Figure 3.4.1 and 3.4.2). When a test specimen is mechanically conditioned, the effective stiffness is obtained, given by the lines OA and OC in Figure 3.4.1 and 3.4.2. In Figure 3.4.1, the area OAB, written as A_{OAB} , is the strain energy of the specimen of Figure 3.1 with a central crack or with two side cracks according to Figure 3.5 (or Figure 3.2) with a width “ b ,” length “ l ” and thickness “ t ,” loaded to the stress σ . During the quasi static crack extension from B to D in Figure 3.4.1, the constant external load σ does work on the specimen of: $\sigma \cdot b \cdot t \cdot \Delta \varepsilon_{BD} \cdot l = \sigma \cdot b \cdot t \cdot \delta_{BD} = A_{ABDC}$, where $\Delta \varepsilon_{BD}$ is the strain increase due to the cracking and δ_{BD} the corresponding displacement. The strain energy after the crack extension is A_{OCD} and the strain energy increase by the crack extension thus is in Figure 3.4.1: $A_{OCD} - A_{OAB} = A_{OCD} - A_{OCB} = A_{CBD} = A_{ABDC} / 2$. Thus half of the external energy: $A_{ABDC} = \sigma \cdot b \cdot t \cdot \delta_{BD} / 2$ is the amount of increase of the strain energy due to the elongation by δ , and the other half is the fracture energy which is equal to this increase of strain energy. The same follows for unloading at yield drop. Because every point of the yield drop curve gives the Griffith strength which decreases with increasing crack length, unloading is necessary to maintain equilibrium. The fracture with unloading step AC in Figure 3.4.2 is the energetic equivalent to

the unloading steps AE and FC and the fracturing step EF at constant stress $EB = FD = (AB + DC)/2$. Thus $A_{ABDC} = A_{EBDF}$. Identical to the first case of Figure 3.4.1, the increase in strain energy due to crack extension is:

$$A_{ODF} - A_{OBE} = A_{ODF} - A_{OBF} = A_{BFD} = 0.5 \cdot A_{EBDF} = 0.5 \cdot A_{ABDC} ,$$

equal to half the work done by the external stresses during crack propagation and thus also equal to the other half, the work of crack extension. It therefore is shown that half the area under the load-displacement curve represents the fracture energy. For mode II, only line OACO in Figure 3.4.1 is measured and A_{OAC} is regarded to be the fracture energy. Because $A_{OAC} = A_{BAC} = 0.5 \cdot A_{ABDC}$, thus equal to half the area under the load displacement curve, the right value is measured and mode II data needs no correction. Because eq. (3.2.2) is based on the total crack length and the strength is a Griffith stress, the initial value $2c$ of the crack length has to be accounted and σ and G_c has to be related to the whole crack length, including the initial value $2c$, and thus should be related to the whole specimen width b and not to the reduced width of the fracture plane: $b - 2c$ as is done now and leads to an energy, dependent on the choice of the initial value of $2c$. Only for the Griffith stress, the energy method of § 6 and § 7 applies for initial failure, based on the energy difference of the cracked and un-cracked state. This has to be corrected together with the correction by a factor 2 for the mode I fracture energy G_c . A third correction occurs when σ_c of eq. (3.3.4) changes. The decrease of the mean G_c -value, starting half way the yield drop stage, shows the decrease of the nominal value of the constant G_c ,

due to the formation of an overcritical crack length by the decrease of intact area at the fracture plane. This is discussed in § 3.6.

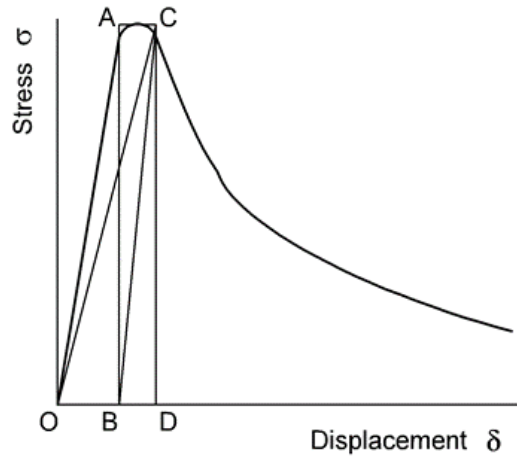


Figure 3.4.1. Stress – displacement curve for tension, of the specimen of Figure 3.5.

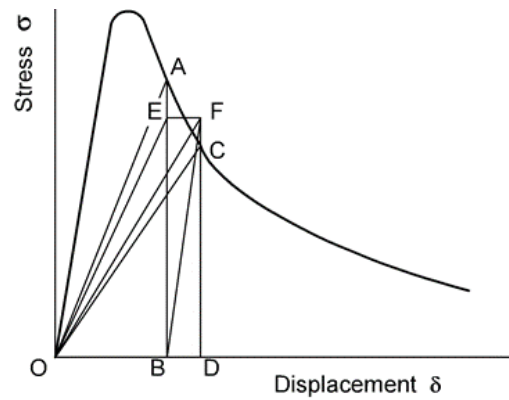


Figure 3.4.2. Descending branch of the stress –displacement curve of Figure 3.4.1.

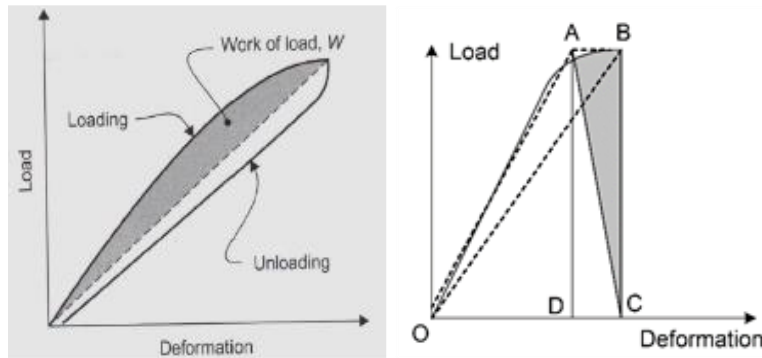


Figure 3.4.3. Mode II fracture energy and similarly start mode I: Area: $OAB = CAB = ABCD/2$.

In [7], not $A_{ABDC}/2$ is regarded as fracture energy but the amount A_{OACO} of Fig 3.4.2. This is the irreversible energy of a loading cycle by a crack increment in the specimen. This consists of: $A_{OEAO} + A_{OEFO} - A_{OFEO} = A_{OEFO} = 0.5 \cdot A_{BEFD} = 0.5 \cdot A_{ABDC}$, thus again half the area under the load-displacement curve. As discussed in [1], the measurements of [7] indicate the presence of a mechanosorptive process, acting in the whole specimen. It thus should be realized, that the area under the loading curve as: A_{OACO} gives no separate information on the fracture process alone of the still intact part of the fracture plane. Other viscoelastic and viscoplastic processes will dominate what has to be corrected by deformation kinetics [5] by determination of the activation energy of all acting processes. After correction, as first lower bound solution, the fracture energy can be regarded to be constant per unit crack length and then the area below the yield drop curve is a measure of the amount of intact ultimate loaded material at the increasing crack extension.

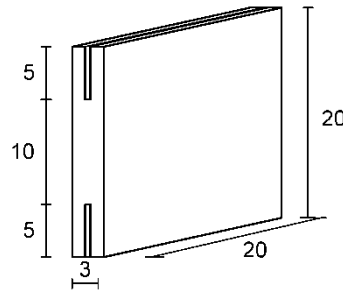


Figure 3.5. Geometry of the specimens of [3].

3.5. EXPLANATION OF MODE I DATA AND THE EMPIRICAL YIELD DROP CURVE

The measurements of [3] are completed by measuring the whole loading and yield drop curve and using the compact tension tests as control, being a control by the different loading case. The graphs of [3], Figure 3.6 and 3.7, are the result of tension tests on the specimen of Figure 3.5. The length of the specimen was $l = 3$ mm, the width and thickness: $b = t = 20$ mm and the notch length $2c = 2 \times 5 = 10$ mm with a notch width of 0.5 mm. In Figures 3.6 and 3.7, the measured stress-displacement is given together with the lines 1 and 2 according to the Griffith locus eq. (3.3.7). The strain ε_g follows from the displacements at the x -axis of the figures divided through 3 mm, the measuring length and length of the specimen. Because of the small length of 3 mm, not the whole width b of the specimen is active. Assuming a possible spreading of 1.2:1 through the thickness of 1.25 mm above and below the side notches, the working width b_{eff} is equal to the length of the fracture plane plus 2 times 1.2 x 1.25 or: $b_{eff} = 10 + 3 = 13$ mm. Thus the notch lengths in Figure 3.5 should be regarded to be 1.5 mm instead of 5 mm. The stresses in the Figures 3.6 and 3.7 of [3],

are related to the length of the fracture plane and not to the width b_{eff} , according to the nominal Griffith stress. Thus the actual stresses have to be reduced by a factor $10/13 = 0.77$. The standard compact tension tests of [3] did show a stress intensity K_{Ic} of $330 \text{ kNm}^{-3/2}$. This value also should follow from the area under the yield drop curve of that compact tension test. When half the area of that diagram is taken to be the fracture energy instead of the total area, then K_{Ic} , mentioned in [3], indeed is corrected to the right value of $467/\sqrt{2} = 330 \text{ kNm}^{-3/2}$ giving an empirical verification of the theory. Regarding the short double edge notched specimens of Figure 3.5, the measured E-modulus should be related to the effective width of 13 mm instead of the width of 10 mm of the fracture plane and therefore is $E = 700 \times 10/13 = 700 \times 0.77 = 539 \text{ MPa}$. The critical energy release rate then is:

$$G_c = K_{Ic}^2 / E = 330^2 / 539 = 200 \text{ N/m} \quad (3.5.1)$$

The measured value of G_c from the area under the stress-displacement curve is given in [3] to be 515 N/m . But, because half this area should have been taken and this value is wrongly related to the length of the fracture plane instead of on b_{eff} , the corrected value is $G_c = 1/2 \times 515 \times 0.77 = 200 \text{ N/m}$, as found above in eq. (3.5.1), giving again an empirical verification of the theory, now by the tests on the short double edge notched specimens.

As shown before, the yield drop curve of Figure 3.6 has (as Figure 3.2) a vertical tangent at the top $d\sigma_g / d\varepsilon_g = \infty$. The critical crack length for yield drop $c_c = \sqrt{bl / 6\pi}$ according to eq. (3.3.3) is:

$$c_c = \sqrt{(b_{eff}l) / (6 \cdot \pi)} = \sqrt{(13 \cdot 3) / (6 \cdot \pi)} \cdot 10^{-3} = 1.4 \cdot 10^{-3} = 1.4 \text{ mm} \quad (3.5.2)$$

This confirms the mentioned initial St. Venant crack length to be as small as about 1.5 mm. In Figure 3.6, at the Griffith maximal stress of $(0.77) \cdot 7 = 5.39$ MPa, is $K_{Ic} = \sigma \sqrt{\pi c}$ or $K_{Ic} = 5.39 \cdot \sqrt{\pi \cdot 1.4 \cdot 10^{-3}} = 0.36 \text{ MNm}^{-3/2}$, ($> 0.33 \text{ MNm}^{-3/2}$) for this strong specimen. The strength level above 4 (to 4.6) Mpa, given by Figure 3.7, is measured in 3 of the 10 specimens of the discussed series. T1309/2309 of [3] and Figure 3.6, shows the highest level, thus the total curve, as given by Figure 3.2 indicating that this strength of the fracture plane, according to crack-pattern A of Figure 3.8, was determining the yield drop. The other specimens of this series did show lower strength values than about 4 MPa, as applied for further unloading due to already extended small cracks. At § 3.3 and § 4.5, it is shown that for the critical small crack density of eq. (3.3.3), the intermediate crack distance is about the crack length as given by row A of Figure 3.8. Line 1 of Figure 3.6 gives the primary crack extension, eq. (3.3.7), by this critical crack density. This curve 1 levels off from the measurements at $\sigma = 4$ Mpa, where the next process starts, given by line 2 of Figure 2.6. This happens when the crack length has become about 3 times the initial critical value $c_{c,0}$, because then 4 MPa is reached according to:

$$\sigma_g = \sqrt{\frac{EG_c}{\pi 3c_{c,0}}} = 0.57 \cdot 7 = 4 \text{ MPa} \quad (3.5.3)$$

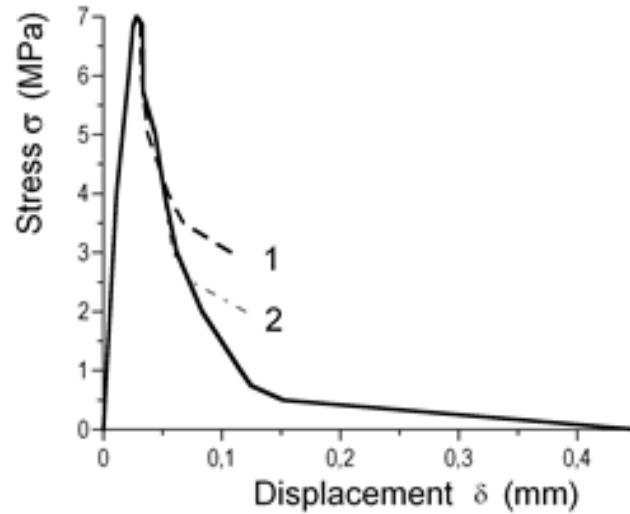


Figure 3.6. Stress - displacement of specimen T 1409.

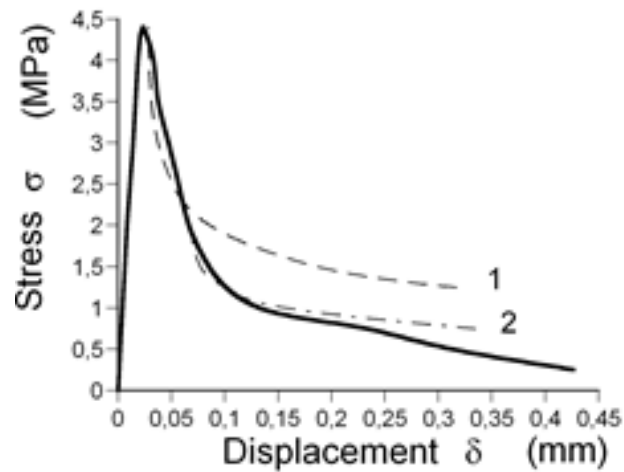


Figure 3.7. Stress – displacement of specimen T 1509 of [3].

This 3 times larger crack length is given by crack row B of Figure 3.8. The top value σ_c of the first process on row A is $\sigma_c = 7$ Mpa, for all values of σ_g between 4 and 7 Mpa. The top value of

the second process B on $3c_{c,0}$ cracks is $\sigma_c = 4$ MPa. This process ends where cracks of $7c_{c,0}$ lengths remain, according to row C of Figure 3.8. Thus when:

$$\sigma_g = \sqrt{\frac{EG_c}{\pi 7c_c}} = \frac{1}{\sqrt{7}} \sqrt{\frac{EG_c}{\pi c_c}} = \frac{1}{\sqrt{7}} \cdot 7 = 0.378 \cdot 7 = 2.65 \text{ Mpa} \quad (3.5.4)$$

This is where line 2 of Figure 3.6 levels off from the data line. This stress is equal to top value σ_c of the next process C, on $7c_{c,0}$ crack lengths, given below line 2 in Figure 3.6. This ends at $(1/\sqrt{15}) \cdot 7 = 0.258 \cdot 7 = 1.81$ Mpa, where the process on $15c_{c,0}$ starts. However, at longer cracks, maximal spreading is reached and the ultimate stress is determining and processes towards the longer cracks of 15, 31 and 63 $c_{c,0}$. They are probably not distinct and it is probable that due to the high actual stress, failure may occur at any point of the still intact part of the ligament. Here applies another hardening effect, because the strongest material will fail the last.

The Griffith law is apparently paradoxical. At a certain stress level there is enough energy to fracture a critical crack length of $2c$ (of Figure 3.1). But at crack extension the stress level lowers. Thus there is not enough energy to extend the now longer crack further. Thus, initial and further crack extension is impossible. The reason of this paradox is that nominal stresses are regarded, while fracture laws only can apply in real, actual stresses. After the first process of row A of Figure 3.8, half of the intact material is fractured, but the stress level is not halved, but 0.57 times lower. The next steps to rows B and C show respectively, the stress levels of 0.378 and 0.258, thus more than 0.25 and 0.125 needed to fracture the

remaining 0.25 and 0.125 intact material. The proof of the increasing sufficient stress level for further fracture is given by eq. (3.2.10), because not only the first derivative but also the second derivative is positive when $c/b > 1/6$.

The Griffith law thus is an extremum principle of limit analysis, which applies for virtual work at the top of the yield drop curve for the regarded initial crack length. In the form of eq. (3.3.2) or eq. (3.3.7) they represent this principle for the yield drop states. It proves the necessity of applying limit analysis as the basis of the new fracture mechanics theory.

At overcritical crack lengths, after some yield drop, K_{Ic} -values decrease, showing that the crack closure energy is lower than the bond breaking energy. Thus it remains, that failure of the post-critical crack lengths is due to the ultimate, uniaxial, clear wood failure stress, by micro-cracking of the adjacent $2c$ parts of Figure 3.8. This is discussed further below.

It is shown that the Griffith yield drop equation, combined with the crack merging model, precisely explains the data of strong specimens. The data of the less strong specimens, given by Figure 4.7, show instability of process A (of Figure 3.8) due to the steep slope near the top of Figure 4.2. This also explains the high variability of the data, found in [3]. Line 1 of Figure 4.7 is the same as line 2 of Figure 4.6, and can be chosen to level off at about 2.2 MPa, in accordance with the uniaxial strength of the still intact area of the ligament, which is half the area at 4.4 MPa, showing again that an ultimate stress criterion is determining for long (overcritical long) small-cracks (thus at low nominal stress). The optimal crack merging mechanism, clearly noticeable at strong specimens, is a chosen lower bound equilibrium system of limit analysis, which precisely follows the measured data (See above and § 3.6).

3.6. CRACK MERGING MECHANISM

As derived in § 4.4 of [5], the activation energy and activation volume parameters of the damage process of wood, show that the change of the site distance parameter $1/\lambda_1$ strongly dominates above bond breaking rate, shown by the decreasing distance, the increase of the flow unit density up to a critical value. Thus, as discussed in § 4.5 about deformation kinetics, macro crack extension is preceded by the formation of a high density of small cracks, providing a mechanism with the least loss of strength with the highest dissipation. Because for a distribution of small cracks, it applies that when the intermediate crack distance is higher than 2 times the St. Venant distance, the strength of the plate is about the same as when each small crack alone, was in the plate. The critical, maximal small crack density thus is determined by the St Venant distance. The critical intermediate small crack distance of a fracture process in “clear” wood in the fracture plane is about equal to the crack length, as given in scheme A of Figure 3.8. In § 3.3, theoretically, a crack distance of 2.2 times the crack length c is found, which for simplicity is rounded down to 2 in Figure 3.8.

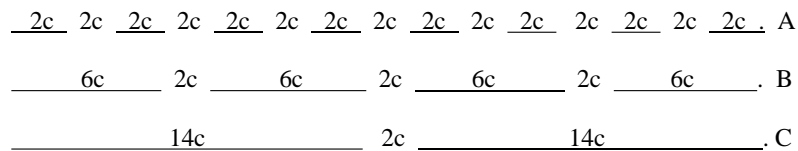


Figure 3.8. Small crack merging.

As shown in § 3.5, eq. (3.3.7) applies for yield drop going from row A to row B, which ends when the stress reaches the value according to eq. (3.5.3). This value is the top value for the next process, going from row B to row C, wherefore again eq. (3.3.7) applies until the stress reaches the value of eq. (3.5.4). The

crack merging mechanism thus can be seen as an extension and correction of the Griffith law and Griffith locus.

For the initial small cracks, the critical crack length according to eq. (3.3.3) is:

$$c_c = \sqrt{lb/6\pi} = \sqrt{2.2 \cdot (2c_0) \cdot 2.2 \cdot (2c_0) / (6\pi)} = 1.0 \cdot c_0, \quad (3.6.1)$$

for the specimen with row A. The distance l between the rows, above each other, is 2.2 times the crack length, being the Saint-Venant distance for building up full stress again behind a crack, to be able to form a new crack. Thus $l = b = 2.2 \cdot 2c$ for row A, and $l = b = 2.2 \cdot 6c$ in row B, and $l = b = 2.2 \cdot 14c$ for row C. Thus when crack pairs of row A join together, a double-crack length of $6c$ occurs. The critical crack length therefore for row B is:

$$c_c = \sqrt{lb/6\pi} = \sqrt{2.2 \cdot 6 \cdot 2.2 \cdot 6 \cdot c_0^2 / (6\pi)} = 0.5 \sqrt{(6 \cdot c_0)^2} = 0.5 \cdot 6c_0 = 3c_0. \quad (3.6.2)$$

Next a double-crack length of $14c$ is formed as row C and then $30c$, etc. However, for very long cracks, the maximal stress spreading is already reached and the ultimate stress criterion applies and it is more probable that random failure of the ultimate loaded remaining intact clear wood parts $2c$ length of rows A, B or C are determining for ultimate tensile failure. Thus micro crack formation and propagation in the remaining high loaded, intact clear wood part of the ligament is determining. This determining clear wood failure also applies from the beginning (as discussed in e.g., § 3.7), so that fracture is always due to the same micro crack extension. This damage process acts in all these parts at the same time during the whole fracture process. Thus, for the whole fracture process, from the beginning to full separation, it applies

that micro-crack formation in the intact part $(b - 2c)$ of Figure 3.1 of the ligament is determining, (despite the strength increase by the spreading effect) and that the concentration is not determined by the merged macro crack length $c_c = \sqrt{lb/6\pi} = \sqrt{b^2/6\pi} = 0.23b$, but by the merged, micro crack length in clear wood of:

$$c_c' = \sqrt{(b-2c)^2/6\pi} = 0.23 \cdot (b-2c). \quad (3.6.3)$$

For every successive process, it applies optimally, that every initial crack merges with one neighbor by extension at one side over a distance of $1 c_0$, leading to halving of the solid area of the ligament, and to an increase of the crack length by:

$$\begin{aligned} 2c_{n+1} &= 2 \cdot 2c_n + 2c_0, \\ \text{giving } 2c_1 &= 6c_0 \text{ and } 2c_2 = 2 \cdot 2c_1 + 2c_0 = 14c_0. \end{aligned} \quad (3.6.4)$$

The increase of the crack length is:

$$\Delta(2c)' = 2c_{n+1} - 2c_n = 2c_n + 2c_0, \quad (3.6.5)$$

Including the initial crack length of $2c_0$, the increase of the total crack length is:

$$\Delta(2c) = 2c_{n+1} - 2c_n - 2c_0 = 2c_n. \quad (3.6.6)$$

More general for all merging cracks at any distance during time Δt this is:

$$\Delta(c) = \beta_1 \cdot c \cdot \Delta t \quad (3.6.7)$$

and as the determining damage deformation kinetics [5] equation this is (see § 5, eq.5.3):

$$dc / dt = \beta_2 \cdot c_0 \cdot \exp(\sigma\phi), \quad (3.6.8)$$

when the initial site concentration c_0 is high, (zero-order reaction) as applies for row A of Figure 3. This equation can be written $\ln(\dot{c}) = \ln(C) + \phi\sigma_v$, or, because $\phi\sigma_{v0} = n$, is constant, independent of stress, due to the time stress equivalence, [5], is:

$$\frac{\sigma_v}{\sigma_{v0}} = 1 + \frac{1}{n} \ln\left(\frac{\dot{c}}{\dot{c}_0}\right) \quad (3.6.9)$$

showing that the combined Griffith – crack-merging model is identical to common damage behavior. Fracture is caused by accumulation of broken bonds, thus following a thermal activated process [5], and also applies for the following micro-crack formation and large cracks formation due to coalescence of micro-cracks (in a coupled process). This occurs when the critical density is reached.

The kinetics for timber show the same behavior as for clear wood, indicating that the same micro-crack propagation is always determining for fracture. As shown in [5], always two coupled processes act, showing the same time-temperature and the same time-stress equivalence of both. A high concentration of micro-cracks delivers the sites for the low concentration of macro-cracks formation. The reaction thus is autocatalytic, which means that one of the reaction products is also reactant and therefore a catalyst in the coupled reaction. The mode I notched specimen, discussed here, shows the coupled low concentration reaction of the macro-crack extension, by its property of a strong yield drop behavior of

the nominal stress. Thus, the initial crack length is the reactant and the reaction product is the newly extended macro crack length. The numerous small-cracks, growing towards each other and to the macro notch provide the site for the macro crack to grow as coupled second low-concentration reaction process. The kinetics of this bond breaking process is discussed in [5].

3.7. MODE II YIELD DROP BEHAVIOR

As shown before, for mode I, yield drop occurs when the rate of the damage process is faster than the rate of loading in a constant strain rate test. This causes unloading, which has nothing to do with softening behavior. Analysis of tests on overcritical crack lengths is necessary to know the properties of yield drop behavior. Therefore first, in paragraph 3.7.1, a prediction of the mode II critical crack length is discussed. This critical length causes the start of yield drop, and thus represents the top of the mode II yield drop curve.

3.7.1. Derivation of the Mode II Critical Crack Length for Yield Drop

Analogous to the mode I derivation in paragraph 3.2, is the fracture energy equal to the strain energy increase W at fracture under constant loading:

$$\frac{2(1+\nu)\tau^2}{2E_{eff}}bt - \frac{2(1+\nu)\tau^2}{2E}bt = W, \quad (3.7.1)$$

and analogous to eq. (3.2.3) and eq. (3.2.2), is for crack closure:

$$W = \pi(\sigma^2 + \tau^2)c^2t / E = \pi\tau^2c^2t / E, \quad (3.7.2)$$

for pure shear. Thus:

$$\frac{2(1+\nu)\tau^2}{2E_{eff}}blt - \frac{2(1+\nu)\tau^2}{2E}blt = \pi\tau^2c^2t / E \quad (3.7.3)$$

giving:

$$E_{eff} = \frac{E}{1 + \pi c^2 / bl(1+\nu)} \quad (3.7.4)$$

The Griffith stress τ_g follows from:

$$\frac{\partial}{\partial c}(W - G_c ct) = 0, \text{ or: } \frac{\partial}{\partial c} \left[\frac{\pi\tau^2c^2t}{E} - G_c ct \right] = 0; \text{ or:}$$

$$\tau_g = \sqrt{\frac{G_c E}{2\pi c}} \text{ or: } c_c = G_c E / (2\pi\tau_g^2) \quad (3.7.5)$$

Substitution of $c_c = G_c E / (2\pi\tau^2)$ into:

$$\gamma = \tau / G_{eff} = 2(1+\nu)\tau / E_{eff} \text{ gives:}$$

$$\gamma = \frac{2(1+\nu)\tau}{E_{eff}} = \frac{2(1+\nu)\tau(1 + \pi c^2 / bl(1+\nu))}{E} = \frac{2(1+\nu)\tau}{E} \left(1 + \frac{\pi(G_c E)^2}{(2\pi\tau^2)^2 bl(1+\nu)} \right) \quad (3.7.6)$$

and the top of the yield drop curve follows, as for mode I, from:

$$\frac{d\gamma}{d\tau} = 0, \text{ giving:}$$

$$\frac{2(1+\nu)}{E} - \frac{3G_c^2 E}{2\pi b l \tau^4} = 0 \text{ or: } \tau_c = \frac{\sqrt{G_c E}}{\sqrt{\sqrt{\pi b l (1+\nu)} 4/3}} = \frac{\sqrt{G_c E}}{\sqrt{\pi c_c}}.$$

Thus:

$$c_c = \sqrt{4(1+\nu) b l / 3\pi} = \sqrt{b l / 0.5\pi} = \sqrt{0.62 b l} = 0.785 \sqrt{b l} \quad (3.7.7)$$

This value of c_c is applied as a_c in paragraph 3.7.2.

3.7.2. Mode II Fracture Strength Criterion

In [8, 9], results of mode II tests, called asymmetric four point bending tests, are given (see Figure 3.9), and applied on very long over-critical initial crack lengths, which clearly represent an identical state of a former yield drop stage, because the measured K_{IIc} -values were a factor 2.5 to 4 lower than normal, thus much lower than the control tests on standard “single edge notched beam” specimens. The, by the numerical VCC- (virtual crack closure) test found too low, value of G_{IIc} , is not the critical energy release rate, but simply the elastic energy for elastic crack closure, (per unit crack length) of the existing very long overcritical crack length, which closure energy, per unit crack length, is much lower than the apparent surface energy. The $f(a/W)$ - factor in eq. (3.7.8) thus is not a geometry factor but an empirical coupling factor of terms in the equation. Because of the zero moment in the

middle of the beam at the location of the cracked, glued-in, specimen (see Figure 3.9), only shear stress loading and energy should be regarded as also follows from the VCC-method. The starting point in [8, 9] is the Griffith eq. (3.7.8), giving:

$$K_{IIc} = \tau_c \sqrt{\pi a_i} \cdot f(a/W) = (\sqrt{EG_{IIc}}), \quad (3.7.8)$$

In this equation G_{IIc} is found by the crack closure method; τ_c , the nominal critical shear stress is measured; a_i , the initial crack length, is wrongly regarded to be the critical crack length and $f(a/W)$ connects empirically τ_c , a_i , and G_{IIc} . The nominal eq. (3.7.8) has to be corrected for the real critical a_c and actual stress $\tau_{a,c}$ values which apply at the fracture site. Thus:

$$\tau_{a,c} \sqrt{\pi a_c} \cdot f(a/W) = \sqrt{EG_{IIc} (a_c / a_i) (\tau_{a,c}^2 / \tau_c^2)} = \sqrt{EG_{IIa,c}} = K_{IIa,c},$$

or:

$$\sqrt{\pi a_c} \cdot f(a/W) = \frac{K_{IIa,c}}{\tau_{a,c}} = C_1 \text{ (constant)} \quad (3.7.9)$$

where $\tau_{a,c}$ is the actual ultimate shear stress and $K_{IIa,c}$ the real critical value of the stress intensity at the critical initial crack length a_c . C_1 is only dependent on dimensions and stiffness factors of the specimen. For instance, eq. (6.2.7), which is based on a compliance method for shear loading and shear deformation, gives:

$$C_1 = K_{IIc} / \tau_{a,c} = \sqrt{0.27 \cdot h(\alpha - \alpha^2) \cdot E / G}, \quad (3.7.10)$$

which is constant, and independent of the crack length βh . The common empirical estimation in [8, 9], wrongly based on nominal stress and on initial crack lengths a_i instead of critical crack lengths a_c , resulted in a not constant C_1 , but on a strong dependency of C_1 on the crack length a/W , which therefore was a factor 2 higher at $a/W = 0.9$, with respect to the value at $a/W = 0.7$. The found factors 2.5 to 4 too low, not critical, not constant, values of G_c , are mainly due to the assumption that the overcritical crack length of $a/W = 0.7, 0.8, \text{ and } 0.9$, are the right initial critical crack lengths of the Griffith theory. According to Figure 12 of [9], there is no difference (by volume effect) between the data for $W = 40$ and 20 mm, thus in the following mean data values of both are regarded. This is necessary because the measured values of τ_c , dependent on W , are not published in [8, 9]. Because the applied initial crack length is overcritical, the clear wood strength, thus micro crack extension, is determining in the still available intact area of: $(W - a) \cdot (W - a)$, adjacent to the long (overcritical) initial cracks a_i . Then the equivalent merged, critical macro-crack length according to eq. (3.3.3) is, (for a constant W in all tests):

$$a_c = 0.78\sqrt{bl} = 0.78\sqrt{(W(1-a/W) \cdot W(1-a/W))} = 0.78 \cdot W \cdot (1-a/W), \quad (3.7.11)$$

Thus, C_1 according to eq. (3.7.9), is, for respectively:

$$\begin{aligned}
 a_i / W = 0.7: \quad \sqrt{\pi a_c} \cdot f(a/W) &= \sqrt{2.46 \cdot W} \sqrt{(1-a/W)} f(a/W) \\
 &= \sqrt{2.46 \cdot W} \cdot \sqrt{0.3} \cdot 1.0 = 0.85 \cdot \sqrt{W} \quad (3.7.12)
 \end{aligned}$$

$$\begin{aligned}
a_i / W = 0.8: \quad & \sqrt{\pi a_c} \cdot f(a/W) = \sqrt{2.46 \cdot W} \sqrt{1-a/W} f(a/W) \\
= \sqrt{2.46 \cdot W} \cdot \sqrt{0.2} \cdot 1.2 &= 0.84 \cdot \sqrt{W}
\end{aligned} \tag{3.7.13}$$

$$\begin{aligned}
a_i / W = 0.9: \quad & \sqrt{\pi a_c} \cdot f(a/W) = \sqrt{2.46 \cdot W} \sqrt{1-a/W} f(a/W) \\
= \sqrt{2.46 \cdot W} \cdot \sqrt{0.1} \cdot 1.67 &= 0.83 \sqrt{W}
\end{aligned} \tag{3.7.14}$$

This gives the necessary constant value of C_1 of eq. (3.7.9), for shear loading. The equations show that only eq. (3.7.12) gives the right value of a_c because $f(a/W)=1$, as should be for the compliance method. Therefore the smaller fracture planes need correction factors (respectively of 1.2 and 1.67) to obtain the same determining ultimate shear strength given by eq. (3.7.18) to eq. (3.7.20). Therefore:

$$a_c = a_{c,0} (f(a/W))^2 \tag{3.7.15}$$

Thus, it also is shown that the initial crack length is not critical, but the actual shear strength is determining for yield drop by overcritical initial crack lengths. The actual stress of actual, still intact material follows from the nominal Griffith stress, corrected by a factor $W/(W-a)$. This stress is determining for all clear wood failure. It is therefore necessary that the found actual clear wood shear strength is the same for the above 3 overcritical cases. Thus, similar to eq. (3.2.9) for mode I, is for (mode II) shear loading:

$$\begin{aligned}
\tau_u = \frac{K_{II}}{\sqrt{\pi a} \cdot f(a/W)} \cdot \frac{W}{W-a} &= \frac{K_{II}}{\sqrt{\pi a} \cdot (1-a/W) \cdot f(a/W)} = \frac{K_{II} / \sqrt{\pi W}}{\sqrt{a/W} \cdot (1-a/W) \cdot f(a/W)}
\end{aligned} \tag{3.7.16}$$

or:

$$\tau_u \sqrt{\pi W} = \frac{K_{II}}{\sqrt{a/W} \cdot (1-a/W) \cdot f(a/W)} \quad (3.7.17)$$

This is constant, independent of a/W because the crack closure value of K_{IIc} of 0.79, 0.71 and 0.52 are not determining factors in this case, but the ultimate shear stress, which is as $\tau_u \sqrt{\pi W}$ equal to:

For

$$a/W = 0.7: \frac{K_{II}}{\sqrt{a/W} \cdot (1-a/W) \cdot f(a/W)} = \frac{0.79}{\sqrt{0.7} \cdot 0.3 \cdot 1} = 3.2 \quad (3.7.18)$$

For

$$a/W = 0.8: \frac{K_{II}}{\sqrt{a/W} \cdot (1-a/W) \cdot f(a/W)} = \frac{0.71}{\sqrt{0.8} \cdot 0.2 \cdot 1.2} = 3.3 \quad (3.7.19)$$

For

$$a/W = 0.9: \frac{K_{II}}{\sqrt{a/W} \cdot (1-a/W) \cdot f(a/W)} = \frac{0.52}{\sqrt{0.9} \cdot 0.1 \cdot 1.67} = 3.3, \quad (3.7.20)$$

giving a mean value of: $\tau_u \sqrt{\pi W} = 3.25 \text{ MPa} \sqrt{\text{m}}$, and with $\bar{W} = 30 \text{ mm}$, this is $\bar{\tau}_u = 10 \text{ Mpa}$ of the clear wood strength of the tested small clear specimen of $30 \times 10 \times 15 \text{ mm}^3$ glued in the centre of the beam specimen (see Figure 3.9). The real value of K_{IIc} follows from eq. (3.7.9) and eq. (3.7.12): $\sqrt{\pi a_c} = K_{IIa,c} / \tau_{a,c}$ or:

$$K_{IIa,c} = \tau_{a,c} \sqrt{\pi a_c} = (3.25 / \sqrt{\pi W}) 0.85 \sqrt{W} = 3.25 \cdot 0.85 / \sqrt{\pi} = 1.56 \text{ MPa} \sqrt{\text{m}}, \quad (3.7.21)$$

as lower bound. This is equal to the in [9], Figure 12, given value of $1.6 \text{ MPa} \sqrt{\text{m}}$, which is measured by the single-edge notched beam test, as control on the data of the asymmetric four point bending tests of [9].

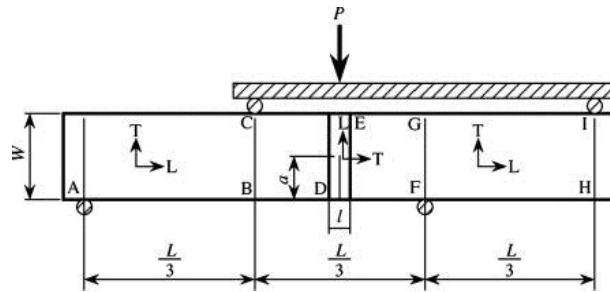


Figure 3.9. Mode II tests, called “asymmetric four point bending tests” of [8, 9].

All measured strength values are at the low side in [8, 9], because the start of viscous non-linearity in the test was regarded as the ultimate fracture state. It however is confirmed by the data of [8, 9], that the actual mean shear strength of the intact part of the fracture plane is determining for overcritical initial crack lengths and not the apparent critical K_{II} - value of crack closure, which is not constant and too low. Thus, macro crack extension is due to apparent ultimate clear wood shear strength, and thus occurs by small crack merging towards the macro-crack tip. The stress intensity is determining for initial crack lengths below $a/W = 0.7$. The test setup is however not stable enough for the higher stresses by lower initial crack lengths.

3.8. REFERENCES

- [1] T.A.C.M van der Put, A new fracture mechanics theory of wood, Nova Science Publishers NY, 2011 C(2011a) or: A new fracture mechanics theory of orthotropic materials like wood, *Engin. Fract. Mech.* 74/5 (2007) pp 771-781, or; [http://iews.nl/C\(2007b\)](http://iews.nl/C(2007b)).
 - [2] G.H. Valentin, L. Bostrom, P.J. Gustafsson, A. Ranta-Maunus, S. Gowda, RILEM state-of-the-art report on fracture mechanics, VTT Report 1262, Espoo, Finland July 1991
 - [3] L. Boström, Method for determination of the “softening” behaviour of wood etc. Thesis, Report TVBM-1012, Lund, Sweden, (1992).
 - [4] T.A.C.M. van der Put, Derivation of the bearing strength perpendicular to the grain of locally loaded timber blocks, *Holz Roh Werkst* (2008) 66: 409–417, or: [http://iews.nl/D\(2008a\)](http://iews.nl/D(2008a)).
 - [5] T.A.C.M van der Put, Deformation and damage processes in wood, Delft University Press, The Netherlands, (1989). Or: [http://iews.nl/B\(1989a\)](http://iews.nl/B(1989a)).
 - [6] I. Smith, E. Landis, M. Gong, Fracture and Fatigue in Wood, *J. Wiley & Sns*, 2003.
 - [7] Y.W. May, On the velocity dependent fracture toughness of wood, *J. Wiley & Sns*, 2003.
 - [8] H. Yoshihara, (2012) Mode II critical stress intensity factor of wood measured by the asymmetric four-point bending test of single-edge-notched specimen etc., *Holzforschung*, 66, pp 989-992.
- H. Yoshihara (2008) Mode II fracture mechanics properties of wood measured by the asymmetric four-point bending test using a single-edge-notched specimen, *Eng. Frac. Mech.* 75 pp.4727-4739.

Chapter 4

CORRECTIONS OF THE SINGULARITY APPROACH

4.1. INTRODUCTION

Only in Chapter 2 is the given non-singularity approach exact, up to initial yield, by applying a statically admissible equilibrium system, which suffices compatibility and boundary conditions and nowhere violates the failure criterion. The singularity approximation, applies not at, but in the neighborhood of the singularity, and is based on collinear crack extension and is therefore not able to show and satisfy the right failure criterion. Therefore, corrective models are applied, to remove the infinite stresses at the singularities. These models, based on plasticity by assumed crack bridging, are known as non-linear fracture mechanics, and are only applicable to singularity solutions. The R-curve is an applied correction for viscous flow and hardening, which is wrongly regarded as crack toughening. The R-curve also is assumed to explain instable crack propagation, although

instability does not occur at a sufficient stiff test assembly (see Appendix I). Thus the viscoelastic, plastic, and other structural change processes in beam type specimens at loading, (known from molecular deformation kinetics [1], see § 4.5), are not regarded separately, but wrongly regarded to be, all together, the response of one toughening fracture process. The start of non-linearity by these processes is wrongly regarded as the start of crack extension, although this happens at the top of the loading curve. This results in many meaningless mutual different R-curves depending on the specimen type. The hardening effect, due to stress spreading, does not show a hardening effect of the nominal apparent surface energy (energy release rate). The decrease of the nominal stress at yield drop is wrongly regarded to be a decrease of the actual stress in the fracture plane, which leads to the assumption of physically impossible strain softening behavior at crack extension.

To correct for combined mode I II loading, the wrong, uncoupled, ultimate uniaxial strength criterion (following from collinear crack extension), additional models are applied to constitute the ultimate state. For instance, the energy methods; numerical crack closure techniques, J-integral, or M- θ - integral, determine the initial strain energy release rate as ultimate state criterion. This however does not remove the influence of the infinite singularity peak stresses which are not corrected by adding an equilibrium system, as assumed by the fictitious crack models (Dugdale, Barenblatt, Hillerborg). This is discussed in § 4.2. The dynamic crack growth models and critical energy criteria are discussed in § 4.3.

The problems with these approximations of the singularity approximation are avoided by applying the given, exact (non-singular) limit analysis approach outlined in Chapter 2.

4.2. THE FICTITIOUS CRACK MODELS

The aim of the fictitious crack models (Dugdale, Barenblatt, Hillerborg) was initially to remove the infinite high stresses of the singularity approach. The model was based on a “fictive” crack length extension, which is loaded by a cohesive flow stress, over such a length that the singularity due to this cohesive flow stress neutralizes the singularity due to the field stress at the extended crack tip. The extended crack length is however not fictitious, but real, because only then, there is a real singularity possible at a real extended crack tip which can be neutralized. The singularity is not neutralized at the actual existing crack tip when this crack extension would not be real. Calculated thus is the strength of an extended crack length in an external stress field, loaded also by a physical and structural impossible, internal opposite applied, dilute viscous stress field, near the crack tips. In principle this is an internal equilibrium system superposed on the Airy stress function solution. But because this added equilibrium system is not present in the equilibrium method solution, it is necessary to subtract the energy of this system from the total failure energy, which is not done. According to virtual work limit analysis theorems, there is no influence of initial stresses and deformations on initial equilibrium systems on the plastic limit or collapse load, when initial dimensions are regarded in the calculations, which always is the case. The addition of corrective equilibrium systems thus has no influence on the collapse load. It remains necessary to regard the uncorrected singularity solution of the Airy stress function. The consequence thus is the rejection of the singularity solution with its infinite high stresses. The fictitious crack models therefore are not exact and superfluous. Instead, the exact boundary value limit analysis approach of Chapter 2, without singularities, leading to the exact, Wu-failure criterion, is determining and has to be

followed. This failure criterion cannot be derived by the singularity approach. The most exact model for uniaxial loading perpendicular to the grain only, is the elastic-plastic Dugdale model, and the results can be compared with the results of the exact solution. Then, the length of that enlarged plastic zone r_p of the extended crack length, according to the Dugdale model is given by eq. (4.2.1) as:

$$r_p = \frac{\pi}{8} \cdot \left(\frac{K_{Ic}}{\sigma_f} \right)^2 = \frac{\pi^2 \sigma^2 c}{8\sigma_f^2}, \quad (4.2.1)$$

where σ_f is the yield stress or is regarded to be a cohesive stress. This leads to a maximal crack opening displacement δ_c at the crack tip of:

$$\delta_c = \frac{8}{\pi E} \cdot \sigma_f \cdot r_p = \frac{K_{Ic}^2}{E\sigma_f} = \frac{\pi\sigma^2 c}{E\sigma_f} \quad (4.2.2)$$

when r_p from eq. (4.2.1) is substituted. This result, based on singularity equations, was necessarily based on very small values of r and r_0 in § 2.2.2, so that all terms containing not the factor $r_0^{-0.5}$ were neglected at the derivation of the equation. For finite values of r_0 this is not a correct result. According to the theory Chapter 2 applies for Mode I, at the crack tip boundary r_0 , at the start of flow, the condition $r_0 = 2c \left(\sigma / \sigma_f \right)^2$ according to eq. (2.3.7) for the elliptic crack tip. This is approximately $r_0 = c\sigma^2 / 2\sigma_f^2$ according to eq. (2.2.16) for the circular crack tip

of the singularity approach, showing a difference by a factor 4. The form of the crack tip determines the value of the tangential tensile stress along the crack-tip boundary. The Dugdale numerical factor $\pi^2 / 8 = 1.23$ (based on an enlarged crack length) is between the values of 0.5 and 2, but is too far away from the elliptic value 2, which applies as the highest lower bound of limit analysis (which bound is equal to the measurements, thus is the solution). Also the theoretical elastic elliptic crack opening displacement of $\delta_c = (2\sigma c) / E$ is far above the Dugdale value. The Dugdale model thus shows an inexact, too low, and thus rejectable lower bound of the strength, which only applies for uniaxial tensile loading perpendicular to crack and grain direction (due to the assumed collinear crack extension). The Dugdale model thus is based on a real, not fictive, extended crack length. Thus the superposed compression closing stress is an impossible, non-existent, external load on the specimen. This is not comparable with the crack problem, which is not loaded perpendicular to the crack boundary by a stress depending on the crack opening, but failure is independent of this, by the determining tangential stress in the crack boundary surface (see Chapter 2). This strength-determining stress is much higher than the regarded maximal stresses of the fictitious crack models, which don't satisfy the real failure criterion. The same applies for the Hillerborg model, which is based on closing stresses, proportional to the yield drop curve, thus proportional to the lowering mean elastic stress far outside the fracture plane and not proportional to the actual spreading stress at the fracture plane. Therefore a zero tangential stress is found at the location of the highest (strength determining) tangential tensile stress. This error is of course far from right because the calculated increasing stress and hardening at the fracture plane (see § 3.2), are opposite to the arbitrary assumed softening.

4.3. APPLIED CRACK GROWTH MODELS

The acknowledged, basically identical crack growth models for wood, of Williams, Nielsen and Schapery, mentioned in [2], are based on linear viscoelasticity and on the Dugdale-Barenblatt model in order to try to derive the empirical crack rate equation:

$$\frac{da}{dt} = A \cdot K_I^n \quad (4.3.1)$$

The followed procedure is contrary to the normal one, and cannot lead to a real solution, because the rate equations are constitutive and have to follow from Deformation Kinetics theory, (see § 4.5 and Section B, [1, 3]) which applies for all materials and is the only way to account for time and temperature dependent behavior. Constitutive equations can only follow from theory and not from general thermodynamic considerations. In [2], it is stated that Fig 4.1 of [2] represents eq. (4.3.1). However, eq. (4.3.1) is a straight line on a double log-plot, while Figure 4.1 gives the semi-log-plot which confirms the applicability of the damage equation of Deformation Kinetics [1] in the form $\dot{a} \approx C \cdot \exp(\phi\sigma_v)$, or:

$$\ln(\dot{a}) = \ln(C) + \phi\sigma_v \quad (4.3.2)$$

This equation is equal to eq. (3.6.9), discussed in § 3.6. More appropriate forms of the exact damage equations and power law forms, with the solutions as the yield drop at the constant strain rate test, are discussed in [1] and the meaning of the power law equation, eq. (4.3.1), is discussed below. The impossibility of the derivation of the fracture rate equation from the Dugdale-

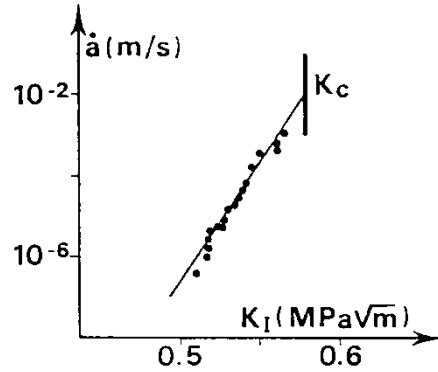


Figure 4.1. Crack growth tests of Mindess (Figure 10 of [2]).

Barenblatt equations follows e.g., from the derivation in [2, § 2.2] of eq. (4.3.3):

$$K_{Ic} = E_0 \cdot \dot{a}^n \cdot \sqrt{\delta_c \varepsilon_y} \cdot r_p^{-n} \quad (4.3.3)$$

based on the relations: $\varepsilon_y = \sigma_c / E$ and $K_{Ic} = \sqrt{E \sigma_c \delta_c}$, with $E = E_0 \cdot t^{-n}$ and $r_p = \dot{a} \cdot t$. These four (interlinked) relations thus also can be used now to eliminate at least 4 parameters, e.g., K_{Ic} , ε_y , r_p and E_0 to obtain an equation in E , t , \dot{a} , σ_c and δ_c . When this is done, eq. (4.3.3) turns to an identity $E = E$, and eq. (4.3.3) thus is not a new derived crack rate equation but an alternative writing of the four relations. The same follows for the other models of § 2.2 of [2] showing comparable parameter manipulations of many critical parameter values which cannot be applied independently because they are part of the same failure condition. The models are further based on linear viscoelasticity which does not exist for polymers. It is shown in [1], page 97, and by the zero creep and zero relaxation tests at page 119, that a

spectrum of retardation or relaxation times does not exist. The superposition integral eq. (28) or eq. (51) of [2]:

$$\varepsilon(t) = \int_{-\infty}^t C(t-\tau) \frac{d\sigma(\tau)}{d\tau} d\tau \quad (4.3.4)$$

thus has no physical meaning. This also applies for the power law models of time and power law eq. (4.3.1), which only apply in a limited range, making predictions and extrapolations outside the fitted range of the data impossible. It is thus necessary to apply the exact theory of Section B, of *iew.s.nl*, for the kinetics of damage and crack growth processes.

4.4. CONTINUUM DAMAGE MECHANICS

Continuum damage mechanics [4], is a simplified application of needed Deformation Kinetics analysis (of [1]), leading to the most elementary damage kinetics equations. But not all possible structural change processes can be given in this simplified form. Regarding fracture mechanics of [4], the analysis is based on the fractured (lost) area A of an initially undamaged section A_0 , leading to the variable:

$$\psi = \frac{A_0 - A}{A_0} \quad (4.4.1)$$

The actual stress σ_a on the material then is (expressed, as wanted, in the nominal stress σ):

$$\sigma_a = \frac{P}{A_0 - A} = \frac{P}{A_0 \psi} = \frac{\sigma}{\psi} \quad (4.4.2)$$

where σ is the nominal stress and σ_a the actual stress on still undamaged, actual area of the section. Now:

- 1) The actual stress on the actual area evidently determines the rate of damage growth, and
- 2) The strain increase due to damage is caused by the actual stress at the damage location.

Thus, the stress-strain behavior of the damaged material can be represented by the constitutive equation of the virgin, undamaged, material with the stress in it, replaced by the actual stress. Thus:

$$\varepsilon = \frac{\sigma_a}{E} = \frac{1}{E} \cdot \frac{\sigma}{\psi} = \frac{\sigma}{E'} \quad (4.4.3)$$

with: $E' = E\psi$. A simple form of the deformation kinetics damage equation for uniaxial tension is:

$$\frac{d\psi}{dt} = -C \left(\frac{\sigma}{\psi} \right)^n \quad (4.4.4)$$

This is comparable with the deformation kinetics equation of § 4.5:

$$\frac{dN}{dt} = -CN_0 \exp\left(\frac{\sigma\lambda'}{kN}\right), \quad (4.4.5)$$

for a forward zero order reaction due to a high reactant concentration and high stress, where this exponential equation is replaced in eq. (4.4.4) by its power law representation (derived in § 4.6). Because the stress is high, the $\sinh(x)$ -form is changed to

exp(x) -form in the equation and initially also $\sigma / N = \sigma_0 / N_0$ is constant, independent of the value of σ_0 and independent of temperature, explaining the time temperature and time stress equivalence. Because the pre-exponential concentration term N is high and does not change much during the reaction, the value of N_0 can be used and the reaction then is of zero order at the start and the solution eq. (4.5.4) then applies for initial failure. After a delay time of relatively small change, eq. (4.4.4) can be used for further failure at high enough stress, leading after integration, for a rod loaded by a constant tensile stress σ_0 , at the initial boundary condition for virgin material, $\psi = 1$ at $t = 0$, and at $\psi = 0$ for complete fracture, to a time to failure of: $t' = [C(n+1)\sigma_0^n]^{-1}$, and for stepwise loading then follows:

$$\sum_{k=1}^s \frac{\Delta t_k}{t'_k} = 1; \quad t'_k = [C(n+1)\sigma_k^n]^{-1} \quad \text{with: } \Delta t_k = t_k - t_{k-1},$$

$$k = 1, 2, \dots, s. \quad (4.4.6)$$

which is Miner's rule, or the principle of linear summation, which evidently also applies for wood and timber. Important conclusions now are:

- 1) It is necessary to apply the actual stress in damage equations, for correct results, as applied in [4, 3 and 1], for all existing solutions, which all are empirically verified by tests.
- 2) Limit analysis deformation kinetics (developed in [1]), have to be applied (e.g., in continuum mechanics), for exact solutions.

- 3) The determining micro-crack equation, which produces macro-crack extension, can be based on an initially high concentration, high loaded, zero order reaction equation.

This is applied and discussed in Chapter 3 and in next paragraphs.

4.5. DEFORMATION KINETICS OF FRACTURE PROCESSES

The basic equations for fracture according to the limit analysis equilibrium theory of molecular deformation kinetics are given in § 4.4 of [1]. The basic concept of this fundamental theory is to regard plastic flow as a matter of molecular bond breaking and bond reformation in a shifted position, which is the same as to state that the flow is the result of a chemical reaction like isomerization. Thus, not the composition changes, but only the bond structure of the molecules. Damage occurs when not all broken side bonds reform, providing the sites of the damage process.

The general theory developed in [1] is based on the limit analysis equilibrium method and is, as such, an exact approach, which is able to predict all aspects of time dependent behavior of materials by the same constitutive equation, because the mathematical derivation of this general theory is solely based on the reaction equations of the bond-breaking and bond- reformation processes at the deformation sites due to the local stresses in the elastic material around these sites. The form of the parameters in the rate equations are according to the general equilibrium requirements of thermodynamics. By expressing the concentration

and work terms of the rate equation in the number and dimensions of the flow units, the expressions for the strain rate, fracture, flow, hardening and delay time are directly derived without any assumptions. To obtain simplifications, series expansion of the potential energy curve is applied, leading to the generalized flow theory, and thus to a proof of this general flow model, and showing the hypotheses of this generalized theory, to be consequences of the series expansion. This theory therefore applies generally, also for structural changes, giving an explanation of the existing phenomenological models and laws of fracture.

The rate equation for fracture then can be given for high stress, as always applies for fracture, by:

$$-\frac{d\rho}{dt} = \frac{2\rho}{t_r} \sinh\left(\frac{W}{kT}\right) \approx \frac{\rho}{t_r} \exp\left(\frac{W}{kT}\right) \quad (4.5.1)$$

where the concentration of activated units per unit volume ρ can be written $\rho = N\lambda A / \lambda_1$ with N flow units per unit area of a cross section, each at a distance λ_1 behind each other with λ as jump distance and A as area of the flow unit. The work of a flow unit W , with area A moving over a barrier, over distance λ is $W = fA\lambda = \sigma\lambda / N$. Because of equilibrium per unit area of the external load $\sigma \cdot 1 \cdot 1$ with the force on the N flow units NfA . Thus $\sigma = NfA$ and eq. (4.5.1) becomes expressed in the nominal macro engineering stress σ , which is the part of the total external stress that acts on N , to be found from tests with different loading paths:

$$-\frac{d}{dt}\left(\frac{N\lambda}{\lambda_1}\right) = \frac{N\lambda}{\lambda_1 t_r} \exp\left(\frac{\sigma\lambda}{NkT}\right), \quad (4.5.2)$$

In this equation t_r is the relaxation time. The value of A can be regarded constant because any change is compensated by a corrected value of f and a corrected value of λ to obtain a correct load on the flow unit and its correct volume. Eq. (4.5.2) can be written with $N' = N/\lambda_1$ (the number of flow units per unit volume) $-d(N'\lambda)/dt = (N'\lambda/t_r)\exp(\sigma\lambda/NkT)$, or:

$$\frac{d}{dt}\left(\frac{\lambda}{N'}\right) = \frac{\lambda}{N' t_r} \exp\left(\frac{\sigma\lambda}{NkT}\right) \quad (4.5.3)$$

For this zero order reaction in wood, when the very high initial reactant concentration does not change much and initially also $\sigma/N = \sigma_0/N_0$ is constant, the solution is:

$$\frac{\lambda}{N'} = \frac{\lambda t_f}{N_0' t_r} \exp\left(\frac{\sigma\lambda}{N_0 kT}\right) + \frac{\lambda}{N_0'}, \text{ or:}$$

$$\left(\frac{\lambda}{N'} - \frac{\lambda}{N_0'}\right) \cdot \frac{N_0'}{\lambda} = \frac{t_f}{t_r} = \frac{t_f}{t_0} \cdot \frac{kT}{\nu h} \exp\left(-\frac{E}{kT} + \frac{\sigma\lambda}{N_0 kT}\right) = \frac{t_f}{t_0} \cdot \exp\left(-\frac{E}{kT} + \frac{\sigma\lambda}{N_0 kT}\right)$$

or

$$\left(\text{with } \frac{kT}{\nu h} = 1\right):$$

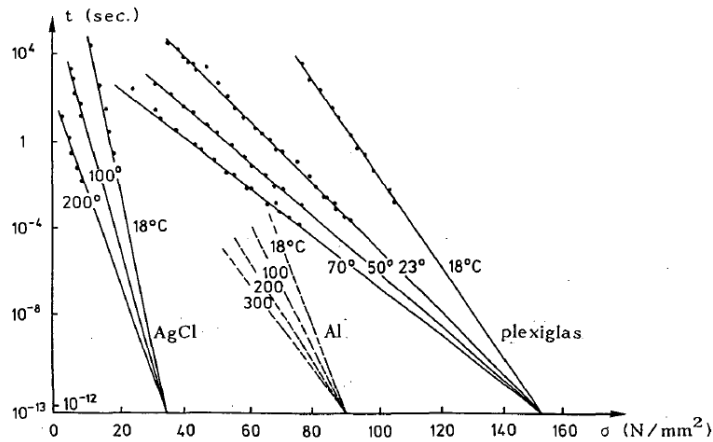


Figure 5. Stress and temperature dependence of the lifetime for structural materials [1].

$$\frac{E}{kT} - \frac{\sigma\lambda}{N_0 kT} = \ln\left(\frac{t_f}{t_0}\right) - \ln\left(\frac{N_0'}{N_f'} - 1\right) = \ln\left(\frac{t_f}{t_0}\right), \quad (4.5.4)$$

Figure 5 shows that eq.(4.5.4) applies generally for structural materials. Thus $N_f' = 0.5 \cdot N_0'$ as experimentally found for fracture. , Thus the crack length is about the same as the crack distance, or the intact area has reduced to 0.5 times the initial area when macro-crack propagation starts due to small crack merging behavior, which explains the measured mode I and mode II final nominal yield drop behavior of fracture.

4.6. DERIVATION OF THE POWER LAW

The power law equation may represent any function $f(x)$, as derived below. . It therefore also may represent, in a limited time

range, a real damage equation giving a meaning of the power n of the power law eq. (4.4.4). This is applied in § 4.4.

Any function $f(x)$ always can be written in a reduced variable x/x_0

$$f(x) = f_1(x/x_0) \tag{4.6.1}$$

and can be given in the power of a function:

$$f(x) = f_1(x/x_0) = \left((f_1(x/x_0))^{1/n} \right)^n \text{ and expanded into the row:}$$

$$f(x) = f(x_0) + \frac{x-x_0}{1!} \cdot f'(x_0) + \frac{(x-x_0)^2}{2!} \cdot f''(x_0) + \dots, \text{ giving:}$$

$$f(x) = \left[\{f_1(1)\}^{1/n} + \frac{x-x_0}{x_0} \frac{1}{n} \{f_1(1)\}^{1/n-1} \cdot f'(1) + \dots \right]^n = f_1(1) \cdot \left(\frac{x}{x_0} \right)^n \tag{4.6.2}$$

when: $(f_1(1))^{1/n} = \frac{1}{n} (f_1(1))^{1/n-1} \cdot f'(1)$ or: $n = f_1'(1) / f_1(1)$,

where: $f_1'(1) = \left(\partial f_1(x/x_0) / \partial (x/x_0) \right)_{(x/x_0)=1}$ and $f_1(1) = f(x_0)$

Thus:

$$f(x) = f(x_0) \cdot \left(\frac{x}{x_0} \right)^n \text{ with } n = \frac{f_1'(1)}{f_1(1)} = \frac{f'(x_0)}{f(x_0)} \tag{4.6.3}$$

Thus the derivation of the power law, using only the first 2 expanded terms, shows that eq. (4.6.3) only applies in a limited range of x around x_0 . Using one x_0 is not limiting for strength problems.

Using this approach on equation: $\dot{a} = 2C \cdot \sinh(\phi\sigma) \approx C \exp(\phi\sigma)$ (for high stresses), gives:

$$\dot{a} = C \cdot \exp(\phi\sigma) \approx \dot{a}_0 \cdot \left(\frac{\sigma}{\sigma_0} \right)^{\phi\sigma_0} \quad (4.6.4)$$

The power $n = \phi\sigma_0$ of the power law equation follows from the slope of the double log-plot:

$$\ln(\dot{a}) = \ln(\dot{a}_0) + n \cdot \ln(\sigma / \sigma_0) \quad (4.6.5)$$

Thus: $n = d \ln(\dot{a}) / d \ln(\sigma / \sigma_0)$ and $n = \phi\sigma_0$ gives a meaning of n as the activation volume parameter $\phi\sigma_0$ of the exact equation. The values of “ n ” and the matching activation energies of the different creep and damage processes in wood, with the dependency on stress moisture content and temperature, are given in [1]. The constancy of the initial value of the parameter $\phi\sigma_0$, independent of applied stress σ_0 , explains the time-temperature and time- stress equivalence and explains, by the physical processes, why and when at high stresses, the in [2] mentioned value of $n + 1 \approx 60$ is measured and at lower stresses, half this value (see [1]).

4.7. J-INTEGRAL APPLICATION

Path-independent integrals are used in physics to calculate the intensity of a singularity of a field quantity without knowing the exact shape of this field in the vicinity of the singularity. They are derived from conservation laws. For the singularity method of wood, the J -integral (Rice integral) and M - θ -integral are applied for estimation of the energy release rate. However, even the finite element applications for wood, appear to lead to quite different

outcomes by different authors at different situations, showing the application to be not exact, as also follows from remarks from [5]: J (near a crack singularity) is the component along the crack-line of a vector integral, having a meaning for not oblique (thus *invalid* for mode II and mixed mode I-II) and (*only for mode I possible*) incipient self-similar growth of a crack in a (nonlinear) elastic material. In this case, J has the meaning of the rate of energy-release per unit of crack-extension. The path-independency of J can be established only when the strain energy density (or stress working density) of the material is a single valued function of strain. In a deformation theory of plasticity, which is valid for radial monotonic loading but *precludes unloading* and which is mathematically equivalent to a nonlinear theory of elasticity, J still characterizes the crack-tip field and is still a path-independent integral. However, in this case, J does not have the meaning of an energy-release rate; it is simply the total potential-energy difference between two identical and identically (monotonically) loaded cracked bodies which differ in crack lengths by a differential amount. Further, in a flow theory of plasticity (*as applies for wood*), even under monotonic loading, the path-independence of J cannot be established. Also, under arbitrary load histories which may include loading and unloading, J is not only not path-independent, but also does not have any physical meaning. The blunting of the top of the loading curve and formation of the fracture zone and the main amount of crack growth with crazing and small crack formation in, (and outside), the process zone, means unloading and non-proportional plastic deformation which also invalidates the deformation theory of plasticity.

Thus the J - integral method of the singularity approach, does not apply to wood (and other structural materials [6]). It is shown in § 2.3 and § 2.4, that oblique crack extension in the isotropic

matrix and skipping across fibers, is necessary for mode II crack extension.

4.8. REFERENCES

- [1] van der Put, T.A.C.M., Deformation and damage processes in wood, Delft University press, 1989, or: [http://iewws.nl/B\(1989a\)](http://iewws.nl/B(1989a)).
- [2] G.H. Valentin, L. Bostrom, P.J. Gustafsson, A. Ranta-Maunus, S. Gowda, RILEM state-of-the-art report on fracture mechanics, VTT Report 1262, Espoo, Finland July 1991
- [3] van der Put, T.A.C.M., Transformations in wood, Delft University, Stevin-laboratory Research Report 2003-3/ME-2, or [http://iewws.nl/B\(2005\)](http://iewws.nl/B(2005)).
- [4] L.M. Kachanov. Introduction to Continuum Damage Mechanics, Martinus Nijhoff Publishers, Dordrecht.
- [5] S. N. Atluri, T. Nishioka and M. Nakagaki, Incremental Path-independent integrals in inelastic and dynamic fracture mechanics, *Engin. Frac. Mech.* Vol. 20, No. 2, pp. 209-244, 1984.
- [6] van der Put T.A.C.M. (1974) Breukcriterium voor beton als ondergrens van de sterkte bepaald volgens de evenwichtsmethode, *Cement* (1974) XXVI No10 pp 420-421 (for concrete).

Chapter 5

ENERGY THEORY OF FRACTURE

5.1. INTRODUCTION

The failure criterion of clear wood, i.e., wood with small defects, is the same as the failure criterion of timber, i.e., notched wood, showing again that the small-crack is dominating and small crack extension towards the macro-crack tip is the cause of macro-crack extension. This small-crack failure criterion thus delivers essential information on macro-crack behavior as discussed in Chapter 10 and in this chapter. The limit analysis derivation of the boundary value problem and applied Airy stress function of the singularity approach of small crack extensions, are given in Chapter 2 and Chapter 10.

5.2. CRITICAL DISTORTIONAL ENERGY AS FRACTURE CRITERION

The failure criterion of wood consists of an anisotropic third degree tensor polynomial (see [1], and Appendix II), which, for the

same loading case, is identical to the Wu-mixed mode I-II-equation [2], eq. (5.2.3). The second degree polynomial part of the failure criterion, eq. (5.2.1), is shown (see Appendix II and [3]) to be the orthotropic critical distortional energy principle for initial yield showing the start of energy dissipation, which is not yet incorporated in the finite element method [4]. By this dissipation according to the incompressibility condition, the minimum energy principle is followed, providing therefore the exact initial yield criterion (see Appendix II) as:

$$\frac{\sigma_x^2}{XX'} + \frac{\sigma_x}{X} - \frac{\sigma_x}{X'} - 2F_{12}\sigma_x\sigma_y + \frac{\sigma_y^2}{YY'} + \frac{\sigma_y}{Y} - \frac{\sigma_y}{Y'} + \frac{\tau^2}{S^2} = 1 \quad (5.2.1)$$

where X, Y are the tension strengths and X', Y' the compression strength in the main directions and S is the shear strength and: $2F_{12} = 1/\sqrt{XX'YY'}$. This value of F_{12} is necessary for the elastic state which also applies at the starting point of initial stress redistribution and micro-crack formation in the matrix. After further straining, F_{12} becomes zero, $F_{12} \approx 0$ at final failure initiation. The absence of this coupling term F_{12} between the normal stresses indicates symmetry, thus (possible random oriented) initial small-cracks are extended during loading to their critical length in the weak planes, the planes of symmetry only. Then, when these small-cracks arrive at their critical crack-density (discussed in § 3.6) and start to extend further, a type of hardening occurs because the reinforcement prevents crack extension in the matrix in the most critical direction. Then, due to hardening, F_{12} and all third degree coupling terms of the tensor polynomial become proportional to the hardening state constants [3] (or see

Chapter 11) and therefore, also dependent on the stability of the test and equipment. For the mixed I-II-loading of the crack plane by tension σ_2 and shear σ_6 , the polynomial failure criterion reduces to:

$$F_2\sigma_2 + F_{22}\sigma_2^2 + F_{66}\sigma_6^2 + 3F_{266}\sigma_2\sigma_6^2 = 1$$

$$\text{or: } \frac{\sigma_6}{S} = \sqrt{\frac{(1 - \sigma_2/Y) \cdot (1 + \sigma_2/Y')}{1 + C\sigma_2/Y'}} \quad (5.2.2)$$

with: $C = 3F_{266}Y'S^2 \approx 0.9$ to 0.99 , depending on the stability of the test. When, due to hardening, C approaches to $C \approx 1$, eq. (5.2.2) becomes eq. (5.2.3), the in § 2.3 exact, theoretically explained, Coulomb- or Wu-equation, with a cut off by the line $\sigma_2 = Y$. Full hardening is thinkable when the testing rig is stiff enough during the test. The solution of the crack problem of Irwin as summation of in-plane and antiplane solutions in order to use isotropic stress functions for the orthotropic case, and to apply descriptions in the three different modes and to sum the result for a general mixed mode case is comparable with this state because it misses the stress interaction term of hardening of eq. (5.2.2), which is not orthotropic by being not quadratic, but contains a third degree term and thus does not show orthotropic symmetry. This hardening coupling term is absent in all general accepted solutions. The stress function which leads directly to the Wu-equation, eq. (5.2.3) is derived in § 2.3.

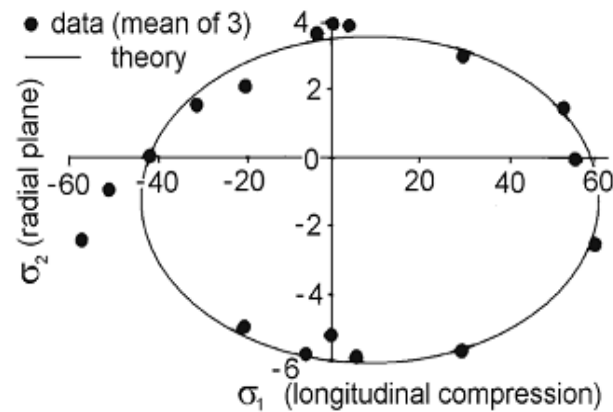
$$\left(\frac{\sigma_6}{S}\right)^2 + \frac{\sigma_2}{Y} \approx 1 \quad \text{or: } \frac{K_{II}^2}{K_{IIc}^2} + \frac{K_I}{K_{Ic}} = 1 \quad (5.2.3)$$

Wrongly, and against the lack of fit test, given by Table 2.1 is for wood and other orthotropic materials, eq. (5.2.2) generally replaced in literature by:

$$\frac{\sigma_2^2}{Y^2} + \frac{\tau^2}{S^2} = 1, \text{ written as: } \frac{K_I^2}{K_{Ic}^2} + \frac{K_{II}^2}{K_{IIc}^2} = 1, \quad (5.2.4)$$

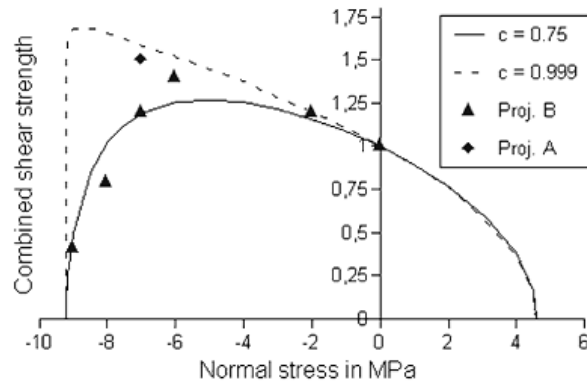
which surely is not a summation of energies as is stated, but is identical to eq. (5.2.1) when it wrongly is assumed that the compression and tension strength are equal for wood and orthotropic materials.

To know the mode of failure, the stresses at the crack boundary should be known. This follows from the exact derivation in [5] and is applied by the VCC- technique of finite element simulation.



Eq. (5.2.2), influence of $3F_{266}\sigma_2\sigma_6^2$,
giving compressional data outside the elliptic curve.

Figure 5.1. (Continued).



The same hardening at compression with (here) dashed parabolic limit eq. (5.2.3).

Figure 5.1.

The influence of $3F_{266}\sigma_2\sigma_6^2$ in eq. (5.2.2), is given by Figure 5.1. The term is not quadratic by containing a third degree term and thus does not show to be orthotropic.

5.3. REVISION OF THE CRITICAL ENERGY RELEASE RATE EQUATION

Based on the failure criterion of § 5.2, adaption of the energy release equation is necessary.

The Griffith strength equation, eq. (3.2.8) of § 3: $\sigma_y^2 = G_c E_y / \pi c$ can be extended by superposition to:

$$\sigma_y^2 + \tau_{xy}^2 = G_c E_y / \pi c \quad (5.3.1)$$

This is only right, when G_c is not constant but may reach values between G_{Ic} and G_{IIc} depending on σ_y / τ_{xy} , because G_c also has to satisfy the failure criterion eq. (5.2.3). In orthotropic stresses, eq. (5.3.1) is $\sigma_y^2 + \tau_{xy}^2 / n_6^2 = G_f E_y / \pi c$ and when $\tau_{xy} = 0$, is $G_f = G_{Ic}$ and $K_{Ic} = \sqrt{E_y G_{Ic}}$. When $\sigma_y = 0$. Is: , $\tau_{xy}^2 \pi c = n_6^2 G_{IIc} E_y = 4n_6^2 G_{Ic} E_y$, because $K_{IIc} = 2n_6 K_{Ic}$ (eq. (2.3.19)). Thus:

$$K_{IIc} = n_6 \sqrt{E_y G_{IIc}} = 2n_6 \sqrt{E_y G_{Ic}} \text{ or: } G_{IIc} = 4G_{Ic} \quad (5.3.2)$$

The failure condition eq. (5.2.3) can be written in fracture energies:

$$\frac{K_I}{K_{Ic}} + \frac{(K_{II})^2}{(K_{IIc})^2} = 1 = \frac{\sqrt{G_I}}{\sqrt{G_{Ic}}} + \frac{G_{II}}{G_{IIc}} = \frac{\sqrt{\gamma \cdot G_f}}{\sqrt{G_{Ic}}} + \frac{(1-\gamma) \cdot G_f}{G_{IIc}} \quad (5.3.3)$$

where, according to eq. (5.3.1):

$$G_f = G_I + G_{II} = \gamma \cdot G_f + (1-\gamma) \cdot G_f \quad (5.3.4)$$

$$\text{Thus: } \frac{\gamma G_f}{(1-\gamma) G_f} = \frac{K_I^2}{K_{II}^2} \text{ or: } \gamma = \frac{1}{1 + \frac{K_{II}^2}{K_I^2}} = \frac{1}{1 + \frac{\tau_{xy}^2}{\sigma_y^2}} \quad (5.3.5)$$

and γ depends on the stress combination τ_{xy} / σ_y in the region of the macro notch-tip and thus not on the stresses of fracture energy

dissipation as generally postulated by the I and II failure modes. This stress combination also may follow from a chosen stress field according to the equilibrium method of limit analysis as is applied in § 6 and § 7. With eq. (5.3.2): $G_{IIc} / G_{Ic} = 4$, eq. (5.3.3) becomes:

$$G_f = 4G_{Ic} / (1 + \sqrt{\gamma})^2 = G_{IIc} / (1 + \sqrt{\gamma})^2 \quad (5.3.6)$$

where γ acts as an empirical constant, explaining the differences in fracture energies depending on the notch structure and shear slenderness of the beam by the different occurring τ_{xy} / σ_y -values according to eq. (5.3.5). Applications of the theory with the total critical fracture energy G_f are given by § 6 and § 7.

The theory is e.g., applied for beams with rectangular end notches as basis of the design rules of the Dutch Timber Structures Code and some other Codes and is a correction of the method of the Euro-Code. In the Euro-Code, an approximate compliance difference is used and a raised stiffness which does not apply for the applied Airy stress function. Further G_{Ic} is used instead of G_f according to eq. (5.3.6). Important is also that the theoretical prediction $G_{IIc} = 4G_{Ic}$ is verified by measuring $G_{IIc} / G_{Ic} = 3.5$ (with $R^2 = 0.64$, thus showing the data to be not very precise).

In comparing results it should be realized that there is a Weibull volume effect of the clear wood strength. Further is a strong hardening possible due to compression, perpendicular to grain at bending failure of small clear single-edge notched specimens, which is wrongly regarded as G_{IIc} resistance increase.

5.4. REFERENCES

- [1] van der Put, T.A.C.M. (1982) A general failure criterion for wood, CIB-W18/IUFRO meeting Boras, Sweden, or: [http://iews.nl/A\(1982\)](http://iews.nl/A(1982)).
- [2] Wu, E.M. (1967) Application of fracture mechanics to anisotropic plates, *ASME J. Appl. Mech. Series E*, 34 4, pp. 967-974.
- [3] van der Put T.A.C.M. (2009) A continuum failure criterion applicable to wood. *J. of Wood Sci*, Vol. 55 No.5. (DOI: 10.1007/s10086-009-1036-2), or: [http://iews.nl/A\(2009\)](http://iews.nl/A(2009)).
- [4] Gopu, Vijaya K. A. (1987) Validity of Distortion-Energy-Based Strength Criterion for Timber Members, *J. Struc. Eng.* 113, No. 12 pp. 2475-2487.
- [5] van der Put T.A.C.M., A new fracture mechanics theory of wood, Nova Science Publishers, Inc. New York, C(2011a) or later publications of <http://iews.nl/seriesC>.

Chapter 6

ENERGY APPROACH FOR FRACTURE OF NOTCHED BEAMS

6.1. INTRODUCTION

The theory of total fracture energy discussed in § 5 was initially developed to obtain simple general design rules for beams with square end-notches and edge joints, loaded perpendicular to the grain design rules of square notches and joints for the Dutch Building Code and later, as correction of the method of [1], published in [2] with the extensions for high beams. Horizontal splitting in short, high beams loaded close to the support, causes no failure because the remaining beam is strong enough to carry the load and vertical transverse crack propagation is necessary for total failure. This is not discussed here because it is shown that also the standard strength calculation is sufficient. In [3, 4] the theory is applied to explain behavior, leading to the final proposal for design rules for the Eurocode, given at § 7.5, and to an always reliable simple design method.

In the following paragraph, the theoretical basis and implementation of the new developments of the energy approach for fracture of notched beams are given and it is shown that the predictions of the theory are verified by the measurements. The presentation of more data can be found in [2].

6.2. ENERGY BALANCE

When crack-extension occurs over the length Δx along the grain, the work done by the constant load V is $V \cdot \Delta\delta$, where $\Delta\delta$ is the increase of the deformation at V . This work is twice the increase of strain energy of the cantilever part: $V \cdot \Delta\delta/2$.

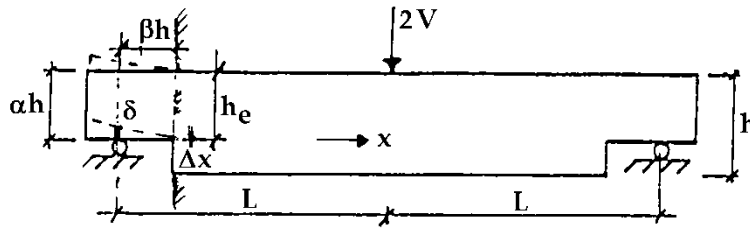


Figure 6.1. Notched beam.

Thus, half of the external work done at cracking is used for crack formation being equal to the other half, the strain energy increase. Thus in general, when the change of the potential energy $\Delta W = V \cdot \Delta\delta/2$ becomes equal to the energy of crack formation, crack propagation occurs. The energy of crack formation is: $G_c b \Delta x = G_c b h \Delta\beta$, where G_c is the crack formation energy per unit crack area. Thus crack propagation occurs at $V = V_f$ when: $\Delta W = V \Delta\delta / 2 = V^2 \Delta(\delta / V) / 2 = G_c b h \Delta\beta$, thus when:

$$V_f = \sqrt{\frac{2G_c b h}{\frac{\partial(\delta/V)}{\partial\beta}}} \quad (6.2.1)$$

and only the increase of the compliance δ/V has to be known. The deflection δ has to be calculated from elementary beam theory representing the first term of the row expansion of the stress division as occurring equilibrium system for virtual work and as a lower bound of the strength. This is close to real behaviour because, according to the theory of elasticity, the deflection can be calculated from elementary beam theory while the difference from this stress distribution is an internal equilibrium system causing no accountable virtual deflection of the beam and also the shear distribution can be taken to be parabolic according to this elementary theory, as only the first order component of this polynomial expansion, contributing to the deflection. As such, influences of initial stresses and deformations have no influence on the strength according to limit analysis theorems.

According to Figure 6.2, the notch can be seen as a horizontal split, case: $a = a'$, and case "a" can be split in the superposition of case "b" and "c," where $b = b'$.

Case "c" now is the real crack problem by the reversed equal forces that can be analyzed for instance by a finite element method, etc. From the principle of energy balance it is also possible to find the critical value of case "c" by calculating the differences in strain energies or the differences in deflections δ by V between case b' and case a' , thus differences in deformation of the cracked and un-cracked part to find $\Delta(\delta/V)$ for eq. (6.2.1). Deformations due to the normal stresses N of case c, are of lower

order in a virtual work equation and should not be accounted. It then follows that case c of Figure 6.2 is equal to a mode I test and $G_c = G_{Ic}$. When the beam is turned upside down, or when V is reversed in direction, then M' and V' are reversed, closing the crack and fracture only is possible by shear, identical to the mode II test and then $G_c = G_{IIc}$. The change of δ by the increase of shear deformation is with $h_e = \alpha \cdot h$:

$$\delta_v = \frac{1.2}{G} \left(\frac{\beta h}{b\alpha h} - \frac{\beta h}{bh} \right) \cdot V \quad (6.2.2)$$

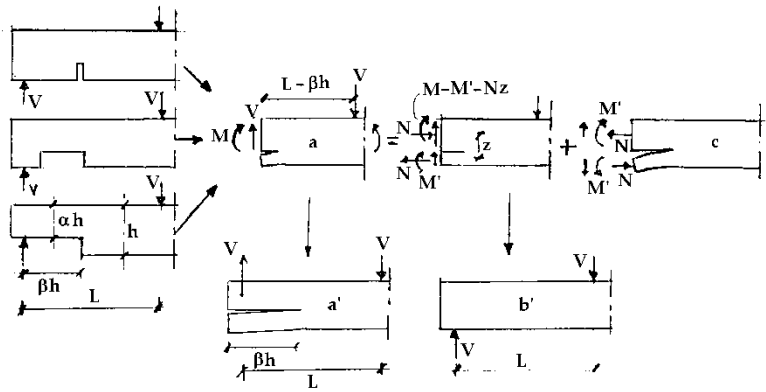


Figure 6.2. Equivalent crack problem according to superposition.

The change of δ by the increase of the deflection is:

$$\delta_m = \frac{V(\beta h)^3}{3Eb(\alpha h)^3/12} - \frac{V(\beta h)^3}{3Eb h^3/12} = \frac{4V\beta^3}{Eb} \cdot \left(\frac{1}{\alpha^3} - 1 \right) \quad (6.2.3)$$

Thus:

$$\frac{\partial(\delta/V)}{\partial\beta} = \frac{1.2}{Gb} \cdot \left(\frac{1}{\alpha} - 1\right) + \frac{12\beta^2}{Eb} \cdot \left(\frac{1}{\alpha^3} - 1\right) \quad (6.2.4)$$

The critical value of V , according to eq. (6.2.1) thus is:

$$V_f = \sqrt{\frac{1.67G_c h b^2}{\frac{1}{G} \left(\frac{1}{\alpha} - 1\right) + \left(\frac{1}{\alpha^3} - 1\right) \cdot \frac{10\beta^2}{E}}} \quad (6.2.5)$$

or:

$$\frac{V_f}{b\alpha h} = \frac{\alpha \sqrt{GG_c/h}}{\sqrt{0.6(\alpha^3 - \alpha^4) + 6\beta^2(\alpha - \alpha^4)G/E}} \quad (6.2.6)$$

For small values of β , eq. (6.2.6) becomes:

$$\frac{V_f}{b\alpha h} = \frac{\sqrt{GG_c/h}}{\sqrt{0.6 \cdot (\alpha - \alpha^2)}} \quad (6.2.7)$$

For high values of β , eq. (6.2.6) becomes:

$$\frac{V_f}{b\alpha h} = \frac{\alpha \sqrt{EG_c/h}}{\beta \sqrt{6(\alpha - \alpha^4)}} \quad (6.2.8)$$

6.3. EXPERIMENTAL VERIFICATION

A verification of the prediction of the theory for high values β , eq. (6.2.8), when the work by shear is negligible, is given by Table

6.1 of an investigation of Murphy, mentioned in [1], regarding a notch starting at $\beta = 2.5$ and proceeding to $\beta = 5.5$. Beams were also tested with a slit at a distance: $\beta = 2.5$. Because the exact eq. (6.2.6) gives a less than 1% higher value, eq. (6.2.8) applies. ($\sqrt{GG_c} = 11.1$ resp. $10.9 \text{ N/mm}^{1.5}$) and: $\sqrt{EG_c} = 48.8 \text{ N/mm}^{1.5}$. This value is used in Table 6.1 for comparison of eq. (6.2.8) with the measurements showing an excellent agreement between theory and measurement. For all specimens was: $\alpha = 0.7$; $\eta = L/h = 10$ (L is distance field loading to support) and $b = 79 \text{ mm}$. The other values are given in Table 6.1.

Table 6.1. Strength of clear laminated Douglas fir with notches in the tensile zone in MPa

H mm	β	number	V/ αbh	
			tests	eq.(6.2.8)
305	2.5	2	0.46	0.47
305	5.5	2	0.24	0.22
457	2.5	2	0.38	0.38
457	5.5	1	0.16	0.17

The fracture energy is: $G_c = (48.8)^2 / 14000 = 0.17 \text{ N/mm} = 170 \text{ N/m}$, which agrees with values of the critical strain energy release rate. The value of K_{Ic} is about: $K_{Ic} \approx \sqrt{0.17 \cdot 700} = 10.9 \text{ N/mm}^{1.5} = 345 \text{ kN/m}^{1.5}$, as is expected by the high density of Douglas fir.

In Table 6.2, data are given for Spruce for low values of β , to verify the then predicted theoretical behaviour according to eq. (6.2.7) with energy dissipation by shear stresses only. It appears for these data that the difference between the mean values

according to eq. (6.2.7) and eq. (6.2.6) are 10% and thus are not negligible and also, the values of eq. (6.2.6) are given to obtain a possible correction factor. It follows from Table 6.2 for Spruce that: $\sqrt{GG_c} = 6.8 \text{ N/mm}^{1.5}$ or: $G_c = 6.8^2 / 500 = 0.092 \text{ N/mm} = 92 \text{ N/m}$.

For Spruce, $K_{Ic} \approx 6.3$ to 7.6 according to [5], depending on the grain orientation and then also applies: $E_2 \approx G$ and: $K_{Ic} = \sqrt{E_2 G_c} = 6.8 \text{ N/mm}^{1.5}$.

Although the fracture energy is shear-stress energy, failure still is by mode I (of Figure 6.2) and not by the shear mode II, as is supposed by other models. Thus the total work contributes to failure, whether it is bending stress energy (Table 6.1) or shear stress energy (Table 6.2) and $\gamma = 1$ (eq. (5.3.5) for failure of this type of notch by the high tensile stress perpendicular to the grain at the notch root.

In [2], more data are given regarding the strength of square notches. The size influence, or the influence of the height of the notched beam on the strength, is tested on beams with notch parameters $\alpha = 0.5$ and 0.75 ; β is 0.5 and heights $h = 50, 100$ and 200 mm with $b = 45 \text{ mm}$ at moisture contents of $12, 15$ and 18% . The strength $\sqrt{GG_f}$ appeared to be independent of the beam depth as expected for macro crack extension along an always sufficient long fracture plane. The value of $\sqrt{GG_f}$ at moisture contents of $12, 15$ and 18% was respectively; $6.7; 7.7$ and $8.0 \text{ Nmm}^{1.5}$. Higher values of $\sqrt{GG_f}$ for Spruce, given in [2], are possible for loads close to the support. Then, horizontal splitting does not cause failure because the remaining beam is strong enough to carry the total load and the derivation is given by regarding vertical crack propagation necessary for total failure (bending failure of the remaining beam).

**Table 6.2. Strength of notched beams, Spruce,
Mohler and Mistler**

h mm	α	β	η/α	b mm	n	V/b α h N/mm ²	var. coef. %	$\sqrt{GG_f}$	
								eq. (6.2.6)	eq. (6.2.7)
								N/mm ^{1.5}	
120	.917	.25	3.4	32	6	2.36	11	(5.8)	(5.5)
	.833		3.8		27	1.93	15	6.4	6.1
	.75		4.2		43	1.68	19	6.6	6.2
	.667		4.7		14	1.52	18	6.5	6.1
	.583		5.4		10	1.5	18	6.8	6.3
	.5		6.3		49	1.59	18	7.4	6.7
	.333		9.5		10	1.48	16	7.0	5.9
	mean								6.8
Testing time more than 1 min., m.c. 11%, $\rho = 510 \text{ kg/m}^3$									

For this mode I, $\sqrt{GG_m} = 57.5 \text{ N/mm}^{1.5} = 1818 \text{ kN/m}^{1.5}$
(comparable with $1890 \text{ kN/m}^{1.5}$ of [5]) For still higher values of α , above $\alpha = 0.875$, compression with shear failure is determining by direct force transmission to the support. In [3] it is shown that Foschi's finite element prediction and graphs, given in [5] can be explained and are identical to eq. (6.2.8).

6.4. REFERENCES

- [1] P.J. Gustafsson, A Study of Strength of Notched Beams, CIB-W18A-21-10-1, meeting 21, Parksville, Vancouver Island, Canada, Sept. 1988.

- [2] T.A.C.M. van der Put, Tension perpendicular to the grain at notches and joints. CIB-W18A-23-10-1, meeting 23, Lisbon, Portugal, Sept. 1990, or: [http://iews.nl/C\(1990\)](http://iews.nl/C(1990)).
- [3] T.A.C.M. van der Put, Modified energy approach for fracture of notched beams. Proceed. COST 508 conf. on fracture mechanics. Bordeaux, April 1992.
- [4] T.A.C.M. van der Put, A.J.M. Leijten, Evaluation of perpendicular to the grain failure of beams, caused by concentrated loads of joints. CIB-W18A/33-7-7, meeting 33, Delft, The Netherlands, August 2000, or: [http://iews.nl/C\(2000\)](http://iews.nl/C(2000)).
- [5] RILEM state of the art report on fracture mechanics, Espoo, 1991.

Chapter 7

ENERGY APPROACH FOR FRACTURE OF JOINTS LOADED PERPENDICULAR TO THE GRAIN

7.1. INTRODUCTION

It was for the first time shown in [1] that fracture mechanics applies for these type of joints. As for square end-notches, the analysis can be based on the compliance change by an infinitesimal crack increase. Because measurements show no difference in strength and fracture energy between joints at the end of a beam (Series G6.1 and G6.2 of [2]) and joints in the middle of the beam (the other G-series), and also the calculated clamping effect difference by crack extension is of lower order, this clamping effect of the fractured beam at the joint in the middle of a beam has to be disregarded. It is necessary to disregard lower order terms of the virtual energy equation of fracture. This applies according to the limit state analysis which is based on the virtual work equations. For end-joints, the split off part is unloaded and

there is no normal force and no vierendeel-girder action at all and the situation and fracture equations are the same as for the notched beams of Chapter 6. For joints in the middle of the beam, splitting goes in the direction of lower moments and is stable until the total splitting of the beam. The analysis in [1, 2] shows this stable crack propagation because the terms in the denominator become smaller at crack length increase, until the shear term remains, giving the maximal value of V according to eq. (7.2.6), the same value as for end-joints. It thus is not true, as is stated in the CIB/W18-discussion of [2], that the analysis and theory are incorrect when virtual lower order terms are omitted in the analysis and that splitting of joints analysis is not comparable to splitting of notched beam analysis. The proof that this neglecting of the vierendeel-action is right, is given (outer the empirical proof by the measurements) by the complete analysis for this case in [3], where also the influence on the strain of normal stresses is accounted, leading to eq. (7.2.5) containing the negligible clamping effect term in the denominator, (based on the assumption that the total splitting of the beam is not the end state).

7.2. ENERGY BALANCE

For a simple calculation of the compliance difference of the cracked and un-cracked state (maintaining the clamping action in the end state), half a beam is regarded, as given in Figure 7.1, loaded by a constant load V . At the start of cracking, the deflection at V increases with δ (see Figure 7.2) and the work done by the force V is: $2\Delta W = V\cdot\delta$, which is twice the increase of the strain energy ($\Delta W = V\cdot\delta/2$) of the beam and therefore the amount ΔW is used to increase the strain energy and the other equal amount of ΔW is used as fracture energy. Because δ is the difference of the

cracked and “un-cracked” state, only the deformation of the cracked part βh minus the deformation of that same part βh in the un-cracked state, needs to be calculated, because the deformation of all other parts of the beam by load V are the same in the cracked and un-cracked states. As discussed at 6.2, the deflection δ has to be calculated from elementary beam theory of elasticity. It thus is not right to regard an additional deformation δ_r , as is done, due to the non-linearity and clamping effect of the cantilevers βh , formed by the crack. The clamping effect change is mathematically of a lower order at an infinitesimal crack extension. If this effect would have any influence, there should be a difference in notched beams in the splitting force for a real square notch of length βh and a vertical saw cut at a distance βh from the support, because that slit has at least twice that clamping effect (see Figure 6.2).

For a connection at the middle of a beam, the following applies after splitting (see Figure 7.1). The part above the crack (stiffness $I_2 = b(1-\alpha)^3 h^3 / 12$) carries a moment M_3 and normal force N and the part below the crack (stiffness $I_1 = b\alpha^3 h^3 / 12$) carries a moment M_1 , normal force N and a shear force V . and at the end of the crack a negative moment of about: $M_2 \approx -M_1$. Further, $M_2 = M_1 - V\lambda$, thus $M_1 = V\lambda / 2$.

The deformation of beam 2 of the cracked part βh is equal to the un-cracked deformation δ_{un} of that part and the deformation of beam 1 is δ_{un} plus the crack opening δ (see Figure 7.1 and 7.2) and δ is:

$$\delta = \frac{1}{2} \cdot \frac{V\lambda^2}{EI_1} \cdot \frac{2}{3} \cdot \lambda - \frac{1}{2} \cdot \frac{M_1\lambda^2}{EI_1} = \frac{1}{3} \cdot \frac{V\lambda^3}{EI_1} - \frac{1}{4} \cdot \frac{V\lambda^3}{EI_1} = \frac{1}{12} \cdot \frac{V\lambda^3}{EI_1} = \frac{V\beta^3}{bE\alpha^3} \quad (7.2.1)$$

The deflection difference of the cracked and un-cracked state is:

$$\delta = \frac{1.2}{G} \left(\frac{\beta h}{b\alpha h} - \frac{\beta h}{bh} \right) \cdot V + \frac{V\beta^3}{bE\alpha^3} \quad (7.2.2)$$

The condition of equilibrium at crack length β is:

$$\begin{aligned} \partial(V \cdot \delta / 2 - G_c b \beta h) / \partial \beta &= 0 \text{ or:} \\ \left\{ \partial(\delta / V) / \partial \beta \right\} \cdot V^2 / 2 &= G_c b h \text{ or,} \end{aligned}$$

with G_c as fracture energy:

$$V_f = \sqrt{\frac{2G_c b h}{\frac{\partial(\delta / V)}{\partial \beta}}}, \quad (7.2.3)$$

where it follows from eq. (7.2.2) that:

$$\frac{\partial(\delta / V)}{\partial \beta} = \frac{1.2}{bG} \left(\frac{1}{\alpha} - 1 \right) + \frac{3\beta^2}{Eb\alpha^3} \quad (7.2.4)$$

and eq. (7.2.3) becomes:

$$V_f = b\alpha h \sqrt{\frac{GG_c / h}{0.6(1-\alpha)\alpha + 1.5\beta^2 G / (\alpha E)}} \quad (7.2.5)$$

For the always relatively small values of β , the previous found eq. (6.2.7):

$$\frac{V_f}{b\alpha h} = \frac{\sqrt{GG_c/h}}{\sqrt{0.6 \cdot (1-\alpha) \cdot \alpha}} \quad (7.2.6)$$

which also applies for notched beams and for end-joints and verifies the lower bound of the strength, predicted by the theory of [2]. This also indicates that only work by shear stresses contributes to fracture. The fit of the equation with vierendeel action, eq. (7.2.5), to the data is not better than the fit by eq. (7.2.6) which shows that the term $1.5\beta^2 G/\alpha E$ is small with respect to $0.6(1-\alpha)\alpha$ and also that β is about proportional to α and is of the same order. Comparison of eq. (7.2.5) and eq. (6.6) shows that the higher value of the end joint is determining for this definition of the strength and the same design rules as for notches are possible for joints when not the joint, but splitting is determining. However, design should be based on “flow “ of the joint before splitting of the beam and the interaction of joint failure and beam splitting has to be regarded as follows.

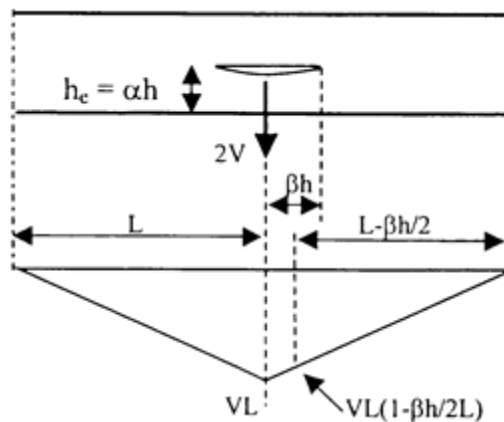


Figure 7.1. Beam with crack by the dowel force of a joint and bending moment.

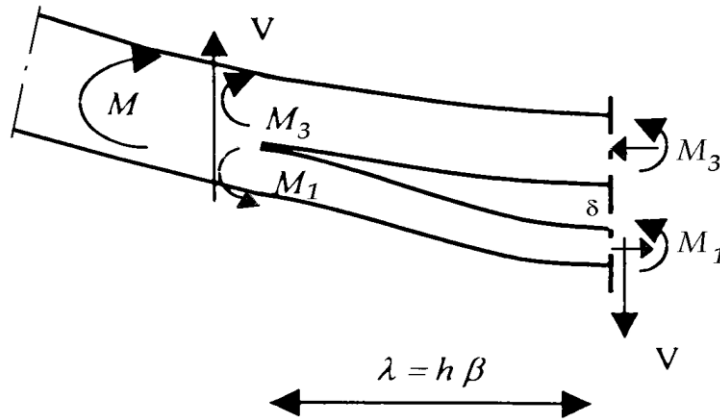


Figure 7.2. Statics of half the crack.

When crack extension starts of a cantilever beam loaded by a constant load V , giving a deflection increase of δ at V , then the applied energy to the beam is $V \cdot \delta$. The energy balance equation then is:

$$V\delta = V\delta/2 + E_c \quad (7.2.7)$$

where $V\delta/2$ is the increase of the elastic energy and E_c the energy of crack extension.

$$\text{Thus: } E_c = V\delta/2 \quad (7.2.8)$$

Thus the energy of crack extension is equal to the increase of elastic energy.

Eq. (7.2.8) can also be written with de incremental deflection $\delta = du$:

$$E_c = V^2 d(u/V)/2 = G_f b h d(\beta) \text{ or:}$$

$$V = \sqrt{\frac{2G_f bh}{\partial(u/V)/\partial\beta}} \quad (7.2.9)$$

where G_f is the fracture energy per unit crack surface and “ $bhd(\beta)$ ” the crack surface increase with “ b ” as width and “ h ” the height of the beam with a crack length $l = \beta h$. When the load on the cantilever beam mentioned above, is prevented from moving, the energy balance, eq. (7.2.7) becomes:

$$0 = E_e + E_c, \text{ or: } E_c = -E_e = -V\delta/2 \quad (7.2.10)$$

for the same crack length and now the energy of crack extension is equal to the decrease of elastic energy in the beam. When the joint at load V becomes determining and is just at the point to start to flow at δ_1 when splitting of the beam occurs, then eq. (7.2.7) becomes:

$$V\delta = (V\delta_1)/2 + V(\delta - \delta_1) + E_c \quad (7.2.11)$$

where again $V\delta_1/2$ is the increase of the elastic energy and $V(\delta - \delta_1)$ the plastic energy of the flow of the joint. From eq. (7.2.11), it then follows:

$$E_c = V\delta_1/2 \quad (7.2.12)$$

the same as eq. (7.2.8), despite of the plastic deformation.

For connections, plastic deformation in the last case will not yet occur because it is coupled with crack extension. When the dowels of the joint are pressed into the wood, the crack opening increases and thus also the crack extension. It can be seen in eq.

(7.2.11), that when flow occurs, the total applied energy $V\delta$ is used for plastic deformation. This is a comparable situation as given by eq. (7.2.10), and the plastic flow coupled crack extension will cause a decrease of the elastic energy. Eq. (7.2.11) thus for joints is:

$$V\delta = (V\delta_1 - \delta_2)/2 + V(\delta - \delta_1) + E_s \quad (7.2.13)$$

where $V\delta_2/2$ is the decrease of the elastic energy by the part of crack extension due to the plastic deformation. From eq. (7.2.13) now follows:

$$E_s = V(\delta_1 + \delta_2)/2 \quad (7.2.14)$$

and eq. (7.2.9) becomes:

$$V = \sqrt{\frac{2G_f bh}{\partial((u_1 + u_2)/V)/\partial\beta}} \quad (7.2.15)$$

From eqs. (7.2.12) and (7.2.14), it follows that $V_c\delta_{1c} = V(\delta_1 + \delta_2)$, where $V_c\delta_{1c}$ is the amount when the connection is as strong as the beam. Thus:

$$\frac{\delta_1 + \delta_2}{\delta_{1c}} = \frac{V_c}{V} = \frac{n_c V_n}{n V_n} = \frac{n_c}{n} \quad (7.2.16)$$

where V_n is the ultimate load of the dowel at flow and n the number of dowels.

Substitution of eq. (7.2.16) into eq. (7.2.15) gives:

$$V = \sqrt{\frac{2G_f bh}{\partial(u_{1c}/V)/\partial\beta} \cdot \frac{n}{n_c}} \quad (7.2.17)$$

which is equal to $\sqrt{n/n_c}$ times the strength according to eq. (7.2.9) for $u = u_{1c}$, thus $\sqrt{n/n_c}$ times the splitting strength of the beam as is applied in [2].

According to eq. (7.2.13), the theoretical lower bound of V according to eq. (7.2.17) occurs at $\delta_1 = \delta_2$, thus when $n/n_c = 1/2$. In [2], the empirical value of 0.5 to 0.4 is mentioned according to the data giving:

$$V = \sqrt{\frac{2G_f bh}{\partial(u_{1c}/V)/\partial\beta}} \cdot \sqrt{0,45} = \sqrt{\frac{2G_f bh}{\partial(u_{1c}/V)/\partial\beta}} \cdot 0.67 \quad (7.2.18)$$

This requirement for “flow” of the joint at failure $\sqrt{GG_f} = 0,67 \cdot 18 = 12 \text{ Nmm}^{-1.5}$ is included in the Eurocode (see § 7.4). This was accepted by CIB-W18 and the Eurocode Committee. The condition $\delta_1 = \delta_2$ means that there is sufficient elastic energy for total unloading and thus full crack extension with sufficient external work for plastic dissipation by the joints. Accordingly, eq. (7.2.14) is for that case:

$$E_c = V\delta_1 \quad (7.2.19)$$

7.3. EXPERIMENTAL VERIFICATION

The value of E_c in eq. (7.2.19) is $12 \text{ Nmm}^{-1.5}$ as follows from the test data given in [2]. In [2], first test-results of 50 beams of [4]

with one or two dowel connections are given for beams of 40x100 and 40x200 mm with α -values between 0.1 and 0.7 and dowel diameters of 10 and 24 mm. In all cases, $n \leq 0.5 \cdot n_c$ and not splitting but “flow” of the connection is determining for failure reaching the (in [2]) theoretically explained high embedding strength by hardening, as expected for the always sufficient high spreading possibility of one- (or two-) dowel joints. The same applies for the 1 and 2 dowel joints of the Karlsruhe investigation. Splitting then is not the cause of failure but the result of post-failure behaviour due to continued extension by the testing device.

Table 7.1 shows that for series B, splitting of the beam is determining. Whether there are 10, 15, 20 or 25 nails per shear plane, the strength is the same $\sqrt{GG_c} = 16.7 \text{ Nmm}^{-1.5}$. This is confirmed by the too low value of the embedding strength of the nails f_c of series B. A more precise value of $\sqrt{GG_c}$ follows from the mean value of $17.1 \text{ Nmm}^{-1.5}$ of series' B2 to B4. Then the value for 10 nails of series B1 is a factor $15.5/17.1 = 0.9$ lower. Thus, $\sqrt{n/n_c} = \sqrt{10/n_c} = 0.9$. Thus, $n_c = 12$ for series B. This means that the number of 5 nails of series A is below $n_c/2 = 6$ and the measured apparent value of $\sqrt{GG_c}$ is the minimal value of $\sqrt{GG_c} \cdot \sqrt{0.5n_c/n_c} = 17.1 \cdot \sqrt{0.5} = 12.1 \text{ Nmm}^{-1.5}$. The same value should have been measured for series C because the number of 3 nails also is below $n_c/2 = 6$. Measured is $11.7 \text{ Nmm}^{-1.5}$. For the 53 beams of all the series G of [2], this is $12.0 \text{ Nmm}^{-1.5}$. As mentioned, a mean value of 12 is now the Eurocode requirement.

Table 7.1 TU-Karlsruhe test data No.1: Joint with nails, [2]

Type	No	d	rows	Col	$a=\alpha h$	a_r	f_c	$\sqrt{GG_c}$	$\eta=L/h$	$F/b\alpha h$
Test	tests		m	N			[2]	eq.(7)		
		mm			mm	mm	MPa	N/mm ^{1.5}		MPa
	beam: b.h=40.180 mm									
A1	8	3.8	5	1	28	76	3.7	13.9	2.37	7.37
A2	4	3.8	5	1	47	76	4.3	13.3	2.37	5.82
A3	3	3.8	5	1	66	76	4.2	11.3	2.37	4.52
A4	3	3.8	5	1	85	76	4.2	10.2	2.37	3.94
A5	3	3.8	5	1	104	76	5.5	11.7	2.37	4.54
	beam: b.h =40.180mm					mean	4.4	12.1		
B1	4	3.8	5	2	47	76	3.5	15.5	2.37	6.77
B2	3	3.8	5	3	66	76	3.8	17.9	2.37	7.15
B3	3	3.8	5	4	85	76	3.3	16.1	2.37	6.21
B4	3	3.8	5	5	104	76	3.6	17.2	2.37	6.69
	beam: b.h = 40.120 m					mean	3.6	16.7		
C1	3	3.8	2	1	28	76	6.8	15.3	2.18	8.51
C2	3	3.8	2	1	28	57	6.2	13.0	2.26	7.21
C3	3	3.8	2	1	28	38	5.6	10.9	2.34	6.07
C4	3	3.8	2	1	28	19	5.7	10.3	2.42	5.73
C5	3	3.8	1	1	28	0	6.9	11.2	2.50	6.21
C6	3	8	1	1	28	0	5.8	9.7	2.50	5.40
	beam: b.h=40.180 mm					mean	6.2	11.7		
L8	1	8	1	1	28	0	5.0	8.8	2.50	4.64

The value of $0.5 \cdot n_c$, depends on the dimensioning of the joint and thus on the amount of hardening by the spreading effect of embedding strength. Thin, long nails at larger distances in thick

wood members are less dangerous for splitting and show a high value of n_c . For series G, with $b = 100$ mm, $n_c/2$ is at least below 8 nails. For series V of [2] with dowels of 16 mm, $n_c = 8.6$. For design, n_c need not be known. But the dimensioning of the joint to meet the requirement of $\sqrt{GG_c} = 12 \text{ Nmm}^{-1.5}$, will lead to the number of nails of $n_c/2$. This dimensioning also determines the value of f_c . The value of $f_c = 4.4$ MPa of series A is lower than $f_c = 6.2$ MPa of series C, in proportion to the square root of the spreading lengths per nail as expected from theory [2].

7.4. DESIGN EQUATION OF EUROCODE 5

As discussed in [2], the shear capacity is (for $h_e \leq 0.7 h$)

$$\frac{V_u}{b\sqrt{h}} = 10.3 \sqrt{\frac{\alpha}{1-\alpha}} = 10.3 \sqrt{\frac{h_e}{h-h_e}} \quad (7.4.1)$$

where $10.3 = (2/3)\sqrt{(GG_c/0.6)}$ is the characteristic value.

This can be replaced by the tangent line through this curve at point $\alpha = 0.5$ giving:

$$\frac{V_u}{b\alpha\sqrt{h}} = 1.7\sqrt{GG_c} = 1.7 \cdot (2/3) \cdot 12 = 13.6 \text{ Nmm}^{-1.5}. \quad (7.4.2)$$

7.4. REFERENCES

- [1] T.A.C.M. van der Put, Tension perpendicular to the grain at notches and joints. CIB-W18A-23-10-1, meeting 23, Lisbon, Portugal, Sept. 1990, or: [http://iews.nl/C\(1990\)](http://iews.nl/C(1990)).
- [2] T.A.C.M. van der Put, A.J.M. Leijten, Evaluation of perpendicular to the grain failure of beams, caused by concentrated loads of joints. CIB-W18A/33-7-7, meeting 33, Delft, The Netherlands, August 2000, or: [http://iews.nl/C\(2000\)](http://iews.nl/C(2000)).
- [3] T.A.C.M. van der Put, DWSF Technical note 11-7, Energy approach of fracture of beams and joints, loaded perpendicular to grain, basic equations, dwsf.nl publication Series 2006, nr.1. ISSN 18-71-675X.
- [4] M. Ballerini: A set of tests on beams loaded perpendicular to the grain by dowel type of joints. CIB-W18/32-7-2. Graz. Austria.

Chapter 8

CONCLUSIONS REGARDING FRACTURE MECHANICS

8.1. CONCLUSIONS OVERVIEW

In this Chapter 8, conclusions are given regarding Chapters 1 to 7.

Conclusions of Chapter 9, regarding the size effect, are given in § 9.5.

Conclusions of Chapter 10 regarding small crack fracture are given in § 10.4.

Conclusions regarding strength theory are given in § 11.5.

8.2. CONCLUSIONS CHAPTER 1 TO 7

- The fracture mechanics of wood is now solely based on the singularity type solutions of the Airy stress function, where collinear crack extension is regarded. This leads to a wrong

mixed mode failure criterion and prevents the possibility of sufficient reliable solutions. The singularity approach thus is not exact and not able to always give the right strength prediction. This leads to the necessary rejection of the singularity approach for strength prediction of new, never measured, cases.

- Wood acts as a reinforced material. The isotropic matrix fails earlier than the reinforcement and determines initial “flow” behavior. It therefore is necessary to solve the Airy stress function for the stresses in the isotropic matrix and then to derive the total (“orthotropic”) stresses from this solution.
- A real failure criterion can only be based on the actual ultimate stress in the material which occurs at the highest stressed crack boundary. A real, physically possible, crack form is the flat elliptical crack, which is the first expanded of any crack boundary form and because the crack is flat, the higher expanded terms have a negligible, in the limit of zero, contribution,
- Strength analysis has to be based on the technical exact theory of limit analysis, at least by applying the lower bound equilibrium method of regarding an equilibrium system which satisfies the boundary conditions and nowhere surmounts the failure criterion. Accordingly, a linear elastic boundary value approach is possible up to the empirical elastic- plastic boundary around the crack tip.
- This stage, after initial “yield,” of confined plasticity near the crack tip can also be replaced by the equivalent linear elastic ultimate stress value, as is also applied for the bending compression strength of wood. Thus, the linear elastic approach is possible up to the crack boundary where an empirical ultimate, uniaxial, cohesive tensile

strength is determining for the strength of general (mixed mode) loading cases.

- This limit analysis approach (which is similar to the Dugdale model), incorporates linear elastic -, as well as non-linear fracture mechanics. There is no distinction between the two.
- Thus, the so called nonlinear fracture mechanics, which only applies for singularity solutions, for instance as correction of infinite stresses, is superfluous, because it is covered by limit analysis.
- It is shown in Chapter 4, that these corrective models of the singularity approach, to replace infinite stresses, as the Hillerborg model, fictitious crack models, J-integral and crack growth models are questionable and not based on theory requirements of Deformation Kinetics and Continuum Damage Mechanics, and therefore have to be replaced by general limit analysis theory, as applied in this publication.
- Determining for the strength is the stress combination at the fracture site, which satisfies the derived, exact mixed mode failure criterion (shown in Chapter 2), which is shown to follow the critical distortional energy criterion for initial crack extension and the Coulomb criterion after “hardening.”
- This mixed mode failure criterion is the consequence of the ultimate uniaxial cohesive strength of the crack boundary near the tip, causing virtual oblique crack extension (which is always possible according to limit analysis theorems). The theory therefore also explains the relations between K_{Ic} and K_{IIc} in TL- and in RL-

direction and the relations between the related fracture energies and energy release rates.

- The derivation in § 2.3, of the mixed mode fracture criterion, shows that fracture mechanics is a two-dimensional problem, and only applies for flat elliptical cracks while for spherical cracks, the ultimate strength theory applies. This explains why the failure criterion equation is the same in both cases. The derivation also shows that Irwin's stress intensity factor is only constant for collinear crack propagation. In § 2.4, it is shown that fracture always occurs in the opening mode for any combined mode I – II stress combination, for any specimen type after some plastic stress redistribution. The mode II shear shift is due to elastic unloading after fracture in the opening mode.
- Based on the reinforced material approach of wood, the mode I and II stress intensities are $K_{Ic} = \sqrt{E_y G_{Ic}}$, $K_{IIc} = n_6 \sqrt{E_y G_{IIc}}$, following from the mode I and II energy release rates, which are related by $G_{IIc} = 4G_{Ic}$ and which are for the total orthotropic stresses for combined mode I – II failure $G_f = G_I + G_{II} = \gamma \cdot G_f + (1 - \gamma) \cdot G_f = 4G_{Ic} / (1 + \sqrt{\gamma})^2$ with $\gamma = 1 / (1 + \tau_{xy}^2 / \sigma_y^2)$ and $n_6 = (2 + \nu_{21} + \nu_{12}) \cdot (G_{xy} / E_y)$.

The theoretical value of $G_{IIc} = 4G_{Ic}$ is verified by reported measurements where ratio 3.5 is found instead of 4 (with $R^2 = 0.64$, explaining the measured difference).

If mode I and/or mode II values are known at combined failure, the following (eq. (5.3.3)) applies:

$$\frac{K_I}{K_{Ic}} + \frac{(K_{II})^2}{(K_{IIc})^2} = 1 = \frac{\sqrt{G_I}}{\sqrt{G_{Ic}}} + \frac{G_{II}}{G_{IIc}} = \frac{\sqrt{\gamma \cdot G_f}}{\sqrt{G_{Ic}}} + \frac{(1-\gamma) \cdot G_f}{4G_{Ic}}.$$

$$\text{Thus: } \frac{\sqrt{G_f}}{\sqrt{G_{Ic}}} = \frac{2}{1+\sqrt{\gamma}}$$

- It is shown in § 2.2.2, that the singularity solution is a special case of the general, exact, non-singular_solution. Therefore it is wrongly stated that when r in that equation goes to zero, σ goes to infinity, but the product is constant by a constant K_A . There is no relation by the applied methods, which confirms this. On the contrary, the derivation of Chapter 2 shows that $r = r_0$ (the boundary of the fracture process zone) is constant and the cohesive strength σ , is also constant for the isotropic matrix. The real singularity is given by $K_A = p\sqrt{\pi c}$, where the applied stress p becomes infinite when the crack length c approaches zero. This follows from the separate exact derivation of the singularity equation in § 10.2, eq. (10.2.4). The external loading stress $\left(Y\sigma / \sqrt{1-(a/x)^2}\right)$ becomes infinite when $x \rightarrow a$, and the crack length $\sqrt{\pi a_c} = \sqrt{\pi 2(x-a)} \rightarrow 0$, when $x \rightarrow a$. However, the product:

$$K_I = \left(Y\sigma / \sqrt{1-(a/x)^2}\right) \sqrt{\pi 2(x-a)} = Yx\sigma \sqrt{2\pi / (x+a)}$$

is constant, equal to $K_I = Y\sigma\sqrt{\pi a}$ for the singularity $x \rightarrow a$. The smallest possible clear wood (micro-) crack length $(x-a)$, is determining for macro-crack extension due to small crack coalescence. It is known from testing

that micro-crack multiplication and merging precedes macro-crack extension.

- As shown by Continuum Damage Mechanics, (§ 4.4), it is necessary for the right theory, that strength analysis is based on the actual stress at the actual intact area, and the strain increase is due to damage caused by the actual stress at the damage location. This explains why approaches based on nominal stresses lead to absurdities, as to the assumption of the existence of strain softening, and negative spring constants, etc. all against basic theorems of science showing the inherent rejection by limit analysis theory.
- The Griffith stress is a nominal stress at the fracture site but, as shown by the stress spreading model, acts as actual stress on the intact, uncracked, not ultimate, but elastic loaded section outside the fracture plane. For fracture, it therefore leads to the following paradox:
 - “At fracture, the elastic energy level is just high enough to cause crack extension of the critical initial crack length. But, at crack extension, the elastic stress level (and thus the elastic energy level) goes down while the crack length increases. Thus there is too little energy to extend this longer crack further. Thus, the Griffith law is not able to explain crack extension at the initial, and following lower stress levels.”
- The formulation of the Griffith law shows that it is an extremum principle and only applies for virtual stresses and displacements and thus only applies for limit analysis approach as necessarily applied in this publication. The reason for this paradox is that nominal stresses are regarded, while fracture laws only apply in real, actual stresses. For the real stress at the fracture site, it applies

that at yield drop, there is an increasingly sufficient high, actual stress level for further fracture as follows from eq. (3.2.10), showing that not only the first derivative but also the second derivative is positive for fracture when critical $c/b > 1/6$.

- In § 3.2, it is shown that, at crack merging of the row of critical small crack density (row A of Figure 3.8), the local strength of adjacent clear material increases by the stress spreading effect (proportional to \sqrt{c}) and therefore gives precisely a constant value of nominal G_{Ic} , (see eq. (3.2.14) to eq. (3.2.17)) which is the reason that the first stage of yield drop still follows the nominal Griffith law. This applies until the maximal possible stress spreading is reached.
- The Griffith, nominal stress law, thus, does not apply for long overcritical initial crack lengths. The energy of elastic crack opening (or closure) is not equal to the crack formation energy for overcritical crack lengths. And because the maximal stress spreading is reached, an ultimate actual stress criterion applies.
- It therefore is shown that strain softening does not exist for real, actual, stress. Softening, called yield drop is only possible for the nominal stress, thus for the actual elastic stress outside the fracture plane and thus represent elastic unloading outside the fracture plane, while the intact part of the fracture plane shows apparent hardening (by the spreading effect) and remains in the ultimate loaded state.
- Yield drop, (wrongly called softening) is only possible when the loading rate is lower than the damage rate, as is normal in a constant strain rate test and is not possible in a

constant loading rate test and not in a dead load to failure test, and thus is not a material property.

- The fracture energy, as area under the yield drop curve should be based on half this area for mode I, as is already applied for mode II. The stress should be, as the Griffith stress, related to the whole width of the specimen, including the initial crack length, and not only to the still intact part of the fracture plane, because then, the fracture energy is different for each different initial crack length. When the fracture energy is related to the whole width, the energy method is correctly based on the energy difference of the cracked and fully un-cracked state of the specimen (as is also the basis of the virtual crack closure method).
- The area of a loading cycle at “yield drop,” divided by the crack length, is indeed equal to the fracture energy, because this area is indeed half the area under the yield drop curve. However, this energy is proportional to the apparent activation energy of all acting processes in the whole test specimen, including visco-elastic and plastic processes, for which responses should be obtained by Deformation Kinetics mainly on a specimen with a blocked crack which then has to be subtracted to obtain the fracture energy. Because this is not applied, and therefore does not lead to crack energy related R-curves, this area method should no longer be applied.
- A derivation of the mode I and II yield drop curves (wrongly called softening curves), according to the Griffith theory is given in Chapter 3. Starting with the critical small crack density, the curve can be explained by an optimal small crack merging mechanism, leading to a row of increasing small crack lengths, showing that this curve is also fully explained by the ultimate state of the decreasing

intact clear wood part in the fracture plane. The yield drop curve follows the so called “stable” part of the Griffith locus. This means that every point of the yield drop curve gives the Griffith strength for the current small crack lengths of the small crack row.

- This yield drop curve depends on only one parameter, the maximal critical Griffith stress σ_c and therefore depends on the critical crack density. This applies until about the 0.38 unloading level. The fracture energy is down to this point equal to the critical energy release rate. After that, the actual strength of the fracture plane of the test specimen becomes determining due to a crack merging mechanism, changing the crack density and intact area of the fracture plane and therefore causing a decrease of σ_c (the top of the yield drop curve) and an apparent decrease of the fracture energy. The strength at every point of the “softening” curve is fully determined by the strength of the intact area of the fracture plane. Yield drop thus is a matter of elastic unloading of the specimen outside the fracture zone and yield drop thus is not a material property.
- Fracture mechanics of wood and comparable materials appears to be determined by small-crack propagation towards the macro-crack tip. This follows from the same failure criterion for “clear” wood and for macro-crack extension. The presence of small-crack propagation is noticeable by the Weibull volume effect of timber strength. There is no influence on macro-crack propagation of the geometry of notches and sharpness of the macro crack-tip in wood (against orthotropic theory). Thus orthotropic fracture mechanics is not determining. This also follows from the nearly same fracture toughness and energy release

rate for wide and slit notches and the minor influence of rounding the notch (also against orthotropic theory). Determining, thus is the influence of small cracks in the isotropic matrix for the total behavior, having the same influence at the tip of wide, as well as, slit notches.

- The theory shows that the Eurocode design rules for beams with rectangular end notches or joints should be corrected to the correct, real compliance difference and the correct, measured uniaxial stiffness.

The verification of the derived theory by measurements shows excellent agreement. The method provides an exact solution and is shown to be generally applicable also for joints and provides simple design equations as wanted

- Because the macro-crack kinetics is the same for timber and clear wood, this small-crack behavior is always determining.
- For long sub critical initial cracks, the ultimate strength of the intact part of the fracture plane, thus the actual stress, is always determining and explains the measured, too low apparent stress intensity which is not determining.
- The ultimate stress of ultimate stress theory, is incorporated in all fracture mechanics laws and is always determining. Therefore it is the complete ultimate stress theory discussed separately in Chapter 11.
- Small-crack coalescence explains precisely the yield drop curve by the strength (or plastic flow stress) of the intact part of the fracture plane, which is always in the ultimate state and is most probable because it requires a lower stress than single macro-crack propagation and shows in rate form, the necessary molecular deformation kinetics equation of this damage process.

-
- The energy approach for the fracture of notched beams and fracture of joints, loaded perpendicular to grain, is simplified by applying the total variable sum of the energy of both modes in the energy balance equation. This leads to the special relation, eq. (5.3.6), of the critical mode I and mode II energies (release rates).
 - It was proposed and accepted by CIB-W18 and the Euro-Code Committee that design for fracture of joints loaded perpendicular to the grain should be based, (as in the past), on the “flow “ of the joint before the splitting of the beam. This is derived and discussed in § 7.2.
At the plastic embedment flow of the dowel, the stress is constant and all external supplied energy by the movement is dissipated. However, by the movement of the dowel crack opening, thus a splitting of the dowel hole occurs, showing dissipation of available elastic energy (see eq. (7.2.13)). This leads to an adapted compliance change equation, showing at which loading level the flow of the dowel is determining for the strength and not splitting of the joint.
 - According to virtual work, limit analysis theorems, there is no influence of initial stresses and deformations, and initial equilibrium systems on the plastic limit or collapse load, when initial dimensions are regarded in the calculations, which is always the case. The addition of corrective equilibrium systems thus has no influence on the collapse load. It remains necessary to regard the uncorrected singularity solution of the Airy stress function. The fictitious crack models thus are not exact and superfluous.
 - There is a negligible, in the limit of zero, influence of the clamping effect of notched beams. Therefore there is no difference in the splitting force for a real square end notch

of length βh and a vertical saw cut at a distance βh from the support, although that slit has at least twice the clamping effect (see Figure 6.2).

Chapter 9

WEIBULL SIZE EFFECT IN FRACTURE MECHANICS OF WIDE ANGLE NOTCHED TIMBER BEAMS

Because the Weibull size effect is normally not regarded as a fracture mechanics subject, this influence is discussed in a separate Chapter.

9.1. OVERVIEW

A new explanation is given for the strength of wide angled notched timber beams by accounting for a Weibull type size effect in fracture mechanics. There the strength of wood is described by the probability of critical initial small crack lengths. This effect is opposed by toughening because of the probability of having a less critical crack tip curvature. The toughening effect dominates at different wide angle notched beams showing different high stressed areas by the different wide notch angles and thus different

influences of the volume effect. This is shown to explain the other power of the depth in eqs. (9.4.7) and (9.4.8), rather than those that apply for the sharp notch value of 0.5 of eq. (9.4.6). It is further explained why, for very small dimensions, also for sharp notches, the volume effect applies. The explanation by the Weibull effect implies that the strength depends on small crack initiation and propagation in the neighbourhood of the macro crack tip. This initial crack population will be different for full scale members, indicating that correction of the applied data is necessary and that additional toughness tests have to be done on full scale (or semi full scale) test specimens. Small cracks fracture mechanics is discussed in Chapter 10.

9.2. INTRODUCTION

Mixed mode fracture of wood shows jumps to the next growth layers at weak spots. This response at randomized stress raisers, near weak spots is indicated by the volume effect of the strength. There is no clear influence on macro-crack propagation of the crack geometry and notch form and sharpness of the macro crack tip, showing orthotropic fracture mechanics, not to be decisive. The determining small crack behavior also follows from the failure criterion of common un-notched, clear wood, being of the same form as the theoretically explained fracture mechanics criterion for notched wood.

The wood matrix is determining for initial failure and not the reinforcement. The failure criterion of unnotched wood shows no coupling term between the reinforcements in the main directions, confirming the orthotropic strength schematization to be non-determining for initial failure. The determining small crack dimension follows from the Weibull size effect. The here treated

strength of wide angle notched beams is an example of a determining size effect in fracture mechanics.

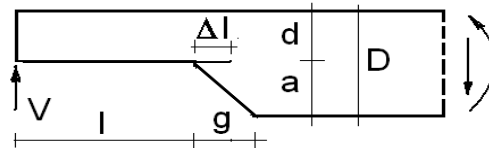


Figure 9.1. Wide angle notched beam element.

The strength analysis of [1], of wide angle notched beams, given in Figure 9.1, was based on the common applied [2], Airy stress function. However, despite the dominant mode I loading, none of the solutions of this function are close enough to the measurements to be a real solution. The reason for this is the absence of the Weibull size effect in the equations as will be shown in this paragraph. The [1] chosen solutions of the biharmonic Airy stress function are $r_1^{\pm n} \cos(n\theta_1)$, $r_1^{\pm n} \sin(n\theta_1)$, $r_2^{\pm n} \cos(n\theta_2)$, $r_2^{\pm n} \sin(n\theta_2)$ resulting in:

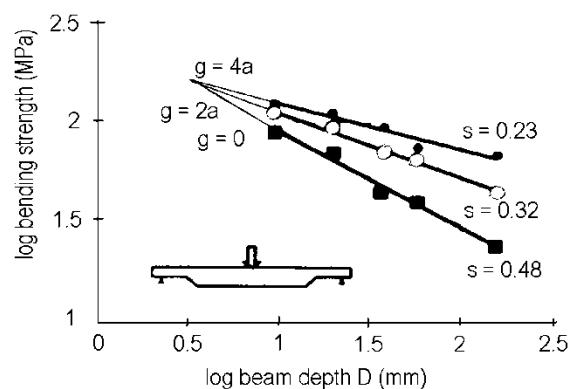


Figure 9.2. Measured bending strengths for different sizes and notch angles.

$$\{\sigma_r, \sigma_\theta, \sigma_{r\theta}\} = \frac{K_A}{(2\pi r)^n} \{f_1(n\theta), f_2(n\theta), f_3(n\theta)\} \quad (9.2.1)$$

where K_A is the stress intensity factor and “ r ” the distance from the notch root. In the direction of crack extension, along the grain ($\theta=0$), the tensile strength perpendicular to the grain σ_θ is determining for fracture. The boundary conditions for the different notch angles a/g , provide different values of the power “ n ” and thus different slopes of the lines in Figure 9.2. However, it is theoretically not possible that these lines intersect through one point, as is measured, because the different boundary conditions by the different notch angles cannot be satisfied at the same time and the chosen mathematical solution of [1] thus has to be rejected. The fact that these lines cross one point at the elementary volume, proves the existence of a volume effect of the strength. This is introduced in the fracture mechanics energy method calculation in § 9.4. In § 9.3, the derivation of the size effect is given to show that the derivation of the toughening size effect in § 9.4 is the same.

9.3. SIZE EFFECT

Due to the initial small crack distribution, clear wood shows a brittle like failure for tension and shear. According to the Weibull model, the probability of rupture due to propagation of the biggest crack in an elementary volume V_0 is equal to $1-P_0(\sigma)$, when P_0 is the probability of survival. For a volume V containing

$N = V/V_0$ elementary volumes the failure probability is:
 $1 - P_s = (1 - P_0)(1 - P_0)(1 - P_0) \cdots = (1 - P_0)^N$.

Thus $\ln(1 - P_s) = N \ln(1 - P_0) \approx -NP_0$ because $P_0 \ll 1$. Thus, the probability of survival of a specimen with volume V , loaded by a constant tensile stress σ , as in the standard tensile test, is given by:

$$P_s(V) = \exp(-NP_0) = \exp\left(-\frac{V}{V_0} \left(\frac{\sigma}{\sigma_0}\right)^k\right) \quad (9.3.1)$$

where $P_0(\sigma) = (\sigma/\sigma_0)^k$ is chosen, because the power law of σ may represent any function of σ around a chosen stress value as the mean failure stress (see § 4.6 for the proof). For a stress distribution, eq. (9.3.1) becomes:

$$P_s(V) = \exp\left(-\int_V \left(\frac{\sigma(x, y, z)}{\sigma_0}\right)^k dx \cdot dy \cdot dz / V_0\right) \quad (9.3.2)$$

This specimen has an equal probability of survival as in the standard test specimen eq. (9.3.1), when the exponents are equal. Thus, when:

$$\int_V \left(\frac{\sigma(x, y, z)}{\sigma_0}\right)^k dV = \left(\frac{\sigma_s}{\sigma_0}\right)^k V_s \quad (9.3.3)$$

For a constant stress $\sigma(x, y, z) = \sigma$, the specimen strength will decrease with its volume V according to:

$$\sigma = \sigma_s \cdot \left(\frac{V_s}{V} \right)^{1/k} \quad (9.3.4)$$

where σ_s is the mean strength of the specimen with volume V_s . The power k depends on the coefficient of variation s/σ according to:

$$\left(\frac{s}{\sigma} \right)^2 = \frac{\Gamma(1+2/k)}{\Gamma^2(1+1/k)} - 1 \quad (9.3.5)$$

From the row-expansion of the Gamma-functions it can be seen that:

$$k \cdot \frac{s}{\sigma} = f\left(\frac{s}{\sigma}\right) \approx 1.2 \quad (9.3.6)$$

where $f(s/\sigma)$ is normally a little varying function. Thus, $1/k = s/(1.2 \cdot \sigma)$

For a stress distribution, eq. (9.3.3) becomes:

$$\int \left(\frac{\sigma_m}{\sigma_0} \right)^k \left(\frac{\sigma(x, y, z)}{\sigma_m} \right)^k dx dy dz = \left(\frac{\sigma_m}{\sigma_0} \right)^k V_{ch} = \left(\frac{\sigma_s}{\sigma_0} \right)^k V_s \quad (9.3.7)$$

where σ_m is the determining maximal stress in volume V and $V_{ch} = \int (\sigma/\sigma_m)^k dV$, a characteristic volume. Eq. (9.3.7) thus becomes:

$$\sigma_m = \sigma_s \left(\frac{V_s}{V_{ch}} \right)^{1/k} = \sigma_s \left(\frac{V_s}{V_{ch}} \right)^{s/1.2\sigma} \quad (9.3.8)$$

This applies for the strength of common unnotched specimens. This strength also is determined by fracture mechanics, in the neighborhood of flat notches. The tensile strength is:

$$f_t = \frac{K_{Ic}}{\sqrt{\pi c}} \text{ or } f_t = f_{t,s} \sqrt{\frac{c_s}{c}}. \quad (9.3.9)$$

where K_{Ic} is the stress intensity factor. Substitution of the strength according to eq. (9.3.4) (or eq. (9.3.8)) leads to:

$$f_t = f_{t,s} \sqrt{\frac{c_s}{c}} = f_{t,s,v} \left(\frac{c_s}{c} \right)^{0.5} \left(\frac{V_s}{V} \right)^{1/k} \quad (9.3.10)$$

This equation gives the probability of a critical Griffith crack length c leading to fracture due to small crack extension from weak spots towards the macro crack tip. Also, in this case, a crack toughening mechanism is thinkable, as discussed in § 9.4, leading to the opposite volume effect with a negative value of the exponent $1/k$. This cannot be distinguished and the resultant value of $1/k$ then is given by eq. (9.3.10). Because for every type of wood material, the value of c is specific, determining the specimen strength, eq. (9.3.8), as shortcut of eq. (9.3.10), is applied in practice.

According to eq. (2.3.7), the stress intensity factor of eq. (9.3.9) is $K_{Ic} = \sigma_t \sqrt{\pi r / 2}$ where σ_t is the equivalent cohesion strength at the crack tip boundary and r is the radius of the elastic-

plastic boundary of the crack tip zone. A constant stress intensity factor K_{Ic} means that $\sigma_t \sqrt{r}$ is constant and only the crack length c is a variable, as for brittle fracture. Toughening means an increase of the plastic zone, thus of r of the small cracks, within the characteristic volume. This influence is visible at the different wide angle notches as discussed in § 9.4.

Because fracture across the grain is tough and the lengths of applied beams don't vary much, the size effect of the length dimension is small, which also implies no volume effect in width direction and the volume effect for bending is replaced by a height effect of the beam only. More probable is that this absence of a width effect is mainly explained by the constant widths of $2b'$ of 2 zones of weakness adjacent to the free sides of the beam due to the cutting action at manufacturing. Then, the height factor of the Codes becomes $(V_s / V_{ch})^{1/k} = (2b'h_s l / 2b'hl)^{1/k} = (h_s / h)^{1/k}$. This width effect is applied in § 9.4, leading to expressions in h / h_s , given as in [1], as D / D_0 .

9.4. SIZE EFFECT OF WIDE NOTCHED BEAMS

The analysis of the strength of notched beams can be based on the energy method where the critical fracture energy is found from the difference of the work done by the constant force due to its displacement by a small crack extension minus the increase of the strain energy due to this displacement. According to this approach of [3, 4], and § 6, the bending stress σ_m at the end of the notched beam at $l = \beta D$ in Figure 9.1 is:

$$\sigma_m = \frac{6V_f \beta D}{b(\alpha D)^2} \approx \frac{\sqrt{6EG_c / D}}{\sqrt{(\alpha - \alpha^4)}}, \quad (9.4.1)$$

when the notch is not close to the support. In [1] it is chosen $\alpha = d/D = 0.5$, which means that $d = a$. Further, the length is $l = 2D$ when $g/a = 0$ and 2 , while $l = 4D$ for $g/a = 4$ in Figure 9.1. E is the modulus of elasticity and G_c the critical energy release rate, given in [3]. Eq. (9.4.1) applies for the rectangular notch ($g = 0$). For wide notch angles a more complicated expression applies because of the changing stiffness over length Δl of the crack extension. However, for given dimensions and loading, the basic form of the equation is the same as eq. (9.4.1), thus:

$$\sigma_m = B\sqrt{EG_c / D} \quad (9.4.2)$$

where B is a constant depending on dimensions and notch angle. According to §2 and [3], it is, as mentioned, $\sqrt{EG_c} \square K_c \square \sigma_t \sqrt{r}$, where σ_t is the equivalent cohesion strength and the crack tip radius r is the only parameter of the notch strength. The volume effect depending on the stress, follows from § 9.3 and the analysis thus can be based on the yield stress and the characteristic volume around the notch tip. For the probability of a critical value of r , of the small initial cracks within the high stressed characteristic volume around the notch tip, the probabilistic reasoning of § 9.3 can be repeated as follows. The probability of having a critical flaw curvature $1/r$ in an elementary volume V_0 is equal to $1 - P_0(1/r)$, when P_0 is the survival probability. For a volume V ,

containing $N = V/V_0$ elementary volumes, the survival probability is in the same way:

$$P_s(V) = \exp(-NP_0) = \exp\left(-\frac{V}{V_0}\left(\frac{r}{r_0}\right)^{-k}\right) \quad (9.4.3)$$

where $P_0(1/r) = (r_0/r)^k$, because the power law may represent any function in $1/r$. At “flow,” this probability is not a function of σ , but of the flow strain, given by a critical r . Equal exponents for the same probability of failure in two cases now lead to:

$$r = r_s (V/V_s)^{1/k} \quad (9.4.4)$$

and eq. (9.4.2) becomes:

$$\begin{aligned} \sigma_m &\approx \frac{B' \sigma_t \sqrt{r_s}}{\sqrt{D}} \cdot \left(\frac{V}{V_s}\right)^{1/2k} \quad \text{or:} \\ \sigma_m &= \sigma_{m0} \left(\frac{D}{D_0}\right)^{-0.5} \left(\frac{V}{V_0}\right)^{1/2k} \end{aligned} \quad (9.4.5)$$

For the notch angle of 90° , ($g = 0$ in Figure 9.1), or for smaller angles, the high stressed elastic region around the crack tip is, as the fracture process zone itself, independent of the beam dimensions. Thus in characteristic dimensions $V = b'l'h' = V_0$ and eq. (9.4.5) becomes:

$$\sigma_m = \sigma_{m0} \left(\frac{D}{D_0} \right)^{-0.5}, \quad (9.4.6)$$

independent of a volume effect. For the widest notch angle of 166° ($g/a = 4$), there is a small stress gradient over a large area and V is proportional to the beam dimensions. Thus, $V (\cdot) b \cdot d \cdot l = \gamma D \cdot \delta D \cdot \beta D = \gamma \beta \cdot \delta D^3$ and $V/V_0 = (\gamma \delta \beta D^3 / \gamma \delta \beta D_0^3) = (D/D_0)^3$. Thus, with $1/k = 0.18$:

$$\sigma_m = \sigma_{m0} \left(\frac{D}{D_0} \right)^{-0.5+3/(2k)} = \sigma_{m0} \left(\frac{D}{D_0} \right)^{-0.23} \quad (9.4.7)$$

For the angle of 153.40° , ($g/a = 2$), the high stressed region dimensions become proportional to the dimensions b and D and:

$V/V_0 = (bdl)/(b_0d_0l) = (\gamma \delta D^2 / \gamma \delta D_0^2) = (D^2 / D_0^2)$ and with $1/k = 0.18$ is:

$$\sigma_m = \sigma_{m0} \left(\frac{D}{D_0} \right)^{-0.5+2/(2k)} = \sigma_{m0} \left(\frac{D}{D_0} \right)^{-0.32} \quad (9.4.8)$$

It follows from Figure 9.2, that the values of exponents of -0.5 , -0.32 , and -0.23 are the same as measured. The coefficient of variation of the tests must have been $1.2 \cdot 0.18 = 0.22$, as is common for wood. According to the incomplete solution of [1], discussed § 9.2, these values of the exponents were respectively 0.437 , -0.363 and -0.327 , thus, too far away from the measurements.

The explanation of a no volume effect of sharp notches due to the invariant characteristic volume, independent of the beam dimensions, explains why for very small beams, also for sharp notches, there is a volume effect because the beam dimensions are restrictive for the characteristic volume. As known, the exponent may also change from -0.5 to -0.23 with the decrease of the beam dimensions. The constant dimensions of the fracture process zone act as a relative increase of the plastic zone for decreasing test beam dimensions and it appears that toughening is the explanation for this volume effect. The lines in Figure 9.2 intersect at the elementary Weibull volume wherefore the depth dimension is $10^{0.6} = 4$ mm with a material bending strength of 147 MPa.

9.5. CONCLUSIONS REGARDING SIZE EFFECT

- A new explanation is given of the strength of wide angled notched beams of [1] by introducing the Weibull type size effect in fracture mechanics, based on the critical small crack length, opposed by the toughening tip curvature of the initial small cracks near the high stressed macro notch tip zone.
- For sharp notch angles, up to 90° , there is no volume effect for full scale specimens, due to the constant characteristic volume of the fracture process zone. Crack extension occurs at the notch tip. For wider notch angles, the peak stresses and stress gradients become lower and are divided over a larger region and influenced by the dimensions of

the specimen and thus a volume effect correction applies. Crack extension towards the notch tip starts at adjacent, high stressed weak spots.

- For very small beams, also for sharp notches, there is a volume effect because then the beam dimensions are restrictive for the characteristic volume. Tests should be repeated on full scale beams for the right effect.
- The intersection of the three lines in Figure 9.2, with different values of “ n ” of eq. (9.2.1), due to different boundary conditions, which cannot apply at the same time for the different notch angles, cannot be explained by the boundary value analysis. This intersection can only be explained due to the volume effect of the strength indicating failure by small crack extension within the high stressed region at the notch tip.
- The measured values of the powers of the depths (or the slopes of the lines of Figure 9.2) are precisely explained by applying the Energy approach and the volume effect correction according to $\sigma_m = \sigma_{m0} (D / D_0)^{-0.5} (V / V_0)^{1/2k}$

9.6. REFERENCES

- [1] R.H. Leicester, Design specifications for notched beams in AS 1720, CIB-W18/38-6-1, meeting 38, Karlsruhe, Germany, August 2005.
- [2] I. Smith, E. Landis, M. Gong, Fracture and Fatigue in Wood, J. Wiley & Sns.

- [3] T.A.C.M. van der Put, Modified energy approach for fracture of notched beams, COST 505 workshop on Fract. Mech. Bordeaux, April 1992.
- [4] T.A.C.M. van der Put, A new fracture mechanics theory of wood, Nova Science Publishers, Inc. New York, 2011.

Chapter 10

SMALL CRACK FRACTURE MECHANICS

10.1. INTRODUCTION

Because small crack behavior is a new subject and has been shown to always be determining for fracture, it is discussed here in a separate chapter as the basis for a necessary, new approach. That small crack extension is determining, is indicated by the volume effect of the strength, as discussed in Chapter 9, and by the unclear influence on the macro-crack propagation of the crack and crack-tip geometry of notches in wood. This behavior is the only possible explanation of yield drop and the dynamics of crack propagation by micro crack extension and small crack merging. The failure criterion of clear wood and of timber [1, 2, 3], and the failure criterion by a single macro notch [3, 4], are the same, showing that small-crack extension towards the macro-crack tip is the cause of macro-crack extension. This is confirmed by the fact that the stress intensity factor is independent on the macro-form of the notch. It is also confirmed by molecular deformation kinetics, showing the same processes in clear and notched wood (see

discussions Annexes B on: iews.nl). Also, the exact solutions given in [4] and below, of the geometric correction factor and of [5] and § 3.7, of the strength behavior of long post-critical crack lengths is totally based on small crack behavior. The small-crack merging mechanism explains in [3] and in § 3.6 and § 3.5, precisely the mode I yield drop curves of [6]. The failure criterion [1], shows no coupling term between the normal stresses at “flow,” and thus shows no dowel action of the reinforcements and there is only a direct interaction of the reinforcement with the matrix and the matrix stresses determine the stresses in the reinforcements. Because the initial small cracks in wood are in the matrix and start to extend in the matrix, the stress equilibrium condition of the isotropic matrix by the matrix-stresses has to be regarded. The isotropic solution of the matrix stresses thus has to be regarded in the end state. The total stresses, due to the reinforcement, then follow by multiplication of the constants factor derived in Chapter 2 and § 2 of [3]. To show that this also applies for the singularity approximation, in § 10.2, (started in [4]), the exact derivation given, of the geometric correction factor of the center notched test specimen, are based on small cracks merging. As known, this geometric correction factor accounts for the difference of finite specimen dimensions with respect to the notch in an infinite plate. Because contrary to macro-crack extension, unloading by yield drop (wrongly called “softening”) by step wise small crack merging is possible at any low mean stress level, it can be postulated that small crack merging always takes place in the high loaded zone near the macro-crack tip and that macro-crack extension is always due to small crack extension and towards the macro-crack tip.

10.2. DERIVATION OF THE GEOMETRIC CORRECTION FACTOR OF THE CENTER NOTCHED SPECIMEN

As mentioned, in eq. (2.3.10), fracture mechanics laws only apply when r_0 (process zone) and σ_t (strength) are constant in $K_{IC} = \sigma_y \sqrt{\pi c_c} = \sigma_t \sqrt{\pi r_0 / 2}$. The singularity approach (called LEFM), as derived in § 2.2.2, as a special case of the exact solution, is shown to be wrongly regarded to be based on $r_0 \rightarrow 0$, and an infinite strength $\sigma_t \rightarrow \infty$. It is necessary in the equation above that $\sigma_y \rightarrow \infty$, $c_c \rightarrow 0$ at the singularity for the right solution. Therefore, the necessary exact derivation of the right geometric correction factor has to be given. For a crack in an infinite plate, which is loaded by a tensile stress σ , the stress distribution along the fracture plane, line AB of Figure 10.2, is:

$$\sigma_{y,\infty} = \frac{\sigma}{\sqrt{1-(a/x)^2}} \quad x > a \quad (10.2.1)$$

where $2a$ is the crack length (including the process zones) and x is the distance from the center of the crack. This stress distribution is according to the solution of the Airy stress function of [7]. Such a solution satisfies the equilibrium, compatibility and boundary conditions and thus is an exact (limit analysis) solution. To obtain the ultimate state of the specimen given in Figure 10.1, we may cut out the specimen dimensions from the infinite plate, as is given in Figure 10.2. Next we may multiply the stress $\sigma_{y,\infty}$ by a (by definition stress independent) factor Y with such magnitude that

the resultant shear loading $2R$ in the planes AD and BC of Figure 10.2 becomes zero. There remains an equilibrium system in those vertical planes giving an internal equilibrium system in the cut-out specimen which, as such, has no influence on the strength when undeformed dimensions are used. Thus, because limit analysis applies with virtual displacements, there is no effect of initial stresses or deformations on the limit collapse load. As a condition for zero values of R , the sum of the normal stresses in the upper plane AB should be equal and opposite to the normal stresses σW in the bottom plane CD, giving:

$$\sigma W = 2 \int_a^{W/2} \sigma_y dx = 2 \int_a^{W/2} \left(Y \sigma / \sqrt{1 - (a/x)^2} \right) dx = Y \sigma W \sqrt{1 - (2a/W)^2} \quad (10.2.2)$$

and the stress multiplication factor thus is:

$$Y = 1 / \sqrt{1 - (2a/W)^2} \quad (10.2.3)$$

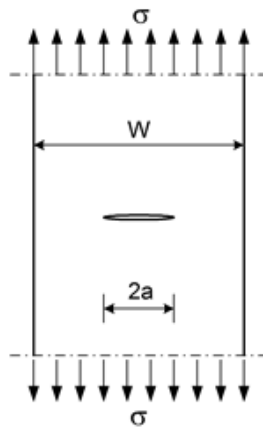


Figure 10.1. CN test specimen.

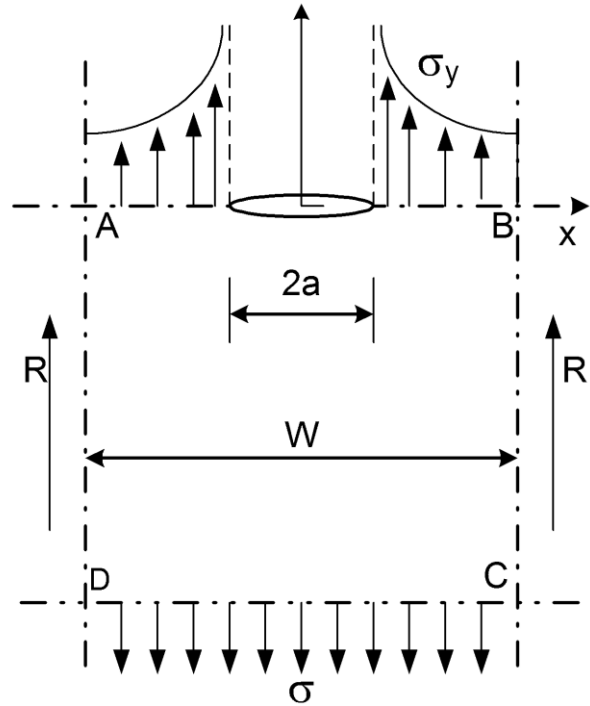


Figure 10.2. Cut out of the specimen from the infinite plate.

The stress intensity factor K_I due to the critical small crack concentration follows from:

$$K_I = \sigma_y \sqrt{\pi a_c} = \sigma_y \sqrt{\pi 2(x-a)} = \left(Y \sigma / \sqrt{1-(a/x)^2} \right) \sqrt{\pi 2(x-a)} = Y x \sigma \sqrt{2\pi / (x+a)} \quad (10.2.4)$$

As shown § 3.6 and in [3], the small crack merging towards the macro-crack tip causes the macro-crack extension. When the nearest, determining small crack tip is situated at a distance x , then the one sided small crack merging distance to the macro-crack tip is $x-a$, which is equal to half the small crack length c of row A of Figure 3.8. Thus, $c = (x-a)$, and total $2(x-a)$ applies to both

sides of the two sided macro-crack extension of the initial crack length of $2a$. This also applies when the macro crack-tip has become sharp enough to take part in the crack merging process. Then, all active crack tips extend over a distance c , which is equal to $c = (x - a)$ in the analysis.

Table 10.1. Comparison of linear elastic geometric correction factors

$2a/W$	$Y = \sqrt{\sec(\pi a / W)}$	$Y = 1/\sqrt{1-(2a/W)^2}$	$Y = \sqrt{(W/\pi a) \cdot \tan(\pi a / W)}$
0.1	1.006	1.005	1.004
0.2	1.025	1.021	1.016
0.3	1.059	1.048	1.040
0.4	1.112	1.091	1.075
0.5	1.189	1.155	1.128
0.6	1.304	1.250	1.208
0.8	1.799	1.667	1.565
0.9	2.528	2.294	2.113
0.95	3.570	3.203	2.918
	Feddersen Koiter et al.	Limit analysis solution, eq.(10.2.3)	Irwin

For $x \rightarrow a$, the lowest, thus first occurring initial flow value for K_I of eq. (10.2.4) becomes:

$$K_I = Y\sigma\sqrt{\pi a} \quad (10.2.5)$$

This is identical to the results of other methods showing the mathematical flat crack, singularity solution, to apply for the smallest initial small crack system and to represent clear wood fracture at the start of “flow” and crack extension (see also § 3.6

and § 3.10). Thus, the derived geometric correction factor Y is comparable to the other solutions of Tada, Feddersen, Koiter, Isida and Irwin [8]. The exact value of Y , according to eq. (10.2.3) $Y = 1/\sqrt{1-(2a/W)^2}$, lies intermediate between the [8] given values of Feddersen and Koiter et al. around $Y = \sqrt{\sec(\pi a/W)}$ and the solution of Irwin $\sqrt{(W/\pi a) \cdot \tan(\pi a/W)}$. In Table 10.1, eq. (10.2.3) is compared with the solution of Irwin and the usual applied Feddersen equation. The precise description by the exact derivation shows that small crack merging does not only explain yield drop, but is the basic mechanism of all crack extension. This is discussed in Chapter 3. The small crack limit behavior is derived in § 10.3. The possibilities of the singularity approach are very limited and extension of the theory for mixed mode loading is not possible by the assumed collinear crack extension.

10.3. SMALL CRACK LIMIT STRENGTH BEHAVIOR

10.3.1. Small Crack Limit Dimensions

The interpretation of the strength data-line of Figure 10.3 on geometrically similar specimens of Bazant, is to regard the inclined line to represent LEFM theory, the horizontal line to be the strength theory and the curved, connecting line to follow nonlinear fracture theory. However, there is no difference between nonlinear and linear elastic (LEFM) fracture mechanics. For both, the linear elastic - full plastic approach of limit analysis applies. The full-plastic zone of the elastic-full plastic approach exists as failure criterion, by a single curve in stress space as shown in Figure 10.3. In this figure from [9], is d/d_0 , the ratio of specimen

size to the fracture process zone size. But, because the line is the result of volume effect tests, the initial crack length is proportional to the test-specimen length. Thus, d/d_0 can also be regarded to be the ratio, initial open crack length to the process zone size. Then, for small values of d , this d/d_0 ratio also may represent the critical small crack density in a macro specimen (d also is small crack interspace).

The curved line of Figure 10.3 follows the equation:

$$\ln \sigma = \ln \sigma_0 - 0.5 \ln(1 + d/d_0) \quad (10.3.1)$$

This can be written:

$$\ln\left(\frac{\sigma}{\sigma_0}\right) = \ln\left(\frac{d_0 + d}{d_0}\right)^{-0.5} = \ln\left(\frac{d_0}{d_0 + d}\right)^{0.5} \quad (10.3.2)$$

$$\text{or: } \sigma \sqrt{\pi(d_0 + d)} = \sigma_0 \sqrt{\pi d_0} = K_c, \quad (10.3.3)$$

This confirms that the curve represents the stress intensity as the ultimate state with K_c as critical stress intensity factor as should be for values of $d/d_0 \gg 1$. For these higher values the curved line approaches the drawn straight, tangent line $\ln \sigma = \ln \sigma_0 - 0.5 \cdot \ln(1 + d/d_0) \approx \ln \sigma_0 - 0.5 \ln(d/d_0)$ with the necessary slope of the curve, (the Bazant - curve): $\frac{\partial \ln(\sigma/\sigma_0)}{\partial \ln(d/d_0)} \approx -0.5$ as limit. The real slope however is:

$$\frac{\partial \ln \sigma}{\partial \ln(d/d_0)} = \frac{\partial \ln(\sigma/\sigma_0)}{(d_0/d) \partial(d/d_0)} = \frac{d}{d_0} \frac{\partial \left(\ln(1 + d/d_0)^{-0.5} \right)}{\partial(d/d_0)} = \frac{d}{d_0} \cdot \frac{-0.5}{1 + d/d_0} = \frac{-0.5}{1 + d_0/d} \quad (10.3.4)$$

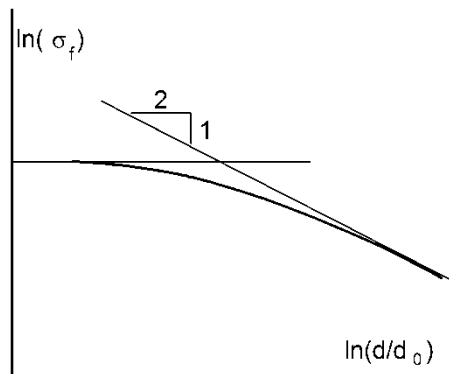


Figure 10.3. From [9]. Limit LEFM behavior as correction of the interpretation of [9].

This slope is -0.5 for $d \gg d_0$ and this slope is zero when $d = 0$.

This shows that for the whole curve, LEFM applies and it is an indication that at zero open crack dimensions, where $d = 0$, the clear wood ultimate strength theory still follows LEFM, because it also applies for the constant initial length d_0 (the fracture process zone length). Thus d_0 acts as a constant minimal blunt small crack length, determining the ultimate strength of strength theory, as shown in § 2.3.

10.3.2. Small Crack Failure Criterion

Softening, called yield drop is explained by the crack merging mechanism and discussed for mode I and II in Chapter 3. Because the isotropic matrix fails before the reinforcement, limit analysis has to be applied for the isotropic stresses in the isotropic matrix. This is not applied by all other fracture mechanics approaches, which therefore don't satisfy the failure criterion and are not able

to give the correct exact mixed mode fracture criterion. At the initial “yield” of the matrix, the stresses of the still elastic reinforcement follow in proportion to the matrix stresses. That the matrix is first determining, follows for Balsa wood, which is highly orthotropic, but is light, and thus has a low reinforcement content and shows total failure soon after matrix failure and shows at failure the isotropic ratio of $K_{IIc} / K_{Ic} \approx 2$ of the isotropic matrix material. For strong clear wood which is failing by shear by single oblique crack extension according to Figure 2.3.2, it appears that the start of crack extension may show the isotropic oblique angle, showing the matrix to be determining for initial failure.

The truss action at the bending failure of a beam, causes a negative contraction coefficient in the bending tension zone. This shows that the reinforcement holds, even after flow in compression and stress redistribution, with increased tension in the reinforcement. It is therefore a requirement for an exact orthotropic solution of the total applied stress, applicable to wood, to also satisfy the isotropic flow solution of matrix-stresses and to look at possible stress redistributions. As discussed in § 5.2 (and Section A of iews.nl), the (small crack) failure criterion for shear with tension is eq. (5.2.1) or eq. (5.2.2), which becomes, as limit behavior, equal to the Wu-equation when due to full hardening, $C \rightarrow 1$ in eq. (5.2.2). Full hardening is possible when the test rig is stiff enough to remain stable during the test. The Irwin solution of the crack problem, as summation of in plane and antiplane solutions in order to use (with minor adaptations) isotropic stress functions for the orthotropic case, and to apply descriptions in the three characteristic modes and to sum the result for the general mixed mode case, is not right for wood. It misses the interaction terms and the failure equation, eq. (5.2.2), is not orthotropic,

because it is not quadratic but contains a third degree term and thus does not show orthotropic symmetry. This coupling term is absent in the general accepted solutions. The strong influence of compression in Figure 5.1 therefore cannot be given. The stress function which leads directly to the Wu-equation is given in § 2.3 and in [3]. Necessary are the stresses at the crack boundary to know the mode of failure. This follows from the exact derivation in Chapter 2 and is applied by numerical simulation by the VCC-technique of the finite element method, and thus cannot be based on a separate calculation of the energy release rates of the normal stress in the opening mode and of the shear stress in the sliding mode according to the method of Sih, Paris, and Irwin, by giving the sum of separate solutions of the 3 modes, without interactions (as $3F_{266}\sigma_2\sigma_6^2$), which are assumed to be possible by assumed isotropic and orthotropic symmetry. Thus, the not orthotropic, “mixed mode,” interactions, as given by Figure 5.1, cannot be described by other methods.

10.4. CONCLUSIONS REGARDING SMALL CRACK FRACTURE MECHANICS

- Part of the conclusions about the need to regard small crack fracture are given in Chapter 8.
- The correct derivation of the geometric correction factor of the center notched specimen is given based on small-crack extension to the macro-crack tip, and based on a constant, finite ultimate cohesion strength and constant dimensions of the process zone and thus is not based on the infinite tensile strength at zero process zone dimensions of all other derivation methods.

- A new interpretation is given of the transition of “strength theory” to “fracture mechanics theory” of Bazant based on tests on geometrically similar specimens. It follows that the whole curve represents LEFM (linear elastic fracture mechanics) and shows that at very small (to zero), open crack dimensions, the clear wood ultimate strength theory still follows LEFM, because it applies also for the adjacent constant initial length of the fracture process zone length. As follows from Chapter 9, the power 0.5 in eq. (10.3.2) shows that a volume effect is acting not as assumed by Bazant.
- Eq. (10.3.3) shows that the crack length should be regarded to consist of an open part plus the process zone length.
- There is no difference between linear elastic- and non-linear fracture mechanics because for both approaches linear elastic behavior is regarded up to failure and plastic flow. This is possible because, by the virtual work approach (regarding no geometrical changes), there is no influence on the strength depending on the loading path followed, and of initial stresses and internal equilibrium systems. The critical energy release rate is, in both cases determined by plastic behavior. In fact, the linear- full plastic approach of limit analysis always applies for the boundary value approach and ultimate state at the crack-tip boundary.
- It is confirmed:
 - that limit analysis applies with elastic-full plastic behavior and may be regarded to be elastic up to fracture, at the confined plastic zone.
- that wood behaves as a reinforced material, and the solutions of the isotropic Airy stress function of the matrix

- stresses as well as the orthotropic Airy stress function of the total stresses are needed.
- that reaction kinetics and the general applicable failure criterion indicate that small-crack processes are always determining for fracture.
 - the explanation of the failure criterion is given. All other methods are not able to give and explain the correct exact Wu-) failure criterion for combined “mixed mode” failure.

10.5. REFERENCES

- [1] van der Put T.A.C.M., A continuum failure criterion applicable to wood, *J Wood Sci* (2009) 55:315–322, or: [http://iewns.nl/A\(2009\)](http://iewns.nl/A(2009)).
- [2] van der Put T.A.C.M., A general failure criterion for wood, Proc. 15th CIB-IUFRO Timber Engineering Group Meeting, Boras, May 1982, or: [http://iewns.nl/A\(1982a\)](http://iewns.nl/A(1982a)).
- [3] van der Put T.A.C.M., A new fracture mechanics theory of wood, Nova Science Publishers, Inc. New York, 2011.
- [4] van der Put T.A.C.M., Exact derivation of the geometric correction factor of the center notched test specimen, based on small cracks merging as explanation of yield drop; *Int. J. Comp. Eng. Res.* Vol. 04, Issue, 7, July 2014, or: [http://iewns.nl/C\(2014a\)](http://iewns.nl/C(2014a)).
- [5] van der Put T.A.C.M., Discussion of: “Mode II fracture mechanics properties of wood measured by the asymmetric four-point bending test using a single-edge-notched specimen of H Yoshihara in *Eng. Frac. Mech.* 75 pp 4727-4739” in *Eng. Frac. Mech.* 90 pp 172-179, or: [http://iewns.nl/C\(2012\)](http://iewns.nl/C(2012)).

- [6] Boström L, Method for determination of the softening behavior of wood etc. Thesis, Report TVBM-1012, Lund, Sweden, (1992).
- [7] Westergaard H.M., Trans. ASME, *J. Appl. Mech.* Vol. 61, 1939, pp A49 – A53.
- [8] Tada H., Paris P.C. and Irwin G.R., The stress analysis of Cracks Handbook.” Del Research Corporation, St. Louis, Missouri, 1985, H. Tada, Paris and G.R. Irwin.
- [9] I. Smith, E. Landis, M. Gong, Fracture and Fatigue in Wood, J. Wiley & Sns.

Chapter 11

STRENGTH THEORY: EXACT FAILURE CRITERION FOR CLEAR WOOD AND TIMBER

11.1. INTRODUCTION

An overview is needed of the development during 3 decades. First, from 1982, [1], to 1993, [2]; second, from 1993 to 2005, [3, 4] and third, from 2005 to now, resulting in this final publication of the general failure criterion. In the first period, the failure criterion, already in the Dutch Code, was adapted for the Draft Eurocode (see [5] – I to IV). In the second period, the anti-theory movement was in charge and replaced sneakily, the exact theory of limit analysis based already, in the past, by CIB-W18 and the Code committee's accepted Code rules ([5]-I to VII), with empirical nonsense rules, which are unacceptable, uneconomical and/or unacceptably unreliable. The new CIB-W18 censorship, based on abstracts selection, prevented any possibility for discussion of theory and of necessary corrections at CIB-W18

meetings. This resulted at last, in a total absence of knowledge of the necessary exact theory and accordingly in withdrawal of the general failure criterion. The now useless Eurocode does not contain any generally applicable continuum failure criterion. This publication thus is necessary to recover this omission.

A general failure criterion for wood was, for the first time derived in [1], which was necessarily based on a tensor polynomial format. This followed from a first derivation of the orthotropic extension of the critical distortional energy principle, in paragraph 2.1.2 of [1], showing this basic principle to have the general form of the second degree tensor polynomial and further by the derivation of paragraph 1.2.4 of [1], showing the third degree tensor polynomial terms to represent hardening behavior up to the exact fracture mechanics mixed mode I - II strength. The further extension to a higher degree tensor polynomial represents the polynomial expansion of the failure criterion, because the measured mean data points represent points of the exact failure criterion, while these points also are the polynomial points, which thus represents the polynomial expansion of the exact failure criterion and as such, as many polynomial terms and data points can be chosen, as is necessary for a fit of the wanted precision.

In the introduction and paragraph 1.1 of [1], the concept of the yield surface of classical plasticity theory is discussed with the conditions of orthotropic symmetry in the main planes. All transformation laws of the stress tensors σ and of the strength tensors F_{ij} are given, making it possible to define the uniaxial strength in any direction. This is shown in paragraph 1.2 of [1], by the fit to test results of tension compression and shear of clear wood. The initial flow properties, perpendicular to grain are fully

and precisely described by the second degree polynomial, confirming the critical distortional energy principle for initial yield. In the longitudinal direction, compressional hardening is possible in the radial plane after this initial yield. This is discussed in paragraph 1.2.4 of [1], leading to the derivation of the Wu-equation of Fracture Mechanics, which also applies for micro-crack extension in clear wood, as explained in [2] and is discussed here in Chapters 1 to 10. In paragraph 1.2.5 of [1], the uniaxial off-grain-axis strength is discussed, leading to the derivation of the Hankinson and Norris equations as initial yield equations. It is shown that the usually applied, von Mises- Hill- Hoffmann- Hankinson- and Norris criteria are special forms of the critical distortional energy principle of yield but are not generally valid. The Hill and Norris criteria only apply for materials with equal compression and tension strengths. Only the Hoffmann criterion accounts for such different strengths. However the Hill and Hoffmann criteria contain a cyclic symmetry of the stresses in the quadratic terms, as applies for the isotropic case which causes a fixed, not free, orientation of the failure ellipse in stress space [1]. These criteria thus cannot apply generally for the orthotropic case. The same prescribed orientation is given by the theoretical Norris equation, being far from wood behavior which shows a zero, or nearly zero, slope of the ellipsoid with respect to the main direction. This explains why the older empirical Norris equation, with zero slope, applied for wood, in the past, in Europe, is not as bad as the later theoretical Norris equation.

A further derivation of [2], discussed in § 11.2, provided the extended Hankinson equations, extended by one hardening parameter, which is able to fit precisely different test results, at different hardening states, by different test methods and the fact

that different values of one parameter are able to precisely fit whole curves of different hardening states of different test types, is the proof that the polynomial third degree terms F_{ijk} determine the hardening state as part of the exact criterion based on a theoretical necessity. This theoretical necessity is explained by the boundary value derivation of the exact mixed mode Wu-equation of fracture mechanics, which is shown to represent these third degree coupling terms (See Chapter 2).

The tensor transformations of F_{ijk} tensors were only given in [1], because the choice was made, in later publications, for the in general more simple stress tensor approach of strengths in the main planes, by expansion of the stresses into the main material planes, providing the fewer number of polynomial terms. However, for information, the general F_{ijk} transformations are also given here in Appendix III.

Paragraph 2 of [1] delivers general information. The method of paragraph 2.2 of determination of hardening rules should not be followed. The method is too complex and only descriptive (phenomenological) and determination of the initial response with gradual “plastic” flow with hardening is not needed for the determination of the ultimate state, which follows from the elastic full plastic approximation of limit analysis.

Extensions of the derivations of [1], given in [2], also involved an alternative derivation of the critical distortional energy criterion of initial yield of orthotropic wood. However the final, exact derivation is given here in Appendix II. A further discussion in [2] is given of the third degree shear coupling terms with special hardening effects due to micro-crack arrest by strong layers occurring after initial yield. It followed, that for a precise fit, without meaningless higher degree polynomial terms, separate

criteria are necessary for tension and for compression. This is obvious because of the different failure mechanisms of tension and compression. This is applied to resolve the initial yield equation, eq. (2.14), into 2 factors, giving a factor for compression and a factor for tension failure, leading to the product of the Hankinson equations for tension and compression. In [2], also the derivation is given of the exact modified Hankinson criterion and of the general form of the higher degree constants and how they can safely be determined from oblique uniaxial loading tests.

An extension of the tensor polynomial method was given [5]-V, by a general approach for anisotropic, not orthotropic, behavior of joints (as punched out metal plates) and the simplification of the transformations by 2 angles as variables.

A confirmation of the results of [1] by means of coherent measurements (only in the radial-longitudinal plane) of [6] provided the generalization to an equivalent, quasi homogeneous, polynomial failure criterion for timber (wood with small defects). These measurements also show a determining influence of hardening on the equivalent main strengths and on the failure criterion of wood. This follows from the theoretical explanation in [2] and Chapter 2, of the Wu fracture mechanics criterion for layered composites.

The mentioned main developments and further developments to [3, 4] contributed to the final derived theory. Design and control calculations have to be based on the exact theory of limit analysis by the lower bound equilibrium method. Essential for design thus is the derivation and estimation of the exact failure criterion for wood. The influence of temperature, moisture content, creep and loading rate on the behavior at “flow” and failure is given in Section B of *iew.s.nl*, or in [7] (see Figure 5.6 of [7]). The molecular deformation kinetics rate equations [7], provide the physical constitutive equations for wood and other materials.

11.2. THE GENERAL FAILURE CRITERION FOR WOOD POLYMERS

11.2.1. General Properties

A yield- or flow-criterion gives the combinations of stresses whereby flow occurs in an elastic-plastic material, like wood in compression. For more brittle failure types in polymers with glassy components like wood at tensile loading, there is some boundary where above the gradual flow of components at peak stresses and micro-crack formation may have a similar effect on stress redistribution as flow, especially for long term loading. It is discussed in [2] and later, that these flow and failure boundaries may be regarded as equivalent elastic-full- plastic flow surfaces of limit analysis. The initial loading line shows gradual flow and hardening and stable micro-cracking up to final “flow” at the top. The following unloading is elastic and reloading shows a linear elastic loading up to flow at the same top. This is independent of the loading history (by unaltered geometry) and the linear elastic loading up to full plastic failure can be chosen to determine the ultimate state. The full plastic state is a line in a cross section of stress space and the flow- or failure criterion is a closed surface in the stress space, i.e., a more dimensional space with coordinates $\sigma_1, \sigma_2, \sigma_3, \sigma_4, \sigma_5, \sigma_6$. A cut, according to Figure 2.1 through the plane of the coordinate axes $x = \sigma_1$ and $y = \sigma_2$, will show a closed curve, and such a curve always can be described by a polynomial in x and y like:

$$ax + by + cx^2 + dy^2 + exy + fx^3 + gy^3 + hx^2y + ixy^2 + \dots = k \quad (11.2.1)$$



Figure 11.1. Failure ellipsoid and definition of positive stresses.

whereby as much as terms can be accounted for as is necessary for the wanted precision. The surface will be concave because of the normality principle, and higher degree terms, causing local peaks on the surface (and thus causing inflection points) are only possible by local hardening effects depending on the loading path and are outside the initial flow-criterion. It can also be seen that the constants f and g are indeterminate and have to be taken as zero because for $y = 0$, eq. (11.2.1) becomes $ax + cx^2 + fx^3 = k$, having the real roots x_0 , $-x_1$, $-x_2$ and thus can be written:

$$(x - x_0) \cdot (x + x_1) \cdot (x + x_2) = 0 \quad (11.2.2)$$

Because there are only two points of intersection possible of a closed surface with a line, there are only two roots by the intersecting x -axis, being $x = x_0$ and $x = -x_1$ and the part $(x + x_2)$, never being zero within or on the surface and thus is indeterminate, and has to be omitted. For a real concave surface “ F ” thus is necessarily zero. The same applies for g , $g = 0$ following from the roots of y when $x = 0$. The equation can systematically be written as stress-polynomial like:

$$F_i \sigma_i + F_{ij} \sigma_i \sigma_j + F_{ijk} \sigma_i \sigma_j \sigma_k + \dots = 1 \quad (i, j, k = 1, 2, 3, 4, 5, 6) \quad (11.2.3)$$

In [1] it is shown that clear wood can be regarded to be orthotropic in the main planes and the principal directions of the strengths are orthogonal (showing the common tensor transformations) and higher degree terms, which are not always due to possible hardening, should be neglected, so that eq. (11.2.3) becomes:

$$F_i \sigma_i + F_{ij} \sigma_i \sigma_j = 1 \quad (i, j = 1, 2, 3, 4, 5, 6) \quad (11.2.4)$$

In [2], and as discussed in Appendix II, it is shown that this equation represents the orthotropic critical distortional energy criterion for initial flow or failure. In eq. (11.2.4), for reasons of energetic reciprocity, $F_{ij} = F_{ji}$ ($i \neq j$) and by orthotropic symmetry in the main planes (through the main axes along the grain, tangential and radial) there is no difference in positive and negative shear-strength and terms with uneven powers in σ_6 thus are zero or $F_{16} = F_{26} = F_6 = 0$; and there is no interaction between normal- and shear-strengths or $F_{ij} = 0$ ($i \neq j$; $i, j = 4, 5, 6$).

Thus eq. (11.2.4) becomes for a plane stress state in a main plane:

$$F_1 \sigma_1 + F_2 \sigma_2 + F_{11} \sigma_1^2 + 2F_{12} \sigma_1 \sigma_2 + F_{22} \sigma_2^2 + F_{66} \sigma_6^2 = 1 \quad (11.2.5)$$

For a thermodynamic allowable criterion (positive finite strain energy), the values F_{ii} must be positive and the failure surface has to be closed and not be open-ended and thus the interaction terms are constrained to:

$$F_{11}F_{22} > F_{12}^2 \quad (11.2.6)$$

($F_{11}F_{22} = F_{12}^2$ gives a parabolic surface and $F_{11}F_{22} < F_{12}^2$ is hyperbolic, both open ended)

For the uniaxial tensile strength $\sigma_1 = X$ ($\sigma_2 = \sigma_6 = 0$) and eq. (11.2.5) becomes:

$$F_1\sigma_1 + F_{11}\sigma_1^2 = 1 \text{ or: } F_1X + F_{11}X^2 = 1 \quad (11.2.7)$$

and for the compression strength $\sigma_1 = -X'$ this is:

$$-F_1X' + F_{11}X'^2 = 1 \quad (11.2.8)$$

It follows from eq. (11.2.7) and (11.2.8) that F_1 and F_{11} are known:

$$F_1 = \frac{1}{X} - \frac{1}{X'}, \text{ and } F_{11} = \frac{1}{XX'} \quad (11.2.9)$$

In the same way, for $\sigma_1 = \sigma_6 = 0$, in the direction perpendicular:

$$F_2 = \frac{1}{Y} - \frac{1}{Y'}, \text{ and } F_{22} = \frac{1}{YY'} \quad (11.2.10)$$

Further it follows for $\sigma_1 = \sigma_2 = 0$ (pure shear), for the shear strength S , that:

$$F_{66} = \frac{1}{S^2} \quad (11.2.11)$$

and according to eq. (11.2.6) is:

$$-1/\sqrt{XX'YY'} < F_{12} < +1/\sqrt{XX'YY'} \quad (11.2.12)$$

It can be shown (as discussed in [1]) that the restricted values of $2F_{12}$, based on assumed coupling according to the deviator stresses, as given by Norris [8], Hill or Hoffmann [9] as $2F_{12} = -1/2XY$, or $F_{12} = -(1/X^2 + 1/Y^2 - 1/Z^2)$ are not general enough for orthotropic materials and don't apply for wood. There is also no reason to restrict F_{12} according to Tsai and Hahn [10] as $2F_{12} = 1/\sqrt{XX'YY'}$ or according to Wu and Stachurski [11] as $2F_{12} \approx -2/XX'$. These chosen values suggest that F_{12} then is about 0.2 to 0.5 times the extreme value of eq. (11.2.12).

The properties of a real physical surface in stress space have to be independent on the orientation of the axes and therefore the tensor transformations apply for the stresses σ of eq. (11.2.5). These transformations are derived from the equilibrium of the stresses on an element, formed by the rotated plane and on the original planes, or simply, by the analogous circle of Mohr construction. For the uniaxial tensile stress then is:

$$\sigma_1 = \sigma_i \cos^2 \theta \quad \sigma_2 = \sigma_i \sin^2 \theta \quad \sigma_6 = \sigma_i \cos \theta \sin \theta$$

Substitution in eq. (11.2.5) gives:

$$F_1\sigma_t \cos^2 \theta + F_2\sigma_t \sin^2 \theta + F_{11}\sigma_t^2 \cos^4 \theta + (2F_{12} + F_{66})\sigma_t^2 \cos^2 \theta \sin^2 \theta + F_{22}\sigma_t^2 \sin^4 \theta = 1 \quad (11.2.13)$$

and substitution of the values of F :

$$\begin{aligned} \sigma_t \cos^2 \theta \left(\frac{1}{X} - \frac{1}{X'} \right) + \sigma_t \sin^2 \theta \left(\frac{1}{Y} - \frac{1}{Y'} \right) + \frac{\sigma_t^2 \cos^4 \theta}{XX'} + 2F_{12}\sigma_t^2 \sin^2 \theta + \frac{\sigma_t^2 \sin^4 \theta}{YY'} + \\ + \frac{\sigma_t^2 \cos^2 \theta \sin^2 \theta}{S^2} = 1 \end{aligned} \quad (11.2.14)$$

It can be seen that for $\theta = 0$, this gives the tensile- and compression strength in e.g., the grain direction $\sigma_t = X$ and $\sigma_t = -X'$, and for $\theta = 90^\circ$, the tensile and compression strength perpendicular to the grain $\sigma_t = Y$ and $\sigma_t = -Y'$, and that a definition is given of the tensile and compression strengths in every direction. These are the points of intersection of the rotated axes with the failure surface. Eq. (11.2.13) thus can be read in this strength component along the rotated x-axis $\sigma_t = \sigma_1$ according to:

$$F'_1 \sigma_1 + F'_{11} \sigma_1^2 = 1 \quad (11.2.15)$$

and eq. (11.2.13) gives the definition of the transformations of F'_1 and F'_{11} . The same can be done for the other strengths. The transformation of F'_{ij} thus also is a tensor-transformation (of the fourth rank) that follows from the rotation of the symmetry axes of the material. Transformation thus is possible in two manners. The stress-components can be transformed to the symmetry directions according to eq. (11.2.5), or the symmetry axes can be rotated,

leaving the stresses along the rotating axes unchanged. For this case the general polynomial expression eq. (11.2.16) applies:

$$F'_{11}\sigma_1 + F'_{22}\sigma_2 + F'_{11}\sigma_1^2 + 2F'_{12}\sigma_1\sigma_2 + F'_{22}\sigma_2^2 + F'_{16}\sigma_1\sigma_6 + F'_{26}\sigma_2\sigma_6 + F'_{66}\sigma_6^2 = 1 \quad (11.2.16)$$

These transformations of strength tensors F' are given in [1] and in Appendix III.

11.2.2. Initial Yield Criterion and Derivation of the Hankinson and Extended Hankinson Equations

As mentioned, eq. (11.2.5) or eq. (11.2.14) for the off-grain-axis tensile- and compression strengths, represents the initial yield condition being the extended orthotropic critical distortional energy principle derived in Appendix II. This “initial yield” equation, eq. (11.2.14), can be resolved into factors as follows:

$$\left(\frac{\sigma_t \cos^2 \theta}{X} + \frac{\sigma_t \sin^2 \theta}{Y} - 1 \right) \cdot \left(\frac{\sigma_t \cos^2 \theta}{X'} + \frac{\sigma_t \sin^2 \theta}{Y'} + 1 \right) = 0 \quad (11.2.17)$$

giving the product of the Hankinson equations for tension and for compression, (where X and X' are the tensile and compressional strengths in grain direction). This applies when:

$$2F'_{12} + 1/S^2 = 1/X'Y + 1/XY' \quad (11.2.18)$$

In this equation, derived in [1], $(1/X'Y + 1/XY')$ is of the same order, and thus about equal to $1/S^2$ so that $2F_{12}$ is of lower order with respect to $1/S^2$. In [2], eq. (11.2.18) was used as a measure for F_{12} which is a difference of two higher order quantities and thus cannot give a precise information of the value of F_{12} , that also can be neglected as first estimate. In [12], the sum of $1/S^2$ and $(1/X'Y + 1/XY')$ is incorrectly taken to be equal to $2F_{12}$, being of higher order with respect to the real value of $2F_{12}$ and it is evident that this value did not satisfy eq. (11.2.12) for a closed surface.

Eq. (11.2.17) shows that the exponent “n” of the generalized Hankinson formula eq. (11.2.19):

$$\frac{\sigma_t \cos^n \theta}{X} + \frac{\sigma_c \sin^n \theta}{Y} = 1 \quad (11.2.19)$$

is: $n = 2$ for tension and compression at initial yield when there are no higher degree terms. A value of n , different from $n = 2$ thus means that there are third degree terms due to hardening after initial yield as in eq. (11.2.21).

The initial yield criterion eq. (11.2.14) or eq. (11.2.17), being for orthotropy, the extended critical distortional energy principle, should satisfy both the elastic and the yield conditions at the same time. Because the Hankinson equation with $n = 2$ also applies for the axial modulus of elasticity and because this modulus is proportional to the strength, the Hankinson equations with $n = 2$, eq. (11.2.17), satisfies this requirement. Thus $n = 2$ is necessary for initial yield. Thus after some strain in the elastic stage, the initial yield is reached and because the modulus of elasticity follows the

Hankinson equation with $n = 2$, also the yield criterion, eq. (11.2.17), containing the Hankinson equations, follows this and has the quadratic form and no higher degree terms. This also is measured. It is mentioned in [13], that for glulam and for clear wood in bending and in tension, $n \approx 2$. The combined compression with shear tests (of Keylwerth by the “Schereisen,” allowing only shear-deformation in one plane) show that for off-axis longitudinal shear, also in the radial plane, $n = 2$, showing no higher degree terms for the shear strength. According to Figure 11.4, this also applies for the tangential plane, but not for the radial plane. The value of n thus depends on the type of test and it is mentioned by Kollmann [14], that $n \approx 2.5$ for compression of clear wood, showing that hardening was possible in the tests and the third degree terms of the yield criterion are not zero [2]. The test method of [6] shows that F_{112} , F_{166} and F_{266} in the radial plane have an influence (what is shown to be the hardening effect due to crack arrest). Thus the test method (early instability by loss of equilibrium of the test or not) has influence on whether only initial yield ($n = 2$), or a more stable failure will occur (n different from $n = 2$). Thus, when $n \neq 2$, higher degree terms are not zero in the failure criterion and eq. (11.2.21) applies.

An equation of the fourth degree (eq. (11.2.21) in σ_t) can always be written as the product of two quadratic equations, eq. (11.2.20). For a real failure surface, the roots will be real and because the measurements show that one of the quadratic equations is determining for compression- and the other for tension- failure mechanisms and must be valid for zero values of C_t and/or C_d as well, this factorization leads as the only possible solution to be the product of extended Hankinson equations for tension and compression as follows:

$$\left(\frac{\sigma_t \cos^2 \theta}{X} + \frac{\sigma_t \sin^2 \theta}{Y} - 1 + \sigma_t^2 \sin^2 \theta \cos^2 \theta \cdot C_t \right) \cdot \left(\frac{\sigma_t \cos^2 \theta}{X'} + \frac{\sigma_t \sin^2 \theta}{Y'} + 1 + \sigma_t^2 \sin^2 \theta \cdot \cos^2 \theta \cdot C_d \right) = 0 \quad (11.2.20)$$

Performing this multiplication, eq. (11.2.20) thus is in general:

$$F_1 \sigma_t \cos^2 \theta + F_2 \sigma_t \sin^2 \theta + F_{11} \sigma_t^2 \cos^4 \theta + (2F_{12} + F_{66}) \sigma_t^2 \cos^2 \theta + F_{22} \sigma_t^2 \sin^4 \theta + 3(F_{112} + F_{166}) \sigma_t^3 \cos^4 \theta \cdot \sin^2 \theta + 3(F_{122} + F_{266}) \sigma_t^3 \sin^4 \theta \cdot \cos^2 \theta + 12F_{1266} \sigma_t^4 \cos^4 \theta \sin^4 \theta = 1 \quad (11.2.21)$$

giving the third degree tensor polynomial, applied in [1, 6], where it appeared that F_{1122} and other possible higher degree terms can be neglected except F_{1266} (for completeness of the factorization).

The values C_t and C_d can be found by fitting of the modified ‘‘Hankinson equations’’ eq. (11.2.20), for uniaxial off-axis tension and compression test results, giving the constants:

$$\begin{aligned} 2F_{12} &= 1/X'Y + 1/XY' - 1/S^2 + C_t - C_d; \\ 3(F_{112} + F_{166}) &= C_t/X' + C_d/X; \\ 3(F_{122} + F_{266}) &= C_t/Y' + C_d/Y; \\ \text{and } 12F_{1266} &= C_t C_d - 12F_{1122} \approx C_t C_d \end{aligned} \quad (11.2.22)$$

A fit of the Hankinson power equation, eq. (11.2.19) always is possible and different n values for tension and compression from $n = 2$ in that equation means that there are higher degree terms and that C_t and C_d are not zero, as follows from eq. (11.2.20).

For timber with defects and grain and stress deviations, the axial strength is determined by combined shear and normal stress perpendicular to the grain. This may cause some stable crack propagation and a parabolic curve of the effective shear strength (according to the Mohr- or Wu-equation, eq. (11.2.27) with $C = 1$) given by a third degree term. For timber n can be as low as $n \approx 1.6$ in eq. (11.2.19) for tension, showing higher degree terms to be present. This also follows from $n \approx 2.5$ for compression. The data of [6], show that F_{166} , F_{266} and F_{112} of the radial plane have influence showing (see Figure 11.3, 11.4, 11.9, and 11.7), the parabolic like curves, different from elliptic curves of 2nd degree, at the longitudinal tension side, of Figure 11.6. It could be expected for clear wood that $F_{166} = 0$ and $F_{122} = 0$ because the longitudinal stress σ_1 is in the plane of the crack and not influenced by the crack tip. However collinear crack propagation is not possible at shear failure and also due to grain deviations in timber there is an influence on F_{166} and F_{122} .

It was shown in [1] that F_{12} is small and cannot be known with a high accuracy. Small errors in the strength values (X, X', Y, Y', S) may switch F_{12} from its lower bound to its upper bound, changing its sign and the value thus is not important and thus negligible for a first estimate. The data of [6] of the principal stresses in longitudinal tension, being close to initial yield, show F_{12} to be about zero at initial yield, thus when $C_d = C_t = 0$ and thus when:

$$1/S^2 = 1/X'Y + 1/XY' \quad (11.2.23)$$

Then eq. (11.2.22) suggests that:

$$2F_{12} = C_t - C_d \quad (11.2.24)$$

due to hardening when C_t and C_d are not zero. This is tested in [2] and it appears that because $F_{12} \approx 0$ for longitudinal tension, S follows, (according to eq. (11.2.22), from $1/S^2 = 1/X'Y + 1/XY' + C_t - C_d$ and S should not be measured separately by a different type of shear test, but follows (as the other strength values), from the uniaxial off-axis tension- and compression tests. Because F_{1122} is negligible, is, according to eq. (11.2.22): $12F_{1266} \approx C_t C_d$, which is also small and negligible. F_{166} will have a similar bound as F_{266} , as follows from eq. (11.2.27) what is given in Figure 2.4.1 and follows by replacing the index 2 by 1 and Y by X . However the determining bound of F_{166} follows from eq. (11.2.22), when F_{112} is known. F_{112} is not discussed in [1], but a general method to determine the bounds of F_{112} is given in [1], for F_{266} . The estimation that in § 11.2.4, of F_{112} , based on σ_1 and σ_2 alone, ($\sigma_6 = 0$) also is sufficient.

It appears not possible to have one failure criterion for the different failure types of longitudinal tension and longitudinal compression. For the longitudinal tension fit, the hardening constants F_{112} , F_{12} and F_{122} are zero by without hardening. For the longitudinal compression fit, these constants are not zero and F_{112} , thus hardening, dominates. For tension, the early instability

of the test, by splitting, determines the strength, while for compression the late instability after hardening defines failure. It thus is necessary for a precise fit, to fit both regions (longitudinal tension and compression) separately and not to apply one overall criterion for longitudinal tension and compression. With the estimates of F_{266} and F_{112} to be close to their bounds for compression, and with zero normal coupling terms for tension, all constants are known, according to eq. (11.2.22), depending on C_d and C_t from uniaxial off-axis tension and compression tests. (see § 11.2.4).

11.2.3. Transverse Strengths

In [1] it is shown that for rotations of the 3-axis, when this axis is chosen along the grain, eq. (11.2.5) and (11.2.16) may precisely describe the peculiar behavior of the compression- tension- and (rolling) shear-strength perpendicular to the grain and the off-axis strengths without the need of higher degree terms. These measured lines of the off-axis uniaxial transverse strength of Figure 11.2, follow precisely from eq. (11.2.15) $F'_1 \sigma_1 + F'_{11} \sigma_1^2 = 1$. When for compression, the failure limit is taken to be the stress value, after that, the same sufficient high amount of flow strain has occurred, then the differences between radial- tangential- and off-axes strengths disappear and one directional, independent, strength value remains (see Figure 11.2). For tension perpendicular to the grain, only in a rather small region (around 90^0 , see Figure 11.2) in the radial direction, the strength is higher and because in practice, the applied direction is not precisely known and avoids this higher

value, a lower bound of the strength will apply that is independent of the direction. The choice of these limits means that:

$$F_1 - F_2 = 0 \quad \text{and} \quad F_{11} - F_{22} = 0 \quad \text{and, that also } F_{12} \text{ is limited}$$

according to: $2F_{12} = F_{11} + F_{22} - F_{66}$.

Further then also is:

$$F'_{66} = 0 \quad \text{and} \quad F'_{66} = F_{66} = 1/\tau_{rol}^2 \tag{11.2.25}$$

From measurement, it can be derived that F_{12} is small, leading to:

$$F_{66} \approx F_{11} + F_{22} \quad \text{or} \quad \tau_{rol} \text{ is bounded by:}$$

$$\tau_{rol} = \sqrt{XX'/2} = \sqrt{YY'/2} \tag{11.2.26}$$

and the ultimate behavior can be regarded to be quasi isotropic in the transverse direction.

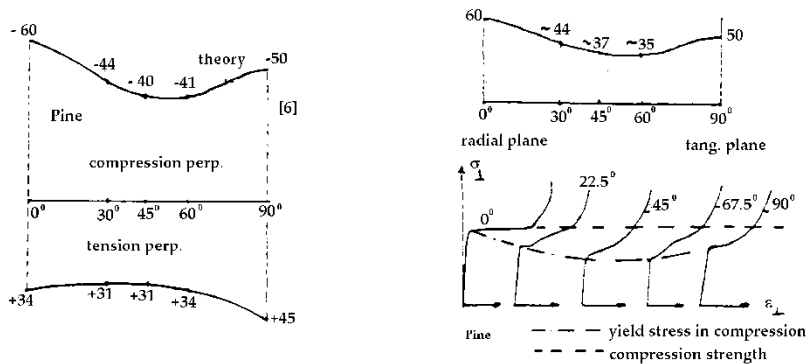


Figure 11.2. Yield stresses and hardening.

The measurements further show for this rotation around the grain-axis that the “shear strengths” in grain direction in the radial- and the tangential plane, F_{44} and F_{55} , are uncoupled or $F_{45} = 0$, as is to be expected from symmetry considerations.

11.2.4. Longitudinal Strengths

When now the 3-axis is chosen in the tangential or in the radial directions, the same relations apply (with indices 1, 2, 6) as in the previous case. The equations for this case then give the strengths along, and perpendicular to the grain and the shear-strength in the grain direction.

In [1] it is shown that this longitudinal shear strength in the radial plane increases with compression perpendicular to this plane according to the coupling term F_{266} (direction 2 is the radial direction” direction 1 is in the grain direction):

$$F_2\sigma_2 + F_{22}\sigma_2^2 + F_{66}\sigma_6^2 + 3F_{266}\sigma_2\sigma_6^2 = 1$$

or:

$$\frac{\sigma_6}{S} = \sqrt{\frac{(1 - \sigma_2/Y) \cdot (1 + \sigma_2/Y')}{1 + C\sigma_2/Y'}} \quad (11.2.27)$$

with: $C = 3F_{266}Y'S^2 \approx 0.9$ (0,8 to 0.99, see Figure 2.4.1).

When C approaches $C \approx 1$ (measurements of project A in Figure 2.4.1), eq. (11.2.27) becomes:

$$\left(\frac{\sigma_6}{S}\right)^2 + \frac{\sigma_2}{Y} \approx 1 \quad (11.2.28)$$

which is equal to the mixed I– II mode Wu- equation of fracture mechanics, showing that the micro-crack and macro crack extensions are the same. The same can be done at the tensile side giving the same equation with Y replaced by $-Y'$. The exact derivation of this equation, in orthotropic stresses, is given in Chapter 2, paragraph 2.3:

$$1 = \frac{\sigma_2}{\xi_0 \sigma_t / 2} + \frac{\sigma_6^2}{\xi_0^2 \sigma_t^2 n_6^2} = \frac{\sigma_2 \sqrt{\pi c}}{\sigma_t \sqrt{\pi r_0} / 2} + \frac{(\sigma_6 \sqrt{\pi c})^2}{(\sigma_t n_6 \sqrt{2\pi r_0})^2} = \frac{K_I}{K_{Ic}} + \frac{K_{II}^2}{K_{IIc}^2}, \quad (11.2.29)$$

because by the transformation from elliptical to circular coordinates $\xi_0 = \sqrt{2r_0/c}$. Critical small crack propagation occurs at a critical crack density, when the intermediate crack distance is about the crack-length and is independent of the crack length and crack tip radius r_0 , when an ultimate strength applies. This then indicates the presence of blunt initial flaws with constant $2r_0/c$ and the second part of eq. (11.2.29) then can be written:

$$1 = \frac{\sigma_2}{\sigma_{2c}} + \frac{\sigma_6^2}{\sigma_{6c}^2} \quad (11.2.30)$$

thus in ultimate strength values σ_{2c}, σ_{6c} of strength theory.

The value of F_{266} of eq. (11.2.27), depends on the stability of the test, and thus is not a constant, but a hardening factor, determining the amount of hardening by the testing instability determined, ultimate state. This is shown in the following Figure 11.8, where parameter values according to more stable torsion tube tests, are used to predict the oblique grain compression strength values. Because of more hardening in the torsion tube test, the peak of 1.1, at 10^0 is predicted, which cannot be measured in the oblique grain test, due to earlier instability due to lack of equilibrium of this test setup, after “initial flow.”

As derived in [2], eq. (11.2.27) does not only apply for tension with shear but also for shear with compression σ_2 perpendicular to the flat crack. For a high stress σ_2 the crack is closed at $\sigma_2 = \sigma_c$ and the crack tip notices only the influence of $\sigma_2 = \sigma_c$ because for the higher part of σ_2 , the load is directly transmitted through the closed crack and eq. (11.2.28) becomes:

$$\frac{\sigma_6}{S} = \frac{-\mu(\sigma_2 - \sigma_c)}{S} + \sqrt{1 - \frac{\sigma_c}{Y}}$$

or:

$$\sigma_6 = C + \mu |\sigma_2| \quad (11.2.31)$$

where σ_2 and σ_c are negative, giving the Coulomb-equation with an increased shear capacity due to friction $\mu |\sigma_2|$. However, inserting the measured values of [6], it appears that the frictional contribution is very small. The micro-crack closure stress σ_c will

numerical be about equal to the tensile strength $\sigma_c \approx -Y$. The shear strength will be raised to its maximum at high compression of $\sigma_c \approx -0.9Y'$, by a factor:

$$\left(1 + \mu(0.9Y' - Y) / S\sqrt{2}\right) = \left(1 + 0.3(0.9 \cdot 5.6 - 3.7) / 9.8 \cdot \sqrt{2}\right) = 1.03.$$

Thus, the combined shear- compression strength is mainly determined by an equivalent hardening effect, caused by crack arrest in the critical direction by the strong layers. At higher σ_2 stresses, compression plasticity perpendicular to the grain (project A of [11], see Figure 2.4.1) or instability of the test (project B of [11] with oblique-grain compression tests) may become determining, showing a lower value of C of eq. (11.2.27) than $C = 1$.

Because the slopes of the lines (at small σ_2) of project A and B of [11] are the same, there is no indication, for clear wood, of an influence of the higher degree terms: F_{112} , F_{122} and F_{166} of project B. When for longitudinal tension F_{12} , F_{122} and F_{112} are zero, then, when $F_{166} = 0$, also $F_{266} = 0$ according to eq. (11.2.22). Then also $C_t = C_d = 0$. Further, the line of B is below the line of A and the C -value of B is lower, closer to the elliptic failure criterion. This is an indication that hardening after initial yield (thus departure from the elliptic equation) of project B, the oblique-grain compression test, is less than that of project A and thus that the test is less stable. (Project C of [11] follows the elliptic failure criterion because of the influence of transverse failure due to rolling shear that is shown before, (§2.3), to be elliptic).

The high value of F_{266} , in the radial plane, (measured with $\sigma_1 = 0$), indicates that for clear wood, F_{122} has to be small according to eq. (11.2.22). It further follows from published Hankinson lines, with $n \approx 2$, of clear wood that third degree terms are zero in the tangential plane, confirming the results of projects A and B of [11], mentioned before. There is an indication that this is a general property of timber [11], because when shear failure is free to occur in the weakest plane, as usually in large timber beams and glulam, it occurs in the tangential plane and $n = 2$, showing no higher degree terms.

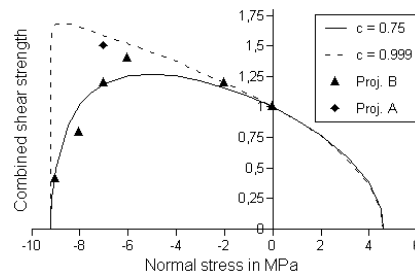


Figure 11.3. (2.4.1 a) - Combined shear-tension and shear-compression strengths. F_{266} .

Determining for compression failure in the radial plane, are the microscopic kinks formation in the cell walls, which is a buckling and plastic shearing mechanism. The kinks multiply and unite in kink-bands and kink-planes at fiber misalignments. Known by everyone is the slip-plane of the prism compression test showing a horizontal crease (shear line, slip line) on the longitudinal radial plane, while on the longitudinal tangential plane the crease is inclined at 45^0 to 60^0 with the vertical axis (depending on the species).

The cause are the rays in the radial planes, which are the main disturbances of the alignment of the vertical cells. For this bi-axial

compression fracture, the same fracture mechanism occurs as for combined mode I-II fracture, discussed above. The shear loading due to micro-crack formation is now caused by the misalignment component of the normal stress.

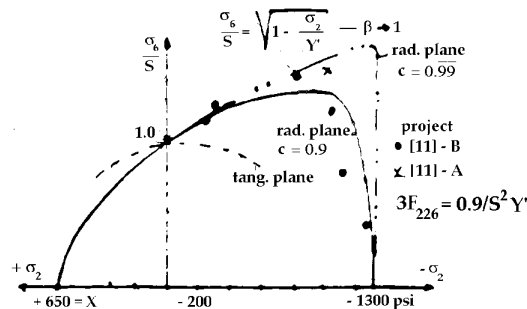


Figure 11.4. Figure 10 of A(1982) of Combined shear-tension -compression strengths. F_{266} .

The general equation now becomes:

$$F_1\sigma_1 + F_2\sigma_2 + F_{11}\sigma_1^2 + F_{22}\sigma_2^2 + 3F_{112}\sigma_1^2\sigma_2 = 1 \quad (11.2.32)$$

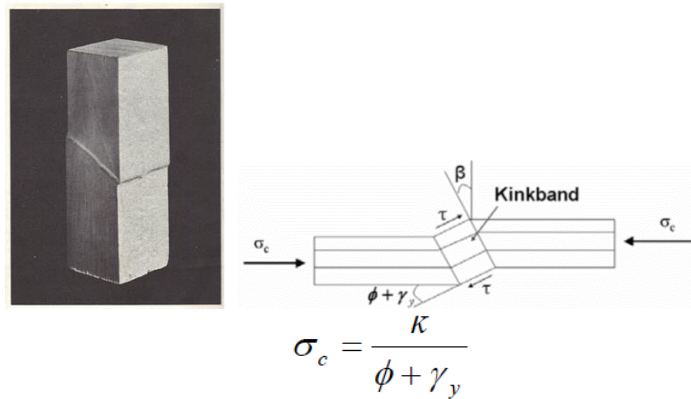


Figure 11.5. Kinkband formation, where K is the plastic shear strength of the matrix (e.g., 11.3 Mpa), $\phi = 15^\circ$ is the misalignment (e.g., for Spruce) γ_y is the longitudinal shear yield strain.

Because $F_{12} = \sigma_6 = 0$ and the contribution of the term with F_{122} is of lower order, not visible in Figure 11.6. The choice of $\sigma_6 = 0$ is made because then, any high value of F_{112} is most determining. Eq. (11.2.32) can be written:

$$\sigma_1 \left(\frac{1}{X} - \frac{1}{X'} \right) + \sigma_2 \left(\frac{1}{Y} - \frac{1}{Y'} \right) + \frac{\sigma_1^2}{XX'} + \frac{\sigma_2^2}{YY'} + 3F_{112}\sigma_2\sigma_1^2 = 1 \quad (11.2.33)$$

Thus:

$$\sigma_1(X' - X) + \sigma_1^2(1 + 3F_{112}\sigma_2XX') = (1 - \sigma_2/Y) \cdot (1 + \sigma_2/Y') \cdot XX' \quad (11.2.34)$$

The critical value of F_{112} , to just have a closed surface, will occur at high absolute values of σ_1 and σ_2 , thus in the neighborhood of $\sigma_1 \approx -X'$. Inserting safely this value in the smallest term of eq. (11.2.34) gives:

$$\sigma_1^2(1 + 3F_{112}\sigma_2XX' + (X' - X)/(-X')) = (1 - \sigma_2/Y) \cdot (1 + \sigma_2/Y') \cdot XX',$$

or:

$$\frac{\sigma_1}{X'} = -\sqrt{\frac{(1 - \sigma_2/Y)(1 + \sigma_2/Y')}{1 + C\sigma_2/Y'}} \approx -\sqrt{1 - \sigma_2/Y}$$

$$\text{where: } C = 3F_{112}Y'X'^2 \quad (11.2.35)$$

Thus when the hardening constant C approaches one $C \approx 1$, the curve reduces to a parabola and the requirement to have a closed curve is $C < 1$, or:

$$3F_{112} < 1/Y' X'^2 \quad (11.2.36)$$

More general, when F_{12} and F_{122} are not fully negligible, the bound $C < 1$ becomes:

$$C \approx 3F_{112}X'^2Y' - 2F_{12}Y'X' + 3F_{122}Y'^2X' < 1 \quad (11.2.37)$$

for longitudinal compression, where besides $\sigma_1 \approx -X'$, also $\sigma_2 \approx -Y'$ is substituted in the contribution of the smallest term, as determining point to just have a closed surface.

The same could be expected to apply for longitudinal tension, giving the same equation (11.2.35) with X' replaced by X . However, because of another type of failure, F_{112} and F_{122} are zero for longitudinal tension (see Figure 11.6) which is an ellipse at the longitudinal tension side, thus is a second degree equation, according to eq. (11.2.33) with $F_{112} \approx 0$ (and with $F_{12} \approx 0$ by the zero slope of the ellipse).

The found (cut-off) parabola eq. (11.2.35) (for C close to $C = 1$) is, as eq. (11.2.27), equivalent to the mixed I–II mode Wu-fracture equation for shear with tension or with compression perpendicular. For wood in longitudinal compression, this failure mechanism acts in the radial plane giving high values of F_{266} and F_{112} close to their bounds of $C \approx 0.8$ to 0.9 .

The parabolic eq. (11.2.35) is shown in Figure 11.6, by the data points outside the points on the ellipse of the longitudinal compression side and is shown as fitted to the theoretical Wu-parabola in Figure 11.7. As mentioned, this hardening of the torsion tube tests, is not found in the uniaxial oblique grain tests, which is earlier unstable, thus showing less hardening. According to Figure 11.6 below, is F_{122} -term of lower order with respect to F_{112} - term and not visible in the figure. Determining is F_{112} , representing hardening by kinking and slip-plane formation (see Figure 11.5). As to be expected, and according to Figure 11.6, is F_{112} zero at the longitudinal tension side (as F_{122} and F_{12}).

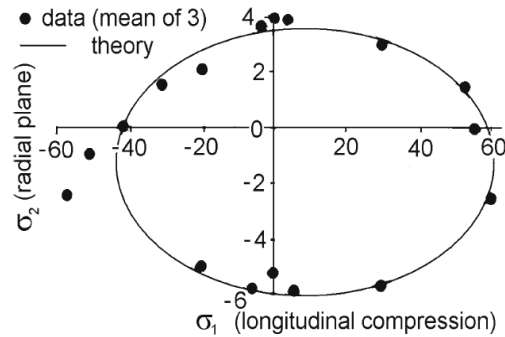


Figure 11.6. Initial yield for $F_{12} = 0$ and $\sigma_6 = 0$.

In [2] is shown that all data may show a different amount of hardening at failure. Because tests in longitudinal compression show other and more hardening than tests in tension, separate data fits for longitudinal tension and longitudinal compression are necessary, as given by eq. (11.2.43) and eq. (11.2.44).

For the parameter estimation by the uniaxial oblique grain tests, it is in eq. (11.2.22):

$$F_{12} = F_{122} = F_{166} = 0;$$

$$3F_{112} \approx 0.9 / ((X')^2 Y'); \quad 3F_{266} \approx 0.9 / (S^2 Y') \quad (11.2.38)$$

Because hardening is mostly not guaranteed in real structures and test situations, the initial flow criterion for the Codes has to be:

$$\frac{\sigma_6^2}{S^2} + \frac{\sigma_1}{X} - \frac{\sigma_1}{X'} + \frac{\sigma_1^2}{XX'} + \frac{\sigma_2}{Y} - \frac{\sigma_2}{Y'} + \frac{\sigma_2^2}{YY'} = 1 \quad (11.2.39)$$

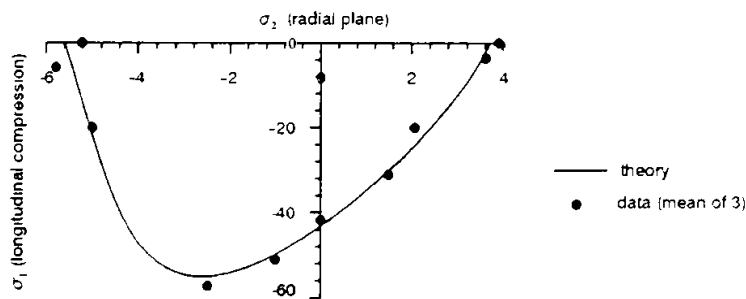


Figure 11.7. Yield criterion for compression F_{112} ($\sigma_1 < 0$) for $\sigma_6 = 0$.

11.2.5. Estimation of the Polynomial Constants by Uniaxial Tests

Based on data fitting of uniaxial tension- and compression tests of [6], the values of C_d and C_t are determinable and by eq. (11.2.22) the polynomial constants are known. This can be compared with the data and fit of the biaxial measurements of [6].

In Figure 11.8, a determination of C_d and of C_t is given. In this figure of [6], the compression- strength perpendicular to the

grain measurement $Y'/X' = 0.204$ is reduced to obtain a value of $Y'/X' = 0.13$ (at 90°) to be able to use the measured constants of the bi-axial tests. It is not mentioned how that can possibly be done but the drawn lines in the figure give the prediction of the uniaxial values based on the measured constants according to the general eq. (11.2.21) (given in [6], as in [1], in the strength tensor form of eq. (11.2.15)). For comparison, the fits of the Hankinson equations are given following these drawn lines.

For tension, the extended Hankinson equation (11.2.20) becomes (by scratching the non zero compression factor of the extended Hankinson product: eq. (11.2.20)):

$$\frac{\sigma_t \cos^2 \theta}{X} + \frac{\sigma_t \sin^2 \theta}{Y} + \sigma_t^2 \sin^2 \theta \cos^2 \theta \cdot C_t = 1 \quad (11.2.40)$$

This equation fits the line for tension in Figure 11.8 when $C_t \approx 11.9/X^2$. The Hankinson equation (11.2.19) fits in this case for $n \approx 1.8$ and all 3 equations (11.2.21), (11.2.40) and (11.2.19) give the same result although for the Hankinson equations only the main tension- and compression strength have to be known and the influence of all other quantities are given by one parameter n or by C_t .

For compression, the same line as found in [6], was found in [1], (see Figure 11 of [1]), by the second degree polynomial with the minimal possible value of F_{12} (according to eq. (11.2.12)), showing that except a negative F_{122} (as used in [6]) also a high negative value of F_{12} may cause the strong peak at small angles. Because such a peak is never measured, the drawn line of [6] is only followed here for the higher angles by the Hankinson

equation. For the small angles, the line (dashed) is drawn through the measured point at 15° , giving the expectable Hankinson value of $n = 2.4$ in eq. (11.2.19) and for eq. (11.2.31) $C_d \approx 4/X^{1.2}$. Because of this low measured value, the predicted peak at 10° in Figure 11.8 is not probable, although the peak-factor of 1.1 is theoretically possible, for a high shear strength, to occur at 18° instead of 10° with $C_d \approx 7.6/X^{1.2}$ in the extended Hankinson equation:

$$\frac{\sigma_t \cos^2 \theta}{X'} + \frac{\sigma_t \sin^2 \theta}{Y'} + \sigma_t^2 \sin^2 \theta \cos^2 \theta \cdot C_d = 1 \quad (11.2.41)$$

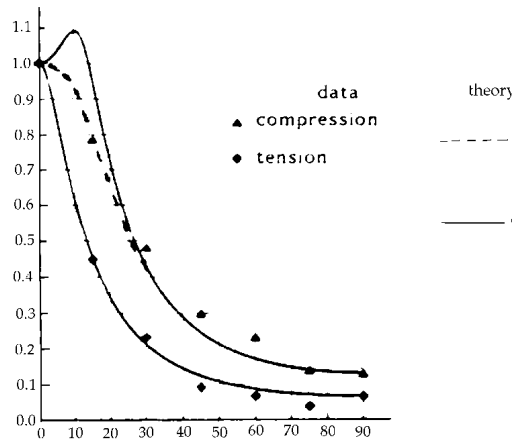


Figure 11.8. Uniaxial tension- and compression strengths
 ----- Compression: Eqs. (11.2.19), (11.2.20), (11.2.41);
 ----- Tension: Eqs. (11.2.19),(11.2.20),(11.2.41).

This shows that the fit of the polynomial constants, based on the best fit of the measurements of [6], is not good for the oblique grain test. The explanation of this deviation is the different state of hardening of the data that can be more or less strong, depending on

the equilibrium stability of the type of test which is less in the uniaxial Hankinson test. This for instance, follows from the ratio of the compression strengths perpendicular to the grain and along the grain of 0.2 in the uniaxial tests and 0.1 in the biaxial tests showing more hardening in the biaxial tests. Further, because the local peak is not occurring in the oblique grain test, the stability is less than in the biaxial test.

An analogous behaviour occurs in the oblique grain test of clear wood [1] where the tensile test shows $C_t = 0$ in eq. (11.2.20) and the compression test shows C_d not to be zero. The tensile test shows unstable failure at yield which needs not to be the case for the compression test that may show additional hardening. For the different hardening states in the different possible types of tests, the lowest possible value should always be used in practice, thus, $C_t = C_d = 0$. It has to be concluded that the strong hardening in the biaxial test in the radial plane will not occur in other circumstances and the hardening parameters should be omitted for a safe, lower bound criterion (in accordance with the oblique grain test).

As generally found in [1] for spruce clear wood, a fit is possible for off-axis tension by a second degree polynomial with $F_{12} = 0$. This also applies for wood with defects, as follows from a fit of the data of [6] by the second degree polynomial (ellipse) in the principal stresses σ_1 and σ_2 ($\sigma_3 = 0$), for longitudinal tension ($\sigma_1 > 0$; $F_{12} = 0$), see Figure 11.6. This fit means that F_{112} and F_{122} are also zero (for $\sigma_1 > 0$) in the radial plane and because the Hankinson value for tension n is different from $n = 2$, there must

be higher degree terms for shear (F_{166} , F_{266}). For fitting these parameters, several starting points are possible.

A first hypothesis of [2]- IV was rejected. It was concluded that C_t and C_d are coupling terms between longitudinal tension and compression and that the different types of failure in longitudinal tension and in compression should be given in separate failure criteria for these cases. However, because of the small values of F_{122} and F_{12} , the best fit for longitudinal tension $\sigma_1 > 0$ is hypothesis 2, when a fit for the total criterion (tension and compression) is wanted for practice.

In Table 11.1, column hyp. 2, this fit is given for $F_{12} = F_{112} = F_{122} = 0$. Because the fit does not change much when data above the uniaxial compression strength $X' = 41.7$ are neglected, the fit may apply for longitudinal compression too, given in column hyp.2, providing the same hardening state as in the oblique grain test (where the strong compression hardening does not occur). Based on the strength values of [6], the constants for this case, eq. (11.2.44), are:

$$C_t = 11.9 / X^2 = 11.9 / 59.5^2 = 0.00336;$$

$$C_d = 4 / X'^2 = 4 / 41.7^2 = 0.00230 \text{ and by eq. (11.2.22)}$$

$$3F_{266} = C_t / Y' + C_d / Y = 0.00332 / 5.95 + 0.0023 / 3.5 = 0.00122$$

or

C of eq. (11.2.27) is:

$$c_{266} = 0.00122 \cdot 9.7^2 \cdot 5.95 = 0.68 \text{ and:}$$

$$3F_{166} = C_t / X' + C_d / X = 0.00336 / 41.7 + 0.0023 / 59.5 = 0.000119,$$

or:

$$c_{166} = 0.000119 \cdot 9.7^2 \cdot 41.7 = 0.47.$$

$$F_1 = \frac{1}{X} - \frac{1}{X'} = 1/59.5 - 1/41.7 = -0.0072;$$

$$F_{11} = \frac{1}{XX'} = 1/(59.5 \cdot 41.7) = 0.00040,$$

$$F_2 = \frac{1}{Y} - \frac{1}{Y'} = 1/3.5 - 1/5.95 = 0.092;$$

$$F_{22} = \frac{1}{YY'} = 1/(3.5 \cdot 5.95) = 0.048 \text{ and:}$$

$$F_{66} = \frac{1}{S^2} = 1/9.7^2 = 0.0106; F_{12} = F_{112} = F_{122} = 0.$$

Eq. (11.2.44) thus also applies for longitudinal compression as follows from Figure 11.6 and Table 1, hyp. 2, showing a better overall fit than according to [6] and to hyp. 4.

To correct the best fit of [6], to obtain a closed curve, the shear strength had to be reduced and a reduced factor 0.8 instead of 0.9 for F_{112} was necessary giving:

$$3F_{122} = 0.8 / (5.6 \cdot 43.1) = 0.000077; \text{ and}$$

$$3F_{166} = C_t / X' + C_d / X - 3F_{122} = 0.000128 - 0.000077 = 0.000051.$$

Thus, giving the C -values: $c_{166} = 0.000051 \cdot 9.4^2 \cdot 43.1 = 0.2$ and $c_{266} = 0.9$ (starting point).

This corrected fit is given in Table 11.1, column 4 (compression fit), and it is seen that the corrected fit is not better than column [6] and needs further improvement. For $\sigma_6 = 0$, the fit for F_{112} , is given in Figure 11.7. For longitudinal compression eq. (11.2.21) then becomes:

$$F_1\sigma_1 + F_2\sigma_2 + F_{11}\sigma_1^2 + 2F_{12}\sigma_1\sigma_2 + F_{22}\sigma_2^2 + F_{66}\sigma_6^2 + 3F_{112}\sigma_1^2\sigma_2 + 3F_{122}\sigma_2^2\sigma_1 + 3F_{166}\sigma_6^2\sigma_1 + 3F_{266}\sigma_6^2\sigma_2 = 1 \quad (11.2.42)$$

Table 11.1. Shear strength σ_6 for combined normal stresses

σ_1	σ_2	σ_6 test	factor: $\sigma_{6,theory} / \sigma_{6,test}$				
			[6]	hyp. 1	hyp. 2 tens.	3 compr.	hyp. 4 compr.
30	1.5	5.8	1.07		1.03		1.02
30	0	8.5	0.88		0.91		0.92
30	-2.5	7.9	0.99		1.10		1.29
7.3	0	9.2	1.04		1.03		1.01
0	2.9	3.7	1.38		1.13		1.19
0	1.5	8.5	0.96		0.89		0.86
0	0	9.0	1.11		1.08		1.04
0	-2.5	10.9	0.96		1.05		1.07
0	-5.4	6.8	0.53		1.12		1.12
-7.7	0	9.6	1.05		1.01		0.96
-20	1.5	7.7	0.84		0.83		0.68
-20	0	9.6	0.99		0.96		0.88
-30	-2.5	11.3	1.04		0.90		0.94
mean factor			0.99		1.0		1.0

Inserting F-values in eq. (11.2.42), this equation becomes:

$$\frac{\sigma_6^2}{S^2} \cdot \left(1 + 0.9 \cdot \frac{\sigma_2}{Y'} + 0.2 \cdot \frac{\sigma_1}{X'} \right) = \left(1 - \frac{\sigma_1}{X} \right) \cdot \left(1 + \frac{\sigma_1}{X'} \right) + \left(1 - \frac{\sigma_2}{Y} \right) \cdot \left(1 + \frac{\sigma_2}{Y'} \right) +$$

$$- \left(1 + 0.8 \cdot \frac{\sigma_2 \sigma_1^2}{Y' X'^2} - 0.77 \cdot \frac{\sigma_1 \sigma_2^2}{X' Y'^2} - 0.41 \cdot \frac{\sigma_1 \sigma_2}{X' Y'} \right) \quad (11.2.43)$$

This equation only applies for the torsion tube test for failure in the radial plane, when it is assumed that negative values of F_{12} and F_{122} (by confined dilatation) are possible. This however is not confirmed enough because its fit [6] in Table 1 is not good enough.

For longitudinal tension ($\sigma_1 \geq 0$), eq. (11.2.21) becomes:

$$\frac{\sigma_6^2}{S^2} \cdot \left(1 + 0.68 \cdot \frac{\sigma_2}{Y'} + 0.47 \cdot \frac{\sigma_1}{X'} \right) = \left(1 - \frac{\sigma_1}{X} \right) \cdot \left(1 + \frac{\sigma_1}{X'} \right) + \left(1 - \frac{\sigma_2}{Y} \right) \cdot \left(1 + \frac{\sigma_2}{Y'} \right) - 1$$

$$(11.2.44)$$

As mentioned, this equation also applies for compression failure in the tangential plane. Because the compression hardening F_{112} , F_{122} , according to eq. (11.2.43) occurs for low values of σ_6 only, and only in the torsion tube test in the radial plane, eq. (11.2.44) more generally represents the failure criterion for tension and compression and shear. However, for tests and structures showing early instability at initial flow, the higher degree hardenings terms will be zero, causing the Hankinson value

of $n = 2$ for timber and glulam. Because this is to be expected in most situations in practice, the determining criterion becomes:

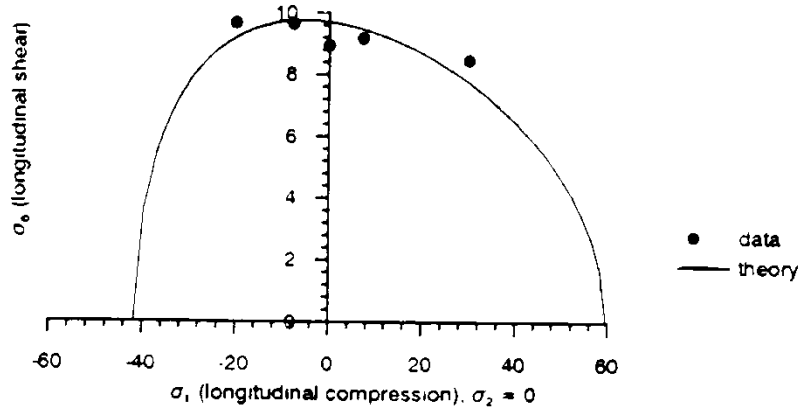


Figure 11.9. Combined longitudinal shear with normal stress in grain direction.

F_{166} .

$$\frac{\sigma_6^2}{S^2} - \left(1 - \frac{\sigma_1}{X}\right) \cdot \left(1 + \frac{\sigma_1}{X'}\right) - \left(1 - \frac{\sigma_2}{Y}\right) \cdot \left(1 + \frac{\sigma_2}{Y'}\right) + 1 = 0,$$

or worked out, identical to eq. (11.2.5) with $F_{12} = 0$:

$$\frac{\sigma_6^2}{S^2} + \frac{\sigma_1}{X} - \frac{\sigma_1}{X'} + \frac{\sigma_1^2}{XX'} + \frac{\sigma_2}{Y} - \frac{\sigma_2}{Y'} + \frac{\sigma_2^2}{YY'} = 1 \quad (11.2.45)$$

It therefore is necessary to use eq. (11.2.45) in the Codes in all cases for timber and clear wood to replace the now still used, not valid Norris-equations. This criterion is, with $F_{12} = 0$, a critical strain energy condition of the wood reinforcements.

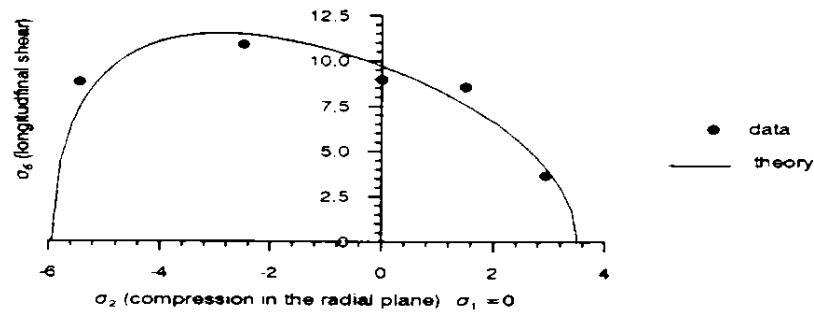


Figure 11.10. Longitudinal shear strength ($\sigma_1 = 0$) depending on the normal stress. F_{266} .

11.3. DISCUSSION OF APPLIED FAILURE CRITERIA

11.3.1. Yield Criterion

A yield- or flow-criterion gives the combinations of stresses whereby flow occurs in an elastic-plastic material. For more brittle failure types in polymers with glassy components like wood at tensile loading, there is some boundary where below the behaviour is assumed to be elastic and where above the gradual flow of components at peak stresses and micro-cracking may have a similar effect as plastic flow with hardening (like metals with gradual plasticity and no yield point).

The loading, damage and hardening behaviour up to failure can be described by deformation kinetics [7]. There are visco-elastic and viscous processes causing early local flow and stable micro-crack propagation (damage increase), while the main part

of the material is elastic and different inelastic and strain rate equations are necessary depending on the loading type and history for a full description.

The failure criterion depends on the ultimate damage process and failure occurs when the standard test becomes unstable (due to loss of equilibrium). Wood can be regarded to be ductile because the critical distortional principle applies and therefore limit analysis should be applied.

11.3.2. Critical Distortional Energy of the Isotropic Matrix

It is not necessary to describe the whole initial loading curve with gradual flow and hardening to describe the ultimate state of flow. The unloading from this ultimate state is linear elastic and on reloading, the loading line is linear elastic up to flow. Thus, the geometry is unaltered and the loading history has no effect on the ultimate state and the linear elastic – full plastic approach of limit analysis is applicable and the initial yield criterion gives the boundary below where the behaviour is elastic.

Because an isotropic matrix of a material may sustain very large hydrostatic pressures without yielding, yield can be expected to depend on a critical value of the distortional energy. This energy is found by subtracting the energy of the volume change from the strain energy (see Appendix II) for the general case in total stresses. For the isotropic matrix material, this subtraction gives, when expressed in matrix stresses:

$$\begin{aligned}
& \left(\frac{1}{2E} \cdot (\sigma_x^2 + \sigma_y^2 + \sigma_z^2) - \frac{\nu}{E} \cdot (\sigma_x \sigma_y + \sigma_y \sigma_z + \sigma_z \sigma_x) + \frac{1+\nu}{E} (\tau_{xy}^2 + \tau_{yz}^2 + \tau_{xz}^2) \right) + \\
& \quad - \left(\frac{1-2\nu}{6E} \cdot (\sigma_x + \sigma_y + \sigma_z)^2 \right) = \\
& = \frac{1+\nu}{6E} \cdot \left((\sigma_x - \sigma_y)^2 + (\sigma_y - \sigma_z)^2 + (\sigma_z - \sigma_x)^2 \right) + \frac{1}{2G} \cdot (\tau_{xy}^2 + \tau_{xz}^2 + \tau_{yz}^2)
\end{aligned} \tag{11.3.1}$$

For plane stress, the distortional energy thus is with $2G = E/(1 + \nu)$:

$$\frac{1+\nu}{3E} \cdot (\sigma_x^2 - \sigma_x \sigma_y + \sigma_y^2 + 3\tau^2) \tag{11.3.2}$$

When σ_x , σ_y and τ are the nominal stresses of a material, having a reinforcement in x and y direction that takes a part of the loading, then the distortional energy of the matrix becomes:

$$\frac{1+\nu}{3E} \cdot \left((1-c_x) \sigma_x^2 - \sigma_x \sigma_y + (1-c_y) \sigma_y^2 + 3(1-c_{tx} - c_{ty}) \tau^2 \right), \tag{11.3.3}$$

where the reinforcement parts are subtracted from the total load. For the reinforcement, taking only normal force and shear, this is:

$$\frac{1+\nu'}{3E_a} \cdot (\sigma_{ax}^2 + 3\tau_a^2) \text{ with: } \sigma_{ax} = \left(\frac{E_a}{E} - 1 \right) \cdot \omega_x \sigma_x$$

where ω_x is the area of the reinforcement per unit area, giving:

$$c_x = \frac{1+\nu'}{1+\nu} \cdot \left(1 - \frac{E}{E_a}\right)^2 \cdot \omega_x^2 \cdot \frac{E_a}{E} \quad (11.3.4)$$

The other values of C_i are analogous.

When the distortional energy is constant at yield then eq. (11.3.3) gives:

$$(1-c_x)\sigma_x^2 - \sigma_x\sigma_y + (1-c_y)\sigma_y^2 + 3(1-c_{tx}-c_{ty})\tau^2 = C \quad (11.3.5)$$

For $\sigma_y = \tau = 0$, this gives the yield stress in x-direction $\sigma_x = X'$. In the same way $\sigma_y = Y'$, when $\sigma_x = \tau = 0$ and is $\tau = S$ when $\sigma_x = \sigma_y = 0$, giving the equation:

$$\frac{\sigma_x^2}{X'^2} - 2F_{12}\sigma_x\sigma_y + \frac{\sigma_y^2}{Y'^2} + \frac{\tau^2}{S^2} = 1 \quad (11.3.6)$$

The Norris equation follows from eq. (11.3.6) when $2F_{12} = 1/X'Y'$. This however is a special value of $2F_{12}$ that need not apply in general.

For the special case that $c_{tx} = c_{ty} = 0$ when, as for concrete, it is assumed that the reinforcement takes no shear, eq. (11.3.5) becomes:

$$\frac{\sigma_x^2}{X'^2} - \frac{\sigma_x \sigma_y}{3S^2} + \frac{\sigma_y^2}{Y'^2} + \frac{\tau^2}{S^2} = 1 \quad (11.3.7)$$

and because $3S^2 \approx X'Y'$, as applies for isotropy and this is assumed by Norris for the cell walls in his derivation, so that this equation becomes:

$$\frac{\sigma_x^2}{X'^2} - \frac{\sigma_x \sigma_y}{X'Y'} + \frac{\sigma_y^2}{Y'^2} + \frac{\tau^2}{S^2} = 1 \quad (11.3.8)$$

giving the Norris equation as critical distortional energy equation of the matrix when the reinforcement “flows” and thus only may carry a normal force.

Wood shows early failure of the matrix. Then the reinforcement carries the total load by the normal and shear forces and the coupling term disappears and the equation gives the apparent critical distortional energy of the reinforcement:

$$\frac{\sigma_x^2}{X'^2} + \frac{\sigma_y^2}{Y'^2} + \frac{\tau^2}{S^2} = 1 \quad (11.3.9)$$

being the older empirical Norris equation. The Norris equations (11.3.8) and (11.3.9) give the possible extremes of F_{12} between zero and the maximal value. Although the Norris-equations are used for wood, they only apply for materials with equal compression and tension strengths.

Because these yield strengths are not equal for wood, different apparent critical distortional energies have been applied for tension and compression as first approximations.

11.3.3. Hankinson Equations

The Hankinson equations apply for the off-axis uniaxial strengths, derived in 11.2 and Appendix II satisfying the exact critical distortional energy equation for initial yield:

$$F_1\sigma_1 + F_2\sigma_2 + F_{11}\sigma_1^2 + 2F_{12}\sigma_1\sigma_2 + F_{22}\sigma_2^2 + F_{66}\sigma_6^2 = 1 \quad (11.3.10)$$

where for uniaxial tensile stress is:

$$\sigma_1 = \sigma_t \cos^2 \theta \quad \sigma_2 = \sigma_t \sin^2 \theta \quad \sigma_6 = \sigma_t \cos \theta \sin \theta$$

Substitution of these stresses gives eq. (11.2.14) which can be resolved into factors giving eq. (11.2.17), which is the product of the Hankinson equation for tension and for compression.

As discussed before, this is possible because:

$$2F_{12} + 1/S^2 \approx 1/X'Y + 1/XY' \quad (11.3.11)$$

In the generalized Hankinson equation, eq. (11.2.19):

$$\frac{\sigma_t \cos^n \theta}{X} + \frac{\sigma_t \sin^n \theta}{Y} = 1 \quad (11.3.12)$$

is the exponent $n = 2$ for the initial yield equation. Measured is also $n = 2$ for the strengths in bending and in tension of clear wood, also for veneer and for shear in the radial plane measured

with the "Schereisen"-device. The measurements thus indicate that also in the radial plane, $n = 2$ applies for initial yield. For $n \neq 2$, as may apply for compression, the extended Hankinson equations, eq. (11.2.20), apply.

11.3.4. Rankine Criterion

The Hankinson equation (11.2.19) for $n = 2$:

$$\frac{\sigma_t \cos^2 \theta}{X} + \frac{\sigma_t \sin^2 \theta}{Y} = 1 \quad (11.3.13)$$

contains the maximum stress condition (or Rankine criterion) of failure for very low and for high angles (see Figure 11.11). For θ in the neighborhood of $\theta = 90^\circ$, eq. (11.58) is about:

$$\frac{\sigma_t \sin^2 \theta}{Y} = 1 \quad (11.3.14)$$

The maximal stress criterion for tension is perpendicular to the grain. This also applies down to 45° , because $1/X$ is of lower order with respect to $1/Y$ and thus the difference of eq. (11.59) with eq. (11.58) is then of lower order. In the same way, for very small values of θ , the ultimate tensile strength criterion in grain direction, eq. (11.60) applies:

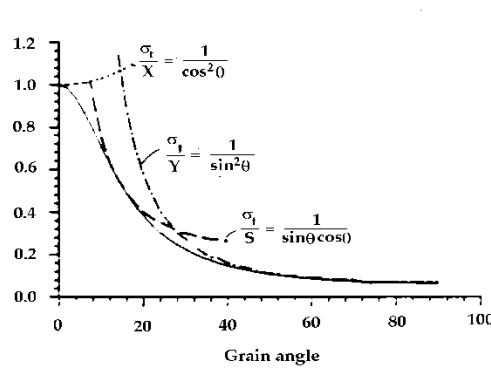


Figure 11.11. Hankinson and Maximal stress criteria.

$$\frac{\sigma_t \cos^2 \theta}{X} = 1 \quad (11.3.15)$$

For values of θ , where the first two terms of eq. (11.3.13) are equal or $\cos\theta/\sqrt{X} = \sin\theta/\sqrt{Y}$, the deviations of eq. (11.3.14) and (11.3.15) from eq. (11.3.13) are maximal (50%). In the neighborhood of this value of θ is $(\cos\theta/\sqrt{X} - \sin\theta/\sqrt{Y})^2 \approx 0$ or $\cos^2 \theta / X + \sin^2 \theta / Y - 2\sin\theta \cos\theta / \sqrt{XY} = 0$ or with eq. (11.3.13):

$$\frac{\sigma_t \sin\theta \cdot \cos\theta}{\sqrt{XY}/2} = \frac{\sigma_t \sin\theta \cdot \cos\theta}{S} = 1 \quad (11.3.16)$$

giving the ultimate failure criterion for shear by the fictive shear-strength $S = \sqrt{XY}/2$.

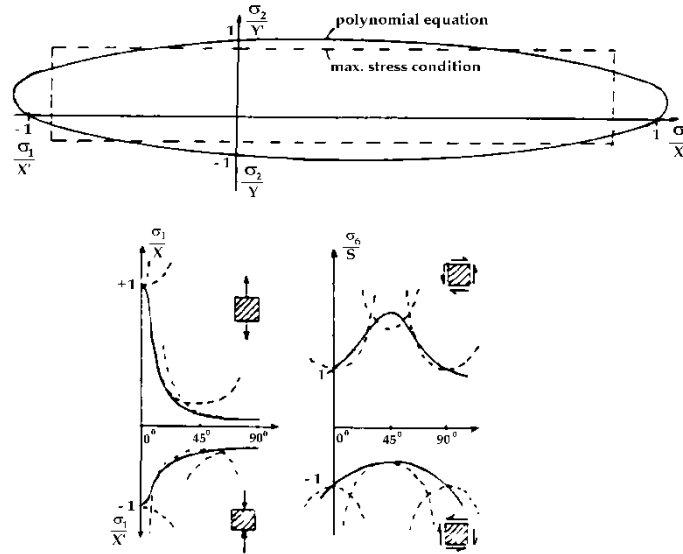


Figure 11.12. Maximal stress failure conditions.

It is easy to show that this value of S is the point of contact of the lines eq. (11.3.16) and eq. (11.3.13). Although eq. (11.3.16) fits precisely at this point where $\operatorname{tg} \theta = \sqrt{Y/X}$, the difference of equations (11.3.14) to (11.3.16) with eq. (11.3.13) is too high at their intersects for application (see Figure 11.11). This also follows from Figure 11.12 for wood and for other comparable polymers.

11.3.5. Norris Equations

The Norris equations follow from the yield equation, eq. (11.3.10), when compression and tension strengths are equal $X = X^c$ and $Y = Y^c$ and thus different equations should be used in each stress quadrant with the strengths $X, Y; X^c, Y^c; X, Y^c; X^c, Y$.

When this is done, Figure 11.13 shows that the Norris equations still do not apply.

The success of these equations follows from the uniaxial applications (in the first and third quadrant) when the Hankinson equations apply.

After substitution of $X = X'$ and $Y = Y'$, the yield equation, eq. (11.2.14), can be resolved in factors like eq. (11.2.17) as:

$$\left(\frac{\sigma_t \cos^2 \theta}{X'} + \frac{\sigma_t \sin^2 \theta}{Y'} - 1 \right) \cdot \left(\frac{\sigma_t \cos^2 \theta}{X'} + \frac{\sigma_t \sin^2 \theta}{Y'} + 1 \right) = 0$$

showing the Hankinson equations to apply and leading to:

$$\frac{\sigma_t^2 \cos^4 \theta}{X'^2} + \frac{\sigma_t^2 \sin^4 \theta}{Y'^2} + \frac{2\sigma_t^2 \sin^2 \theta \cos^2 \theta}{X'Y'} = 1 \quad (11.3.17)$$

This is equal to the Norris-criterion:

$$\frac{\sigma_t^2 \cos^4 \theta}{X'^2} + \frac{\sigma_t^2 \sin^4 \theta}{Y'^2} - \frac{\sigma_t^2 \sin^2 \theta \cos^2 \theta}{X'Y'} + \frac{\sigma_t^2 \sin^2 \theta \cos^2 \theta}{S^2} = 1 \quad (11.3.18)$$

when $1/S^2 \approx 3/X'Y'$. This value of S is measured and can be found in literature (see [1]) showing that the Norris equations are the same as the Hankinson equations for the uniaxial stress case.

For tension (replacing X' by X and Y' by Y in eq. (11.3.18)), it follows in the same way that $S^2 = XY/3$, which may be different from the value for compression, showing that fictive values of S are needed in the other quadrants. Further, the yield criterion eq. (11.3.10) is an ellipsoid, having a small, (or zero) slope with respect to the σ_1 -axis and thus a negligible F_{12} . The center of the ellipse in the 1-2-plane is point $((X - X')/2; (Y - Y')/2)$. When the part of this ellipse in the compression-compression quadrant

has to be approximated by an ellipse with the center at the point (0,0) (as applies for the Norris equation), then F_{12} of that ellipse has a pronounced value. In the tension – compression quadrant, the apparent F_{12} even has the opposite sign. An improvement of eq. (11.3.18) thus will be to have a free slope of the ellipses and to use eq. (11.3.6) instead as an extended Norris equation.

From eq. (11.3.17) it follows that:

$$\frac{\sigma_t^2 \cos^4 \theta}{X'^2} + \frac{\sigma_c^2 \sin^4 \theta}{Y'^2} + \frac{\sigma_t^2 \sin^2 \theta \cos^2 \theta}{S'^2} = 1 \quad (11.3.19)$$

when $1/S^2 \approx 2X'Y'$ in eq.(11.3.17), giving the older empirical Norris equation, that has a zero F_{12} and fits better than the later proposed equation (11.3.18), but still does not fit in all quadrants (see Figure 11.13) because of the assumed equal compression and tension strengths. Further in all four stress quadrants, another, fictive shear strength has to be used.

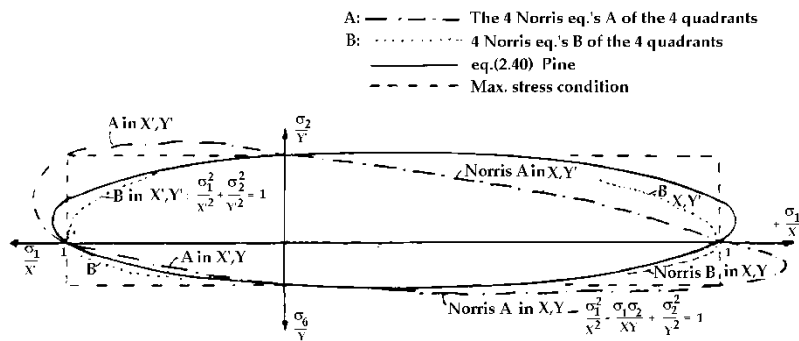


Figure 11.13. Norris equations for $\sigma_6 = 0$.

It can be concluded that the Norris equations can only be applied for uniaxial stress loading being equivalent to the Hankinson equations for initial yield.

Because the Norris equations in the general form are not right, they should not be used anymore.

As discussed before, hardening is mostly not present in tests and structures and a lower bound should be used where also F_{12} can be neglected. Thus for plane stress:

$$F_1\sigma_1 + F_2\sigma_2 + F_{11}\sigma_1^2 + F_{22}\sigma_2^2 + F_{66}\sigma_6^2 = 1 \quad (11.3.20)$$

in all cases, which is easier to use than the invalid Norris criteria.

In general, eq. (11.3.21) applies for the 3-axial stress state, as also is discussed in [1]:

$$\begin{aligned} \sigma_1 \left(\frac{1}{X} - \frac{1}{X'} \right) + (\sigma_2 + \sigma_3) \cdot \left(\frac{1}{Y} - \frac{1}{Y'} \right) + \frac{\sigma_1^2}{XX'} + 2F_{12}(\sigma_1\sigma_2 + \sigma_1\sigma_3) + \frac{\sigma_2^2 + \sigma_3^2 + 2\sigma_4^2}{YY'} + \\ + \frac{\sigma_5^2 + \sigma_6^2}{S^2} = 1 \end{aligned} \quad (11.3.21)$$

This 3-d approach is applicable when there are no initial flat cracks. In this eq. (11.3.21), σ_4 is the rolling shear and, σ_2 and σ_3 are the normal stresses in the tangential and radial planes. In this equation too, $F_{12} = 0$ should be assumed.

It thus can be concluded that the critical distortional energy criterion, reduced when $F_{12} = 0$, to the critical strain energy criterion, also has to be used as a lower bound of the ultimate failure condition.

11.4. CONCLUSIONS REGARDING THE FAILURE CRITERION

- The tensor polynomial failure criterion is shown to be regarded as a polynomial expansion of the real failure criterion.
- It is also shown (Appendix II), that the second degree tensor-polynomial yield criterion represents the critical orthotropic distortional energy principle for initial yield.
- Initial yield in transverse direction, thus follows the second degree polynomial eq. (11.2.15). For compression (perpendicular to grain), strong hardening is possible leading to the isotropic strength behavior (independent of orientation), at the strain where all empty spaces are pressed away.
- For longitudinal initial yield in the radial plane, the third degree polynomial eq. (11.2.42), (with $F_{12} = F_{122} = 0$), applies in a stable test, while in the tangential plane $F_{122} = F_{112} = F_{12} = 0$. When early failure instability occurs in the test at initial crack extension, as for instance in the oblique-grain tension test, or for shear with compression in the “Schereisen” test, there are no third and higher degree terms also not in the radial plane. Higher degree terms thus are due to hardening, depending on the type of test, and due to meta stable crack propagation after initial yield.
- The third degree polynomial hardening terms of the failure criterion are shown to represent (in Chapter 2 or in § 10.5 of [3]), the theoretically derived, Wu-mixed-mode I-II fracture equation, showing hardening to be based on hindered micro-crack extension and micro-crack arrest.

This also applies for kink-band and slip line formation of compression failure, eq. (11.2.35), which is a variant of shear failure according to the mixed mode Wu-equation. Important is the conclusion that the failure criterion shows that micro-crack extension is always involved in fracture processes. The derivation of the new fracture mechanics theory, is therefore based on micro-crack extension. In § 10.2, the exact derivation is given of the geometric correction factor for small crack extension towards the macro-crack tip. This correction factor appears to be numerical the same as for macro-crack extension.

- Because in limit analysis, the extremum variational principle applies for initial “flow” and thus the virtual work equations apply, where the variations are sufficiently small enough to get a linear irreversible process, so that the plastic potential function exists, which is identical to the yield function at flow, and for which the normality rule applies. This applies for the derived orthotropic critical distortional energy criterion, making complete exact solutions possible, and thus reliable strength predictions in all circumstances.
- Wood behaves like a reinforced polymer. The absence of coupling term $F_{12}=0$, between the normal stresses in the main planes, means that the reinforcement takes only normal loading, causing the wood-matrix to carry the whole shear loading. Therefore also, $F_{122}=0$. The reinforcement then is the most effective, as flow of the reinforcement occurs.
- Failure of the matrix occurs before flow of the reinforcement. This follows for Balsa wood, which is highly orthotropic, but shows the isotropic ratio of the

critical stress intensities of the isotropic matrix material at failure at initial flow. For dense, strong (thus with a high reinforcement content), clear wood, this is shown by the oblique crack extension Figure 2.3.2, showing the isotropic oblique angle at the start of shear crack extension, and thus shows the matrix to be determining for initial failure. It is therefore a requirement for an exact orthotropic solution, applicable to wood, to satisfy the equilibrium condition for the total orthotropic stresses, as well as for the isotropic stresses in the matrix at failure. This last condition is not satisfied in all other existing fracture mechanics models.

- Early failure of the matrix causes stress redistribution of mainly shear with compression in the matrix and increased tensile stress in the fibres. The measured negative contraction for creep in tension indicates this mechanism. As in reinforced concrete, truss action is possible, as noticeable by the strong negative contraction coefficient (swelling instead of contraction) in the bending tensile zone of the beam. Failure in compression is determined by the difference in the principal compression stresses. Thus the maximal shear stress or Tresca criterion applies. The necessary validity of the Tresca criterion is confirmed by § 11.5, [15, 16], where the strongly increased (sixfold) compression strength under the load of locally loaded blocks and the increased embedding strength of dowels is explained by the construction of the equivalent slip line field in the specimen based on the Tresca criterion. In addition, the many apparent contradictions of the different investigations are explained by this theory. This strong increase of the compression strength is due to confined dilatation by real hardening (when the empty spaces in wood are pressed away).

-
- The initial yield equation for uniaxial loading can be resolved into factors containing the Hankinson equation for tension and compression for $n = 2$. Thus when the Hankinson parameter n in eq. (11.2.19) is $n = 2$, in tension and in compression, all higher degree terms are zero. This applies for clear wood, depending on the type of test. It also is probable that this is a general property for timber [11], due to preferred failure of the tangential plane.
 - The yield equation for uniaxial loading which contains higher degree terms, can be resolved in factors of the extended Hankinson equations, eq. (11.3.1) for tension and compression when n in eq. (11.2.19) is different from $n = 2$.
 - For wood, at least in the radial plane, after hardening in a stable test, the combined compression - shear strength depends on the third degree coupling term F_{266} , or F_{166} giving the parabolic Mohr- or Wu- equation of fracture. This is theoretically explained in [9] by micro-crack propagation in grain direction. This increase of the shear strength is an equivalent hardening effect due to crack arrest in the worst direction by strong layers. It is shown that the increase of the shear strength, by compression perpendicular to the shear plane, is not due to Coulomb friction which is too small for wood.
 - Because of the grain deviations from the regarded main directions, there is always combined shear-normal stress loading in the real material planes where eq. (11.2.27) applies. F_{112} is due to misalignment of the vertical cells by rays in the radial planes.
 - Therefore, for wood in longitudinal compression in the radial plane, this micro-crack failure mechanism is

determining, giving high values of F_{266} and F_{112} , close to their bounds of $C \approx 0.8$ to 0.9 .

- The same that is found for F_{266} as a function of σ_2 , is to be expected for F_{166} as a function of σ_1 . This is given in Figure 11.9.
- For wood in longitudinal tension, F_{12} , F_{112} and F_{122} are zero and only F_{166} and F_{266} remain in the radial plane as higher degree terms, in stable tests showing a different type of failure than for longitudinal compression.

For longitudinal compression, at $\sigma_6 = 0$, equivalent slip line hardening (high F_{112}), as well hardening by confined dilatation is possible (showing a negative F_{122} and F_{12}). This last type of hardening occurs only in the torsion tube test, because the negative F_{122} and F_{12} of [6] predict the compression peak of Figure 11.8 in the oblique grain test, that does not occur by the lack of hardening in the oblique grain test. This will also be so for structural elements and the lower bound criterion with only F_{166} , and F_{266} (and zero F_{12} , F_{112} and F_{122}) is probably more reliable (hyp 2 fits better than hyp 4 in Table 1) for longitudinal compression failure in the radial plane. In the tangential plane F_{166} and F_{266} are also zero, making the second degree criterion determining.

In general eq. (11.3.21) applies for the 3-axial stress state, as is discussed in [1]:

$$\sigma_1 \left(\frac{1}{X} - \frac{1}{X'} \right) + (\sigma_2 + \sigma_3) \cdot \left(\frac{1}{Y} - \frac{1}{Y'} \right) + \frac{\sigma_1^2}{XX'} + \frac{\sigma_2^2 + \sigma_3^2 + 2\sigma_4^2}{YY'} + \frac{\sigma_5^2 + \sigma_6^2}{S^2} = 1$$

where σ_4 is the rolling shear and σ_2 and σ_3 are the normal stresses in the tangential and radial planes and where it is assumed that $F_{12} = 0$ as applies for longitudinal tension.

- Equations (11.2.28) and (11.2.44) can be used for analyzing test data. Because it is questionable that the hardening by confined dilatation or crack arrest may occur in all circumstances, because it depends on the type of test, the hardening contained by the third degree terms should be omitted for a general application.
- Therefore the second degree polynomial, eq. (11.3.20) or eq. (11.2.45), for plane stress is:

$$\frac{\sigma_6^2}{S^2} + \frac{\sigma_1}{X} - \frac{\sigma_1}{X'} + \frac{\sigma_1^2}{XX'} + \frac{\sigma_2}{Y} - \frac{\sigma_2}{Y'} + \frac{\sigma_2^2}{YY'} = 1$$

which should be used for initial yield and for ultimate failure for the Codes and, as initial yield equation, it applies for the 5th percentile of the strength as well.

- Only this derived extension of the von Mises criterion contains (for orthotropic materials), the necessary independent value of the interaction constant as F_{12} and accounts for different tension- and compression strengths, and is able to give the strength in any direction in the strength tensor form.
- The ultimate stress principle for failure, eqs. (11.3.14), (11.3.15) and (11.3.16), does not apply for the general loading case and only applies locally and approximately for uniaxial loading. These equations are also predicted by the fracture mechanics singularity method [2], showing

that this method, which always is applied in fracture mechanics for all materials, is not right and should not be used.

- The Norris equations are not generally valid and are only for uniaxial loading identical to the Hankinson equation with $n = 2$, when the proper (mostly) fictive shear-strength is used. This equation thus should not be used anymore.
- There thus is no reason not to apply the exact general criterion for the future Codes for all cases of combined stresses. Only this criterion gives the possibility of a definition of the off-axis strength of anisotropic materials.
- It was shown for the first time in A(1982) of iews.nl, that the tensor polynomial failure criterion applies to wood. Also shown is, that the fourth-degree and higher-degree polynomial terms have no physical meaning and thus are zero. Only the third-degree polynomial part is identical to the real initial flow criterion, while the third degree terms represent deviations from orthotropic behavior and represent post initial flow hardening behavior, the numerical value of which depends on the stability of the test specimen and testing device.
- For uniaxial loading, the failure criterion can be resolved in factors leading to the derivation of extended Hankinson equations. This provides a simple method to determine all strength parameters by simple uniaxial, oblique grain compression and tension tests. Based on this, the numerical failure criterion is given with the simple lower bound criterion for practice and for the codes.
- The existence of an isotropic matrix in wood (lignin with branched hemicellulose) follows not only from material analysis, but as mentioned, from the high compression strength at confined dilation with the absence of failure by

triaxial hydrostatic compression which is not the case for orthotropy, because then, for equal triaxial stresses, the strains then are not equal and yield remains possible.

- Plastic flow in wood, starts with the propagation of empty spaces by segmental jumps, just as the dislocation propagation in steel and the possibility should be accounted that there is no change in density at initial flow (as for steel) and the plastic incompressibility condition should be accounted for as a possibility, and as follows from the normality rule of flow in combination with perfect plasticity, the Tresca criterion (maximal shear stress criterion) then should also apply. By the dissipation according to the incompressibility condition, the minimum energy principle is followed providing the lowest possible upper bound and therefore the closest to the exact flow criterion. Limit analysis of the matrix therefore has to be based on incompressibility and the Tresca criterion.
- It has to be stressed, for the virtual work equations of limit analysis, that neither the chosen equilibrium, nor the compatible strain and displacement set need not be the actual state, nor do the equilibrium and compatible sets need to be related in any way to each other.
- The loading curve up to yield and failure also should be described by deformation kinetics [7] to adapt for temperature, time and loading rate influences.

11.5. REFERENCES

- [1] van der Put, T.A.C.M., A general failure criterion for wood, Proc. IUFRO meeting Boras, (or: <http://iew.s.nl/> A(1982), Stevinrapport 4-82-5 HA-14, feb. '82, Delft University NL).

- [2] van der Put T.A.C.M. I: Explanation of the failure criterion for wood, (1993), II: Post yielding behavior of wood. (1993), III: Explanation of the mixed mode interaction equation, all 3 in Proc. of the Cost 508 workshop on Fracture mechanics Bordeaux and on yield and failure of wood, Limerick 1992 and 1993. IV: Discussion and proposal of a general failure criterion of wood, CIB-W18/26-6-1, [http://iews.nl/A\(1993\)](http://iews.nl/A(1993)),
- [3] van der Put T.A.C.M. The tensorpolynomial failure criterion for wood, DWSF-Publication Series 2005, nr.2, ISSN 1871-675X, or: [http://iews.nl/A\(2005\)](http://iews.nl/A(2005)).
- [4] van der Put, T.A.C.M., A continuum failure criterion applicable to wood, *J Wood Sci* (2009) 55: 315-322, or: [http://iews.nl/A\(2009\)](http://iews.nl/A(2009)).
- [5] van der Put T.A.C.M. I (1990) Stability design and code rules for straight timber beams. CIB-W18/23-15-2. Lisbon, Portugal [http://iews.nl/E\(1990\)](http://iews.nl/E(1990)) II:(1990) Tension perpendicular to the grain at notches and joints. CIB-W18/23-10-1. Lisbon, Portugal [http://iews.nl/C\(1990\)](http://iews.nl/C(1990)) III: (1991) Discussion of the failure criterion for combined bending and compression, Appendix a: bearing strength perpendicular to the grain of locally loaded blocks. CIB-W18/24-6-1. Oxford, United Kingdom. [http://iews.nl/D\(1991\)](http://iews.nl/D(1991)), IV: van der Put, T.A.C.M, (1993) Discussion and proposal of a general failure criterion for wood. CIB-W18/26-6-1. Athens, USA. [http://iews.nl/A\(1993\)](http://iews.nl/A(1993)), V: van der Put, T.A.C.M., Discussion of the design of nail-plate connections, Proceed. Pacific timber Eng. Conf., Auckland, New Zealand, I.E.G.N.Y. May 1984 VI: van der Put, T. A. C. M. and Leijten, A. J. M. (2000) Evaluation of perpendicular to grain failure of beams caused by concentrated loads of joints. CIB-W18/33-7-7. Delft, nl, [http://iews.nl/C\(2000\)](http://iews.nl/C(2000)), VII: van der Put, T. A. C. M. and van de Kuilen, J. W. G.

- (2009) Derivation of the shear strength of continuous beams. *European Journal of Wood Wood Production*. doi:10.1007/s00107-010-0473-3. [http://iews.nl/A\(2009\)](http://iews.nl/A(2009)).
- [6] Hemmer, K., Versagensarten des Holzes der Weisstanne unter mehrsichtige Beanspruchung, Dissertation, Karlsruhe 1985.
- [7] van der Put T.A.C.M. Deformation and damage processes in wood. Delft University Press 1989. Or: [http://iews.nl/B\(1989a\)](http://iews.nl/B(1989a)).
- [8] Norris C.B. The elastic theory of wood failure. *ASME Trans.*, vol. 61, 3, 1939.
- [9] Hoffmann O.J. *Composite Materials*, p. 200, 1967.
- [10] Tsai S.W. and Hahn H.T. Introduction to composite materials. Westport, CT: Technometric Publ. Co., Inc. 1980.
- [11] Wu R.Y., Stachurski Z., Evaluation of the normal stress interaction parameter in the polynomial strength theory of anisotropic mater. *J. Comp. Mater.* 1984.
- [12] Leichti R.J, Tang R.C. Predicting the load capacity of wood composite I-beams using the tensor polynomial strength theory. *Wood Sci. and Technol.* 23, 1989.
- [13] Möhler K., Consideration of combined stresses for lumber and glued laminated timber CIB-W18-9-6-4, 1978 en CIB-W18-11-6-3, 1979.
- [14] Kollmann F. Technologie des Holzes und der Holzwerkstoffe, *Springer Verlag* 1951.
- [15] van der Put, T. A. C. M. (2008) Derivation of the bearing strength perpendicular to the grain of locally loaded timber blocks. *European Journal of Wood Production*, doi:10.1007/s00107-008-0258-0, or: [http://iews.nl/D\(2008a\)](http://iews.nl/D(2008a)).
- [16] van der Put, T. A. C. M. (2008) Explanation of the embedding strength of particle board. *European Journal of Wood Wood Production*, doi:10.1007/s00107-008-0234-8.

or: <http://iewws.nl/> D(2008b). See also: Stevin Report TU-Delft 25-88-63/09-HSC-6 or: EC-project MA1B-0058-NL, 1988, and the theoretical explanation of the strength of nailed particle board to wood connections in: Stevin Reports 4-79-6/HSC-3; 4-80-3/HSC-4; and 4-81-7/ HSC-5.

Files of: van der Put of Section A, B, D, are on: dwsf.nl, or: iewws.nl or: Researchgate.net, for information and discussion.

Chapter 12

CONCLUSION

APPENDIX I: DYNAMICS OF CRACK PROPAGATION

The dynamic extension of the Griffith theory is given by Berry in: Some kinetic considerations of the Griffith criterion for fracture I and II: J. Mech. Phys. Solids, 8, (1960) 194-206 and 207-216.

Regarding the test specimen of Figure 3.1, assuming plane stress, the work done by the external forces is:

$$W_i = bl\sigma_i^2 \left[1 + 2\pi c_i^2 / bl \right] / 2E \quad (\text{A1})$$

Including the apparent surface energy $4\alpha c_i$ gives as total energy:

$$V_i = bl\sigma_i^2 \left[1 + 2\pi c_i^2 / bl \right] / 2E + 4\alpha c_i \quad (\text{A2})$$

When the crack extends at constant σ_i , the total energy V will be:

$$V = bl\sigma_i^2 \left[1 + 2\pi c_i^2 / bl \right] / 2E + 4\alpha c_i + K \quad (\text{A3})$$

where K is the stored kinetic energy. The work $W - W_i$ done by σ_i during the extension is:

$$W - W_i = bl\sigma_i(\varepsilon - \varepsilon_i) \quad (\text{A4})$$

where $\varepsilon, \varepsilon_i$ are the strains corresponding to crack lengths c, c_i . Thus:

$$W - W_i = 2\pi\sigma_i^2(c^2 - c_i^2) / E \quad (\text{A5})$$

Equating this to $V - V_i$ gives:

$$\pi\sigma_i^2(c^2 - c_i^2) / E = 4\alpha(c - c_i) + K \quad (\text{A6})$$

Writing: $n = 4\alpha E / \pi c_i \sigma_i^2$ this is:

$$K = \pi\sigma_i^2 c^2 (1 - c_i / c) [1 - (n-1)c_i / c] / E \quad (\text{A7})$$

On dimensional grounds is:

$$K = k\rho\sigma_i^2 c^2 v_c^2 / 2E^2 \quad (\text{A8})$$

where $v_c = dc / dt$ velocity of crack extension, ρ the density and k is a constant. From the last 2 equations, it follows:

$$v_c^2 = \frac{2\pi E}{k\rho} \left(1 - \frac{c_i}{c} \right) \left[1 - (n-1) \frac{c_i}{c} \right] = v_m^2 \left(1 - \frac{c_i}{c} \right) \left[1 - (n-1) \frac{c_i}{c} \right] \quad (\text{A9})$$

where $v_m = \sqrt{2\pi E / k\rho} = 0.38\sqrt{E/\rho}$ is the maximum velocity of crack extension.

Differentiating eq. (A9) gives the acceleration of the moving crack tip:

$$\frac{dv_c}{dt} = \frac{\pi E c_i}{k \rho c^2} \left[n - 2(n-1) \frac{c_i}{c} \right] \quad (\text{A10})$$

It follows from eq. (A9) that the crack velocity is zero when $c = c_i$ and from eq. (A10), that for $n = 2$, the acceleration of crack extension is zero also. For $n = 2$ is $\pi c_i \sigma_i^2 = 2\alpha E$, which is the Griffith equation. Thus the crack of Griffith length is in unstable equilibrium but does not propagate. For $n < 2$, is $\sigma_i > \sigma_g$, the Griffith stress, the crack propagates. This explains why the whole yield drop curve could be measured by Boström in his thesis, see: § 3.8 - [3], without instable crack extension.

APPENDIX II: DERIVATION OF THE ORTHOTROPIC CRITICAL DISTORTIONAL ENERGY PRINCIPLE

It was shown for the first time for wood, in A(1982), that the second degree tensor-polynomial describes initial “flow,” which is shown, to represent the orthotropic extension of the critical distortional energy criterion providing an exact flow criterion as the necessary basis for exact solutions according to limit analysis.

Because the matrix of wood material is isotropic and therefore may sustain large hydrostatic pressures without yielding, yield depends on a critical value of the distortional energy. This energy

W_d is found by subtracting the energy of the volume change from the total strain energy. Thus for the isotropic matrix material this is:

$$\begin{aligned}
 W_d &= \left(\frac{1}{2E} \cdot (\sigma_x^2 + \sigma_y^2 + \sigma_z^2) - \frac{\nu}{E} \cdot (\sigma_x \sigma_y + \sigma_y \sigma_z + \sigma_z \sigma_x) + \frac{1+\nu}{E} \cdot (\tau_{xy}^2 + \tau_{yz}^2 + \tau_{xz}^2) \right) + \\
 &\quad - \left(\frac{1-2\nu}{6E} \cdot (\sigma_x + \sigma_y + \sigma_z)^2 \right) = \\
 &= \frac{1+\nu}{6E} \cdot \left((\sigma_x - \sigma_y)^2 + (\sigma_y - \sigma_z)^2 + (\sigma_z - \sigma_x)^2 \right) + \frac{1}{2G} \cdot (\tau_{xy}^2 + \tau_{xz}^2 + \tau_{yz}^2)
 \end{aligned}
 \tag{B.1}$$

where σ_i are the normal matrix stresses, τ_i the shear stresses, E the modulus of elasticity, G the shear modulus and ν Poisson's ratio of the matrix material following $2G = E/(1 + \nu)$.

Wood has to be regarded as a reinforced material and initial failure is due to failure of the isotropic matrix. This is shown in § 3.8 – [1], leading to a new fracture mechanics theory and a new transformation of the Airy stress function, making exact solutions possible as applied for the derivations of the Wu mixed mode I-II fracture criterion and the derivations of the correct fracture energies and the relation between mode I and II stress intensities and energy release rates. According to § 3.8 – [1], the matrix stresses can be expressed in orthotropic stresses as follows:

The stress in wood $\sigma_{x,or}$ is n_1 times the stress in the matrix σ_x due to the reinforcement in x-direction: $\sigma_{x,or} = (E_x / E) \cdot \sigma_x = n_1 \cdot \sigma_x$, while the reinforcement in y-direction is regarded to belong to the matrix, thus $\sigma_{y,or} = \sigma_y$ and $E_y = E$ of the matrix. For the shear

stress, the multiplying factor is $n_6 = (2 + \nu_{xy} + \nu_{yx}) \cdot G_{xy} / E$. Thus, E_x , E_y , G_{xy} , ν_{xy} and ν_{yx} are the orthotropic values of wood due to the reinforcements.

Eq. (B1) applies for a material with equal tension and compression strength. For unequal axial strengths, the failure condition in x-direction is $(\sigma_x - X) \cdot (\sigma_x + X') = 0$, where X is the tensile strength and $-X'$ is the compression strength, as given in Figure 1a.

This condition can be written as:

$$\left(\sigma_x - \frac{X - X'}{2} \right)^2 = \left(\frac{X + X'}{2} \right)^2 \text{ or: } \sigma_x - p_x = \pm \bar{X} \quad (\text{B.2})$$

The behavior is identical to that of a material with equal tension and compression strengths of \bar{X} being pre-stressed by stress p_x .

This result follows from the applied linear transformation. Because eq. (B.1) is a physical property, it should be independent of the chosen vector space and according to the additivity rule of linear mapping (linear transformation) is $f(\mathbf{x} + \mathbf{y}) = f(\mathbf{x}) + f(\mathbf{y})$, or in this case $f(\boldsymbol{\sigma} - \mathbf{p}) = f(\boldsymbol{\sigma}) + f(-\mathbf{p})$ giving:

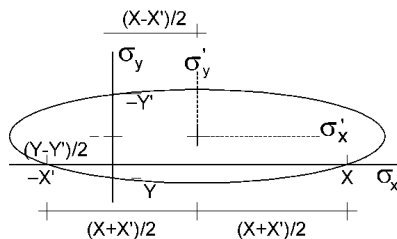


Figure 1a. von Mises criterion for wood.

$$f(\boldsymbol{\sigma}) = f(\boldsymbol{\sigma} - \mathbf{p}) - f(-\mathbf{p}) \quad (\text{B.3})$$

Substitution of $\sigma_x - p_x$, $\sigma_y - p_y$ and $\sigma_z - p_z$ respectively for σ_x , σ_y and σ_z in eq. (B.1) gives:

$$\begin{aligned} & \left(\frac{\sigma_{x,or}}{n_1} - \frac{p_{x,or}}{n_1} - \sigma_{y,or} + p_y \right)^2 + (\sigma_{y,or} - p_y - \sigma_{z,or} + p_z)^2 + \left(\sigma_{z,or} - p_y - \frac{\sigma_{x,or}}{n_1} + \frac{p_{x,or}}{n_1} \right)^2 + \\ & + 6\Sigma \tau_{ij}^2 / n_i = 2C \quad (= 6EW_d / (1+\nu)) \end{aligned}$$

and after subtraction of $f(-\mathbf{p})$ this is:

$$\begin{aligned} & \frac{\sigma_{x,or}^2}{n_1^2} + \sigma_{y,or}^2 + \sigma_{z,or}^2 - \frac{\sigma_{x,or}\sigma_{y,or}}{n_1} - \sigma_{z,or}\sigma_{y,or} - \frac{\sigma_{x,or}\sigma_{z,or}}{n_1} + \left(p_y + p_z - \frac{2p_{x,or}}{n_1} \right) \frac{\sigma_{x,or}}{n_1} + \\ & + \left(p_y - 2p_z + \frac{p_{x,or}}{n_1} \right) \sigma_{z,or} + \left(p_z - 2p_y + \frac{p_{x,or}}{n_1} \right) \sigma_y + 3\Sigma \tau_{ij}^2 / n_i = -C_p \\ & + f(-\mathbf{p}) + C = C = 3EW_d / (1+\nu) \quad (\text{B.4}) \end{aligned}$$

with:

$$f(-\mathbf{p}) = p_{x,or}^2 / n_1^2 + p^2 + p_z^2 - pp_{x,or} / n_1 - pp_z - p_z p_{x,or} / n_1 = C_p.$$

This follows from inserting $\sigma_x = p_x$, $\sigma_y = p_y = p$ and $\sigma_z = p_z$ in eq.(B.1).

Of interest for failure by flat crack propagation is the plane stress equation with $\sigma_z = p_z = 0$; $\tau_{xz} = \tau_{yz} = 0$ and with $p_y = p_{y,or} = p$, giving for eq. (B.4):

$$\frac{\sigma_{x,or}^2}{C' \cdot n_1^2} - \frac{\sigma_{x,or} \cdot \sigma_{y,or}}{C' \cdot n_1} + \frac{\sigma_{y,or}^2}{C'} + \frac{\sigma_{x,or}}{C' \cdot n_1} \left(p - 2 \frac{p_{x,or}}{n_1} \right) - \frac{\sigma_y}{C'} \left(2p - \frac{p_{x,or}}{n_1} \right) + 3 \frac{\tau_{or}^2}{C' \cdot n_6^2} = 1 \quad (B.5)$$

For $\sigma_{y,or} = \tau_{or} = 0$, eq. (B.5) becomes:

$$\frac{\sigma_{x,or}^2}{C' \cdot n_1^2} + \frac{\sigma_{x,or}}{C' \cdot n_1} \left(p - 2 \frac{p_{x,or}}{n_1} \right) = 1$$

This is identical to $(\sigma_{x,or} - X)(\sigma_{x,or} + X') = 0$, or to:
 $\sigma_{x,or}^2 + (X' - X)\sigma_{x,or} - XX' = 0$, showing that:
 $(pn_1 - 2p_{x,or}) = X' - X$, and $C' \cdot n_1^2 = XX'$. The same applies in the perpendicular y-direction for the uniaxial tension and compression strengths Y and Y' giving $C' = YY'$ and $(p_{x,or} / n_1 - 2p) = Y' - Y$.

This last result is to be expected because according to the molecular theory, the strength is proportional to the E-modulus and thus is $YY' = XX' / n_1^2$ and $X' - X = n_1(Y - Y')$. Then also is $p = p_{x,or} / n_1 = Y - Y' = (X - X') / n_1$, and eq. (B.5) becomes:

$$\frac{\sigma_{x,or}^2}{C' \cdot n_1^2} - \frac{\sigma_{x,or} \cdot \sigma_{y,or}}{C' \cdot n_1} + \frac{\sigma_{y,or}^2}{C'} - p \frac{\sigma_{x,or}}{C' \cdot n_1} - p \frac{\sigma_{y,or}}{C'} + 3 \frac{\tau_{or}^2}{C' \cdot n_6^2} = 1$$

or: (B.6)

$$\frac{\sigma_{x,or}^2}{XX'} + \frac{\sigma_{x,or}}{X} - \frac{\sigma_{x,or}}{X'} - 2F_{12} \sigma_{x,or} \sigma_{y,or} + \frac{\sigma_{y,or}^2}{YY'} + \frac{\sigma_{y,or}}{Y} - \frac{\sigma_{y,or}}{Y'} + \frac{\tau_{or}^2}{S^2} = 1 \quad (B.7)$$

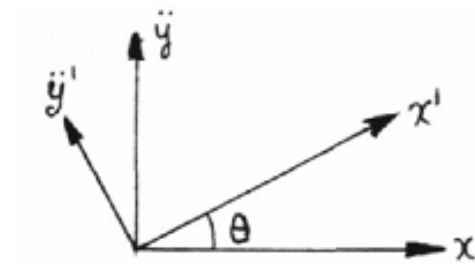
where S is the shear strength and:

$$2F_{12} = 1/C'n_1 = 1/\sqrt{XX'YY'} \quad (\text{B.8})$$

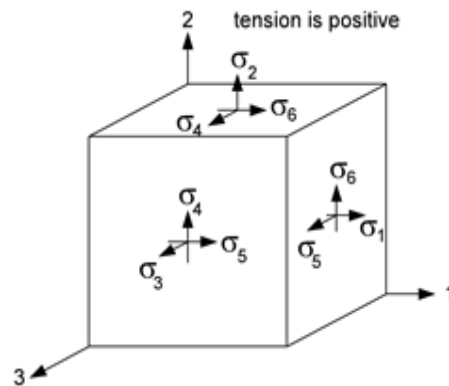
This value of F_{12} applies for the elastic state. At initial stress redistribution and micro-cracking of the matrix and F_{12} becomes lower, reaching a near zero value at yield or failure initiation. This may indicate an early dissipation of the elastic distortional energy for formation of initial micro-cracks. This dissipation of distortional energy is according to the incompressibility condition and thus follows a minimum energy principle of yield. At the end of this stress redistribution, yield occurs according to eq. (B.7) with $F_{12} = 0$. This means an absence of coupling terms between the normal stresses. This is only possible when the reinforcement takes the whole normal loading and no shear, causing the matrix to fail by shear and the critical distortional energy principle thus reduces to the Tresca criterion. The necessary validity of the Tresca criterion is confirmed in [17, 18] of § 11.5, where the strongly increased (6-fold) compression strength under the load of locally loaded blocks and the increased embedding strength of dowels and nails is explained by the construction of the equivalent slip line field in the specimen, using the Tresca criterion. The Tresca criterion satisfies the normality rule and thus inherently the theorems of limit analysis for matrix failure. The normality rule thus does not apply for hardening. This condition is shown to be replaced by the minimum work condition for dissipation represented by the yield equation and the hardening state constants C_d and C_t of eq. (11.2.20). Thus, after initial yield, shear strength hardening is possible according to the mixed mode Wu equation

and finally when the empty spaces in wood are pressed away, real hardening is possible by confined dilatation at locally compression loading of the isotropic matrix. This is discussed in Section D – publications of iews.nl.

APPENDIX III: TRANSFORMATION OF STRENGTH TENSORS: F_{II}



Positive rotation about the main 3-axis (z-axis).



Positive signs in right handed coordinate system.

Sign convention for shear: If an outward normal of a plane points to a positive direction, the plane is positive, and if on a positive plane the stress component acts in the positive coordinate direction, this component is positive.

In the x' , y' coordinates of figure above the strength tensors are:

$$F_i = \begin{pmatrix} F'_1 \\ F'_2 \\ F'_3 \\ F'_4 \\ F'_5 \\ F'_6 \end{pmatrix}; F_{ij} = \begin{pmatrix} F'_{11} & F'_{12} & F'_{13} & F'_{14} & F'_{15} & F'_{16} \\ & F'_{22} & F'_{23} & F'_{24} & F'_{25} & F'_{26} \\ & & F'_{33} & F'_{34} & F'_{35} & F'_{36} \\ & & & F'_{44} & F'_{45} & F'_{46} \\ & & & & F'_{55} & F'_{56} \\ & & & & & F'_{66} \end{pmatrix}$$

symmetry

The principal strength components are:

$$F_i = \begin{pmatrix} F_1 \\ F_2 \\ F_3 \\ 0 \\ 0 \\ 0 \end{pmatrix}; F_{ij} = \begin{pmatrix} F_{11} & F_{12} & F_{13} & 0 & 0 & 0 \\ & F_{22} & F_{23} & 0 & 0 & 0 \\ & & F_{33} & 0 & 0 & 0 \\ & & & F_{44} & 0 & 0 \\ & & & & F_{55} & 0 \\ & & & & & F_{66} \end{pmatrix}$$

sym.

Transformation about the 3- axis gives:

$$F'_1 = \frac{F_1 + F_2}{2} + \frac{F_1 - F_2}{2} \cos(2\theta); F'_2 = \frac{F_1 + F_2}{2} - \frac{F_1 - F_2}{2} \sin(2\theta)$$

$$F'_6 = -(F_1 - F_2) \sin(2\theta); F'_3 = F_3; F'_4 = F'_5 = 0$$

F'_{ij}	invariant	$\text{Cos}2\theta$	$\text{Sin}2\theta$	$\text{Cos}4\theta$	$\text{Sin}4\theta$
F'_{11}	I_1	I_2	0	I_3	0
F'_{22}	I_1	$-I_2$	0	I_3	0
F'_{12}	I_4	0	0	$-I_3$	0
F'_{66}	$4I_5$	0	0	$-4I_3$	0
F'_{16}	0	0	$-I_2$	0	$-2I_3$
F'_{26}	0	0	$-I_2$	0	$+2I_3$
F'_{13}	I_6	I_7	0	0	0
F'_{23}	I_6	$-I_7$	0	0	0
F'_{36}	0	0	$-I_7$	0	0
F'_{44}	I_8	I_9	0	0	0
F'_{55}	I_8	$-I_9$	0	0	0
F'_{45}	0	0	I_9	0	0
F'_{33}	F_{33}	0	0	0	0

Read e.g., $F'_{11} = I_1 + I_2\cos2\theta + I_3\cos4\theta$

$$I_1 = (3F_{11} + 3F_{22} + 2F_{12} + 3F_{66})/8;$$

$$I_2 = (F_{11} - F_{22})/2;$$

$$I_3 = (F_{11} + F_{22} - 2F_{12} - F_{66})/8;$$

$$I_4 = (F_{11} + F_{22} + 6F_{12} - F_{66})/8;$$

$$I_5 = (F_{11} + F_{22} - 2F_{12} + F_{66})/8;$$

$$I_6 = (F_{13} + F_{23})/2;$$

$$I_7 = (F_{13} - F_{23})/2;$$

$$I_8 = (F_{44} + F_{55})/2;$$

$$I_9 = (F_{44} - F_{55})/2.$$

AUTHOR'S CONTACT INFORMATION

Dr. T.A.C.M. van der Put

TU-Delft, Civil Engineering and Geosciences,

Timber Structures and Wood Technology,

Delft, Netherlands

Email: vanderp@xs4all.nl

INDEX

A

airy stress function, xi, 2, 3, 5, 7, 11, 12,
14, 16, 75, 91, 97, 123, 124, 133, 137,
151, 160, 226

C

crack growth models, 3, 5, 74, 78, 125
crack multiplication, 128
cracks, 162

D

deformation, 6, 28, 34, 37, 44, 46, 67,
71, 78, 80, 83, 90, 115, 116, 125, 130,
221
derivations, xi, 3, 166, 226

E

energy, xii, 13, 49, 59, 91, 95, 98, 99,
100, 109, 110, 121, 147, 201, 223,
225
energy density, 13
energy release rate, xi, 1, 31, 35, 41, 54,
65, 74, 88, 126, 131, 132, 143, 159,
160, 226
engineering, 161

F

fictitious crack models, 4, 5, 36, 49, 74,
75, 77, 125, 133
fracture mechanics, xi, xii, 1, 2, 3, 5, 6,
13, 22, 24, 33, 34, 36, 58, 71, 72, 73,
80, 90, 98, 107, 109, 123, 125, 126,
131, 132, 135, 136, 137, 138, 141,
146, 148, 151, 155, 157, 160, 161,
164, 166, 167, 183, 213, 214, 217,
220, 226

- G**
- geometry, 53
 growth, 78
 growth models, xii
- J**
- joints, 109
- K**
- kinetics, 28, 44, 46, 78, 83, 125, 130
- L**
- lead, 130
 limit analysis, xi, 1, 2, 4, 13, 23, 36, 37, 44, 58, 74, 75, 77, 82, 83, 91, 97, 101, 124, 125, 128, 133, 151, 154, 155, 157, 160, 163, 166, 167, 168, 201, 213, 219, 225, 230
- M**
- materials, i, ii, iii, 34, 221
 matrix, 201
 measurement(s), xii, 25, 27, 28, 33, 52, 53, 55, 77, 100, 104, 109, 126, 132, 137, 145, 167, 176, 181, 182, 191, 192, 193, 206
 micro crack processes, xi
 models, xii, 75, 78
 multiplication, 1
- P**
- polymer(s), xi, 6, 30, 79, 168, 200, 208, 213
 propagation, 29, 223
- R**
- requirement(s), 83, 117, 118, 120, 125, 158, 175, 189, 214
 root(s), 9, 10, 105, 120, 138, 169, 176
- S**
- science, i, ii, iii, iv, 6, 71, 98, 148, 161
 shear, 197
 shear strength, 197
 showing, 36
 simulation(s), 28, 94, 159
 singularity approach, xi, 2, 11, 13, 16, 19, 73, 75, 77, 89, 91, 124, 125, 151, 155
 solution, 11, 13, 16
 stability, 220
 state(s), xiii, 6, 31, 33, 37, 44, 48, 50, 65, 70, 71, 74, 83, 90, 92, 93, 107, 109, 110, 112, 129, 130, 132, 150, 151, 156, 160, 166, 168, 170, 184, 193, 195, 201, 211, 216, 219, 230
 strain energy, 3, 31, 36, 38, 39, 49, 63, 74, 89, 100, 104, 110, 142, 170, 199, 201, 211, 226
 strain energy density, 89
 strength theory, xi, xii, 15, 21, 123, 126, 155, 157, 160, 183, 221
 strength theory of wood, xi
 stress, 7, 51, 56, 72, 86
 stress intensity factor, 72, 156
 substitution, 44, 64, 116, 141, 172, 205, 228
- plastic deformation, 1

T

tension, 81, 107, 121, 191, 220, 229
testing, 106
transformation(s), 2, 12, 14, 22, 90, 164,
166, 167, 170, 172, 173, 174, 183,
226, 227, 231, 232

U

uniaxial tension, 193

W

wood, i, iii, 6, 34, 71, 124, 147, 162, 163,
168, 201, 204, 221, 226

Y

yield drop, xii, 3, 4, 35, 36, 37, 42, 43,
44, 45, 46, 47, 48, 49, 50, 52, 53, 54,
55, 58, 59, 62, 63, 65, 68, 74, 77, 78,
86, 129, 130, 131, 132, 149, 155, 157,
161, 225